

**A New Method of Temporal Phase Shifting using
Principle of Stroboscopy for Characterizing
Microstructures**

Davoud Mohammad Ali Zadeh

A Thesis

In

The Department

Of

Mechanical and Industrial Engineering

Presented In Partial Fulfilment of the Requirements

for the Degree of Master of Applied Science (Mechanical Engineering) at

Concordia University

Montreal, Quebec, Canada

July, 2009

© Davoud Mohammad Ali Zadeh, 2009



Library and Archives
Canada

Bibliothèque et
Archives Canada

Published Heritage
Branch

Direction du
Patrimoine de l'édition

395 Wellington Street
Ottawa ON K1A 0N4
Canada

395, rue Wellington
Ottawa ON K1A 0N4
Canada

Your file *Votre référence*
ISBN: 978-0-494-63123-2
Our file *Notre référence*
ISBN: 978-0-494-63123-2

NOTICE:

The author has granted a non-exclusive license allowing Library and Archives Canada to reproduce, publish, archive, preserve, conserve, communicate to the public by telecommunication or on the Internet, loan, distribute and sell theses worldwide, for commercial or non-commercial purposes, in microform, paper, electronic and/or any other formats.

The author retains copyright ownership and moral rights in this thesis. Neither the thesis nor substantial extracts from it may be printed or otherwise reproduced without the author's permission.

AVIS:

L'auteur a accordé une licence non exclusive permettant à la Bibliothèque et Archives Canada de reproduire, publier, archiver, sauvegarder, conserver, transmettre au public par télécommunication ou par l'Internet, prêter, distribuer et vendre des thèses partout dans le monde, à des fins commerciales ou autres, sur support microforme, papier, électronique et/ou autres formats.

L'auteur conserve la propriété du droit d'auteur et des droits moraux qui protègent cette thèse. Ni la thèse ni des extraits substantiels de celle-ci ne doivent être imprimés ou autrement reproduits sans son autorisation.

In compliance with the Canadian Privacy Act some supporting forms may have been removed from this thesis.

Conformément à la loi canadienne sur la protection de la vie privée, quelques formulaires secondaires ont été enlevés de cette thèse.

While these forms may be included in the document page count, their removal does not represent any loss of content from the thesis.

Bien que ces formulaires aient inclus dans la pagination, il n'y aura aucun contenu manquant.


Canada

Abstract

A New Method of Temporal Phase Shifting using Principle of Stroboscopy for Characterizing Microstructures

Davoud Mohammad Ali Zadeh

Temporal Phase Shifting Interferometry is the most common method for characterization of surface, profile and displacement properties of micro devices. Common methods of phase shifting require PZT based devices that have inherent errors due to non-linearity. To avoid these errors during phase shifting, a new phase shifting technique is presented in this work. A detailed analysis of the temporal phase shifting technique was performed and an optimized methodology for phase shifting was also established. This technique utilizes the advantage of stroboscopic interferometry to create phase shifted images without requiring any component for phase shifting. The feasibility of the proposed method of phase shifting was demonstrated using the developed Acoustic-Optic Modulated Stroboscopic Interferometer (AOMSI) on simple 1D and 2D micro structures designed specifically for this purpose.

The proposed method was used for surface profiling and static characterization of the microstructures. Experiments were performed on microcantilevers in order to extract the curvature of the device due to residual stress on it. The same device was tested under a commercial surface profiler with 1\AA resolution and the results were found to be in good agreement with the results from the proposed technique. Static characterization was performed to identify the tip deflection and profile variation of the microcantilever in

response to various DC voltages. A capacitor-based cantilever was tested under varied electrostatic loads and the deflection of the cantilever was extracted using the proposed method. The deflection of the cantilever was predicted using a theoretical model based on energy method. Static characterization results from the proposed technique were found to be in good agreement with the predicted results.

To extend the applicability of this technique without affecting the spatial resolution for micro devices larger than the field of view of the interferometer, stitching method was proposed and three different stitching configurations were also presented. The same device was tested in full-field of view under the commercial profiler. Good agreement between the result of presented stitching methods and commercial profiler demonstrates the reliability of the presented methods for stitching large structures.

Acknowledgments

The author would like to express his sincere thanks to his supervisors Dr. Muthukumaran Packirisamy and Dr. Sivakumar Narayanswamy for their support and encouragement. It was a pleasure to carry out research under them. I am grateful to Dr. Narayanswamy who shared his knowledge for developing a new method of temporal phase shifting. I am also grateful to Dr. Packirisamy for sharing his knowledge on MEMS and giving significant feedback on the experiments. Also the encouragement that I received from both of my supervisors to attend in various conferences and helping me for the publication are unforgettable. Their genuine enthusiasm for this research topic created an atmosphere that was truly instrumental in the success of this presented work.

It is also my pleasure to extend my gratitude to Mr. Murali Manohar Pai for helping in the experimental setup. I owe my thanks to Ms. Ramak Motamedi and Mr. Mohammad Kamal for their help and friendly discussions during my program. The author appreciates the many discussions and outings with friends and colleagues and would like to acknowledge Gino Rinaldi , Arvind Chandrasekaran, Hamid Sadabadi, Etienne Mfoumou, Jayan Ozhikandathil and Stefan Stoenescu. To all a heartfelt thanks.

I would like to express my sincere thanks to my wife, my daughter and my son for their love and encouragement during my program.

Table of Contents

List of Figures	ix
List of Tables	xiii
List of Symbols & Abbreviations	xiv
Chapter 1	Introduction
1.1 Introduction	1
1.2 History of MEMS	2
1.3 Need for Mechanical Characterization Tools in MEMS	4
1.3.1 Non-optical methods	5
1.3.2 Optical based methods	8
1.3.3 Focus sensing techniques	9
1.3.4 Interferometry technique	10
1.4 Interferometry Technique for Surface Profile and Static Behaviour	10
1.4.1 Stroboscopic interferometer	12
1.4.2 Digital laser micro interferometer	14
1.5 Processing of a Fringe Pattern	15
1.5.1 Fringe tracking	16
1.5.2 Fourier transform method	17
1.5.3 Phase shifting method	18
1.6 Objective and Scope of the Thesis	19

Chapter 2 Study of Phase Shifting Interferometer

2.1 Introduction and Background	20
2.2 Available Methods for Shifting the Phase	21
2.2.1 Introduction	21
2.2.2 Linear reference surface displacement	21
2.2.3 Using a glass plate	24
2.2.4 Using a grating plate	25
2.2.5 Polarization based phase shifting	25
2.3 Phase Shifting Algorithms	26
2.4 Phase Shifting Methods	28
2.4.1 Three step method	28
2.4.2 Four step method	29
2.4.3 Carré method	30
2.4.4 The five step method	30
2.5 Error in Phase Shifting Method	31
2.5.1 Vibration and air turbulence	32
2.5.2 Phase-shifter errors	32
2.5.3 Non-linearity due to the detector	34
2.5.4 Quantization of the detector	34
2.6 Conclusion	34

**Chapter 3 New Temporal Phase-Shifting Technique For Characterization
of Microstructures**

3.1 Introduction	35
3.2 Stroboscopic Interferometry	37
3.3 Experimental Methodology	40
3.4 Experimental Set up	43
3.5 Design of Microstructures	45
3.6 Results and Discussion	46
3.7 Conclusion	53

**Chapter 4 Static Characterization of Microstructures Using Developed
AOMSI and Temporal Phase-Shifting**

4.1 Introduction	55
4.2 Theoretical Analysis	57
4.3 Experimental Methodology	60
4.4 Results and Discussion	62
4.5 Conclusion	66

**Chapter 5 Stitched Acousto-Optic Modulator Stroboscopic Interferometry
for Characterizing Large Structures**

5.1 Introduction	67
5.2 Stitching Methods	70

5.2.1	Size reference method	70
5.2.2	Geometric reference	72
5.2.3	Combination of size and geometrical reference	74
5.3	Results and Discussions	75
5.4	Conclusion	87
Chapter 6		
Conclusions and Future Work		
6.1	Conclusions	88
6.2	Future Work	89
References		91
Appendix		
List of Publications		

List of Figures

Figure 1.1 Schematic of Scanning Electron Microscopy [16]	6
Figure 1.2 A scematic of Atomic Force Microscopy [17]	7
Figure 1.3 Schematic layout of Confocal microscopy	9
Figure 1.4 A schematic layout of Microscopic Mirau interferometer system	11
Figure 1.5 Stroboscopic interferometer block-diagram. RM [24]	13
Figure 1.6 Schematic layout of a digital laser micro-interferometer with a stroboscopic illumination [30]	15
Figure 1.7 Result of analysing a holographic interferogram by automatic fringe analysis with a computer image processing system [32]	17
Figure 2.1 Phase shifting by linear displacement of the reference surface using piezoelectric	22
Figure 2.2 A schematic of a setup for phase shifting [44]	23
Figure 2.3 The profile of metallic electrodes on a glass substrate extracted by Phase Shifting method [44]	23
Figure 2.4 Phase shifting with rotating a glass plate	24
Figure 2.5 Phase shifting by moving grating and Bragg cell	25
Figure 2.6 Dependency of non-linear phase error to linear error in different algorithms [52]	33
Figure 3.1 The phase motion because of existing small differences between two frequencies[14]	38

Figure 3.2 (a) Bragg angle, and (b) Vector of diffracted beam in AOM	39
Figure 3.3 The vibration of mounted cantilever on PZT	41
Figure 3.4 Capturing situations of four equal phase-shifted images	42
Figure 3.5 A digital image of used stroboscopic interferometer set up	43
Figure 3.6 Schematic arrangement for the Acoustic-Optic Modulated Stroboscopic Interferometer for performing temporal phase shifting	44
Figure 3.7 SEM image of designed micromirror for the test	45
Figure 3.8 SEM image of an SOI MicraGem technology design cantilever array	46
Figure 3.9 Four interferograms which are taken in stroboscopic interferometry from micromirror, a is the first, b, c and d are the second, third, and fourth taken image respectively	47
Figure 3.10 Wrapped image obtained from Micromirror	48
Figure 3.11 Extracted out of plane variation of micromirrors using new method of temporal phase shifting method	49
Figure 3.12 Captured interferograms from MicraGem technology cantilever array	51
Figure 3.13 The wrapped phase value of pixels along of selected cantilever	52
Figure 3.14 Surface-height information of the selected cantilever	53
Figure 4.1 An array of three MEMS RF switches [3]	56
Figure 4.2 (a) A capacitor-based fixed-free cantilever beam, (b) Deformed beam under electrostatic force	56
Figure 4.3 Schematic of assumed capacitor-base cantilever for the experiment	57
Figure 4.4 Predicted displacement of the cantilever under applied voltages	60
Figure 4.5 Electrostatic excitation of microcantilever	61

Figure 4.6 Tip deflection of the beam because of the electrostatic loads	62
Figure 4.7 Four equally phase-shifted images from DUT when no voltage was applied	63
Figure 4.8 Displacement of the cantilever because of applied voltage in AOMSI.	64
Figure 4.9 Comparison of the results in developed AOMSI and theoretical model	65
Figure 5.1 Scheme for the dimension of a specimen for stitching using size reference method	70
Figure 5.2 A 2-D specimen in which the FOV of taken adjunct images and the reference edges for stitching using size reference has been illustrated	71
Figure 5.3 The area of the adjunct images and references for stitching them on the basis of geometric reference	73
Figure 5.4 The area of two images and references for stitching them on the base of geometric reference	73
Figure 5.5 Scheme of a 2-D specimen and its dimension for stitching using combination of size and reference method	74
Figure 5.6 A sample 2-D specimen in which the FOV of the images with overlap areas is shown, can be analyzed using combination of size and geometric references	75
Figure 5.7 MicroGem made cantilever array and selected cantilever for the test	76
Figure 5.8 Four unknown but equally phase-shifted captured images from used microcantilever for the test in the sequence of acquiring in the first step	78
Figure 5.9 Extracted deflection information for the root portion of the DUT	79
Figure 5.10 Four unknown but equally phase-shifted captured images from used microcantilever for the test in the sequence of acquiring in the second step	80

Figure 5.11 Extracted surface information for the tip portion of the DUT	81
Figure 5.12 Extracted surface information for DUT after stitching using geometric reference	82
Figure 5.13 Extracted surface information for DUT after stitching with size reference and considering whole tip configuration	82
Figure 5.14 Extracted surface information for the DUT after stitching with size reference and considering whole root configuration	83
Figure 5.15 Extracted surface information for the DUT after stitching with averaging overlapping areas	83
Figure 5.16 Extracted information for DUT after compensating the tilt	84
Figure 5.17 Extracted information for the test cantilever after considering the tilt using AOMSI and profilometer	86

List of Tables

Table 1.1 Comparison of common microscopes [18]	8
Table 1.2 Comparison of different fringe analyzing method [35]	18
Table 3.1 Designed microstructures for the test	53
Table 4.1 Used parameters for the calculation	59
Table 5.1 Comparing the result in four used stitching methods and profilometer	86

List of Symbols

c_n	Deflection coefficients of the cantilever
d	Gap between cantilever and base
E	Young's modulus of elasticity
f	Frequency
L	Length
n	Refractive index
n	Diffraction order
Δp	Optical path differences
t	Material thickness
K_α	Acoustic wave vector
Q	Raman-Nath parameter
U_b	Strain energy
U_p	Electrostatic potential energy
V	Applied voltage
V_α	Speed of sound in the material
$W(x)$	Flexural deflection
w	Material width
\hat{w}	Width of AOM
$\acute{\alpha}$	Bragg angle for an incident light
α	Phase shift
β	Phase step size

$\delta(x, y)$	Phase of each pixel
$\delta(\varphi)$	Value of phase
ϵ_0	Permittivity of the free space
ϵ_r	Relative permittivity of the dielectric medium,
θ	Angle
λ	Wavelength of the light source
λ_i	Wavelength of incident light
λ_a	Wavelength of acoustic wave
$\varphi(x, y)$	Values of phase
$\Delta\varphi$	Phase differences
ϕ_n	Orthogonal polynomials
$\phi_0(x)$	Parent polynomial in x
$\phi_i(x)$	i^{th} orthogonal polynomial in x
$\phi_j(x)$	j^{th} orthogonal polynomial in x
$\phi''_i(x)$	Second derivative of i^{th} orthogonal polynomial in x
$\phi''_j(x)$	Second derivative of j^{th} orthogonal polynomial in x

Used Abbreviations:

MEMS	Microelectromechanical system
PZT	Piezoelectric actuator

AOMSI	Acoustic-Optic Modulated Stroboscopic Interferometer
AOM	Acousto-Optic Modulator
PS	Phase shifting
TPS	Temporal phase shifting

Chapter 1

Introduction

1.1 Introduction

Micro Electro Mechanical Systems (MEMS) is a technology suited for the integration of mechanical elements, sensors, actuators, and electronics using batch-level microfabrication technology. MEM is diverse technology that could significantly impact every category of products [1]. Already, MEMS is used for many applications ranging from neural probes to active suspension systems for automobiles. The nature of MEMS technology and its diversity for useful applications make it a far more enabling technology than integrated circuit microchips [2].

Manufacturing processes that can make small features have been developed in recent years. Electrostatic, magnetic, electromagnetic, pneumatic and thermal actuators, motors, valves, gears, cantilevers, diaphragms, and tweezers of less than 100 micron have been fabricated using this technology. The MEMS devices have been used as sensors for pressure, temperature, mass flow, velocity, sound, and chemical composition, as actuators for linear and angular motions, and as simple components for complex systems, such as

lab-on-a-chip, robots, micro heat-engines and micro heat pumps. They have been fabricated using integrated circuit batch-processing technologies. Current manufacturing techniques for MEMS include micromachining, bulk micromachining, lithography, electro deposition, plastic moulding, etc [3].

1.2 History of MEMS

The invention of transistor at Bell Telephone Laboratories in 1947 was a start of fast-growing microelectronic technology. The first integrated circuit (IC) in 1958 using germanium (Ge) devices was built by Jack Kilby and later Robert Noyce developed a planar double-diffused Silicon IC [4]. The complete transition from the original Ge transistors with grown and alloyed junctions to silicon (Si) planar double-diffused devices took about 10 years. The success of Si as an electronic material was due to its lower material costs relative to other semiconductors.

In 1954 it was discovered that the piezo resistive effect in Ge and Si had the potential to produce Ge and Si strain gauges with 10 to 20 times greater sensitivity than those based on metal films. As a result, Si strain gauges were developed commercially in 1958[4-5]. The first high-volume Si pressure sensor was marketed by National Semiconductor in 1974[5]. This sensor included a temperature controller for constant-temperature operation. Improvements in this technology since then have included the utilization of ion implantation for improved control of the piezo resistor fabrication [5].

Around 1982, the term micromachining was introduced to designate the fabrication of micromechanical parts. They were fabricated by etching selectively the areas of the

silicon substrate in order to leave behind the desired geometries. Isotropic etching of silicon was developed in early 1960s for transistor fabrication. Anisotropic etching of silicon was introduced in 1967. Various etch-stop techniques were subsequently developed to provide further process flexibility. Bulk micromachining is a process in which the bulk of the silicon substrate is etched to leave behind the desired micromechanical elements. Bulk micromachining is a useful technique for the fabrication of micromechanical elements. However, the need for flexibility in device design and performance improvement has motivated the development of new concepts and techniques for micromachining [4-7].

Since 1990, the MEMS have advanced from the early stage of technology development, device exploration, and laboratory research, to the mature stage of mass production and applications. It also helped exploration and research in many new areas [8]. Since then, remarkable research progress has been achieved in MEMS under strong capital promotions from both government and industries. Many new Frontiers of research and application are developing in biological research and medical instruments, micro-energy sources—micro-fuel cells, environmental energy converters, remote energy supply techniques, radio frequency and optical/IFR communication, environmental monitoring, and protection, ocean and water-way studies, and nano-micro-mixed technology [8].

Equivalent terms for MEMS are micro systems in Europe and micro machines in Japan [3]. In addition to the commercialization of some integrated MEMS devices, such as micro accelerometers, inkjet printer head, micromirrors, etc., the concepts and feasibility of more complex MEMS devices have been proposed and demonstrated for many

applications in varied fields of micro fluidic, aerospace, biomedical, chemical analysis, wireless communications, data storage, display, optics, etc.[2].

Advanced research in MEMS covers the potential uses of not only silicon and semiconductors but also other new innovative materials [9-10].

The rapid growth of MEMS technology has generated diverse developments in many different fields, ranging from automotive to medicine, pharmaceuticals, manufacturing, space, consumer products, and bioengineering. MEMS technology features small size, fast response time, high precision, and integration of transducers with control electronics. In addition, MEMS fabrication achieves low cost through batch fabrication techniques [2].

1.3 Need for Mechanical Characterization Tools in MEMS

Many experts have indicated that commercialization of MEMS technology must include an improvement in reliability and reduction in costs, particularly packaging costs [9]. Mechanical characterization of MEMS materials is increasingly important in view of improving reliability and assessing the life time of new devices. Various types of characterization would be required based on the application of the specimen. These methods include, surface profiling, static and dynamic characterization, tensile, and torsion and fatigue testing of specially designed microstructures, particle characterization, performance characterization, etc.

Rapid development in microsystem technology made the development of various actuated MEMS structures possible [54-55]. Most microstructures, because of being used

in highly accurate sensors and components, extremely depend on their mechanical specification. For example controlling the thickness of the deposition thin film is critical during manufacturing of the semiconductors and optical components [56] as its properties after deposition vary base on processing conditions [57]. Similarly boundary conditions of micromechanical structures such as AFM probes are non-classical in nature, and they influence the modal response and natural frequencies of the cantilever that cannot be modeled on purely classical boundary conditions [58]. Theoretical modeling could give a feedback for microstructures but in order to obtain exact information of microstructures, an appropriate testing method is required [59-60].

Various tools and techniques are always developed for this purpose on the basis of product type and required accuracy. In this report available tools and techniques for in-plane and out-of-plane characterization of microstructures are classified into two different methods, contact or non-contact type and optical or non-optical method [7].

1.3.1 Non-optical methods

Different techniques that do not use light for characterizing have been developed over the last few years. The four most common techniques are reviewed here. Scanning electron microscope (SEM) images the sample surface by scanning it with a high-energy beam of electrons in a raster scan (see Figure 1.1). In this technique the electrons interact with the atoms and make up the sample producing signals that contain information about the sample's surface topography, composition and other properties such as electrical conductivity. SEM images have a very large depth of field which can be useful for

extracting three-dimensional information of the sample. This technique has the limitation on the specimen size and the sample should be located in a vacuum environment [19-18].

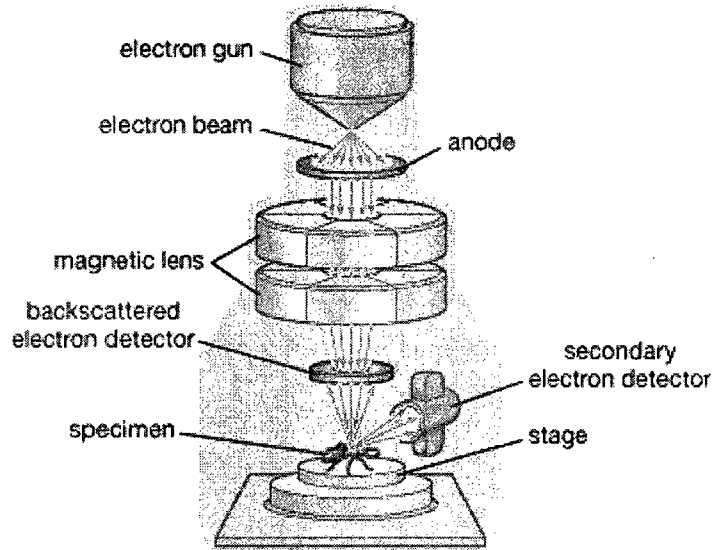


Figure 1.1 Schematic of Scanning Electron Microscopy [16].

Gerd Binnig and Heinrich Rohrer [17] developed the atomic force microscope (AFM) in the early 1980s and Scanning Tunneling Microscope (STM) in 1981. AFM consists of a micro scale cantilever with a sharp tip (probe) at its end that is used to scan the specimen surface. The forces between the tip and the sample leads to a deflection of the cantilever that is measured using a laser spot reflected from the top surface of a cantilever into an array of photodiodes as shown in Figure 1.2. STM is based on the concept of quantum tunnelling and considered as a powerful technique for viewing surfaces at the atomic level. When a conducting tip is brought very near to a metallic or semiconducting surface, a bias between the two can allow electrons to tunnel through the vacuum between them. STM can be a challenging technique, as it requires extremely clean surfaces and sharp tips. The advantage of AFM is that they can be used in ultra high

vacuum, air and various other liquid or gas ambient, and at temperatures ranging from near zero Kelvin to a few hundred degrees Celsius. However in contact type of surface measurement by AFM, soft material or bio-medical samples, might be damaged or scratched.

In Scanning Capacitance Microscopy (SCM) there is a narrow probe electrode which is held just above the surface of a sample and scans across the sample and extracts profile of the surface through the information obtained from the change in electrostatic capacitance between the surface and the probe. Table 1.1 illustrates the capability and limitation of four presented microscopes comparing with optical Microscope.

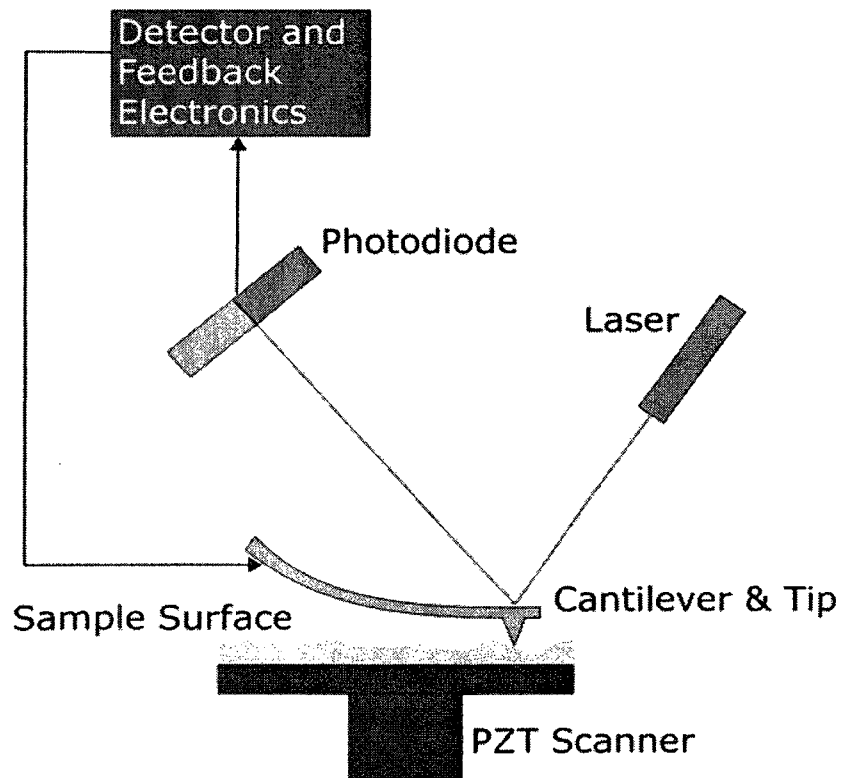


Figure 1.2 A scematic of Atomic Force Microscopy [17].

	Optical microscope	SEM/STM	SCM/AFM
Operating Environment	Ambient air, liquid or vacuum	Vacuum	Ambient air, liquid or vacuum
Depth of Field	Small	Large	Medium
Resolution: X, Y	1.0 μ m	5nm	0.1nm
Resolution: Z	n/a	n/a	0.05nm
Effective magnification	1X – 2E6X	10X – 10E6X	500X – 10E8X
Sample preparation requirement	Little	Little to substantial	Little or none
Characteristics required for sample	not be completely transparent to light wavelength used	be vacuum compatible while not building up charge	not have local variations in surface height >10 μ m

Table 1.1. Comparison of common microscopes [18].

1.3.2 Optical based methods

Ability to make high accuracy, non-contact, non-destructive and full-field measurements make optical metrology appropriate for characterization of microstructures [61]. Each of them is essential in some application. As an example, in vibration pattern of a piezo-motor, the monitoring of the whole surface rather than a single point is necessary [37].

Urgent needs of biomedical, data storage, actuators, and sensors industries have promoted the development of various techniques with the ability to produce ultra high precision surface profiling [15]. Optical characterization technique is considered as one of the best methods for characterizing microstructures due to its ability to provide high accuracy, non-contact, non-destructive and full-field measurements [14]. Optical based

characterization techniques can be broadly classified into focus sensing and interferometric technique [15, 19].

1.3.3 Focus sensing techniques

Confocal microscopy is one of the most important optical focus-sensing techniques that is commonly used in scientific and industrial applications for surface profiling. It can be considered as a replacement technique for stylus instruments, while non-contact nature of this technique makes this method faster than stylus instruments. Figure 1.3 shows schematic layout of Confocal microscopy. Unlike wide-field images such as fluorescence microscope it is using a pinhole in an optically conjugate plane in front of the detector to eliminate out of focus information and provide better image quality. By scanning over the specimen it can provide 2D or 3D imaging of the specimen [15].

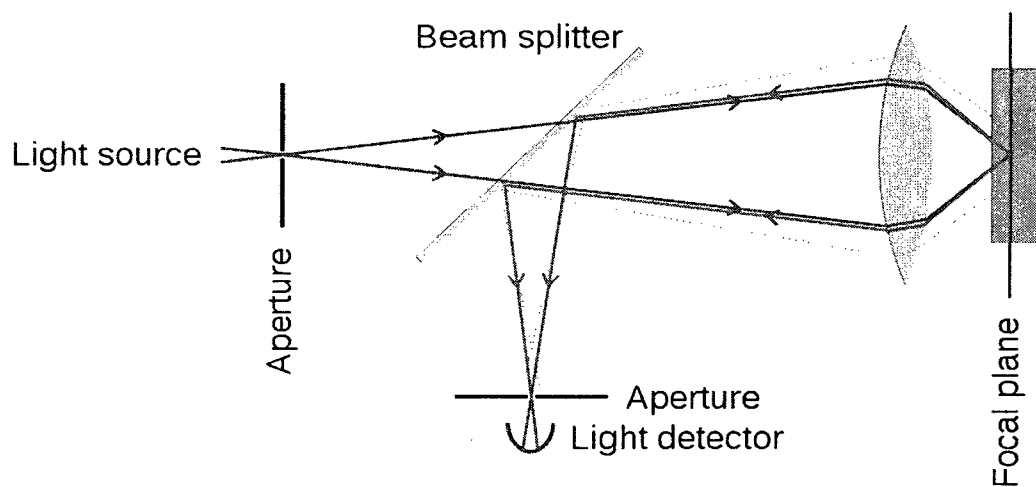


Figure 1.3 Schematic layout of Confocal microscopy [15].

While focus sensing devices are considered useful for surface profiling, they can not be used for dynamic characterization of the microstructure for which Interferometric technique are necessary.

1.3.4 Interferometry technique

Interferometric technique is an extension of the optical focusing technique, and it increases the sensitivity of optical stylus concept by using interference of light [15]. This technique makes use of the principle of superposition to combine separate waves together to have some meaningful property that is diagnostic of the original state of the waves. Most interferometers use light or some other form of electromagnetic wave. The outcome of all interferometry techniques is one or a few interferograms, they are obtained as a result of path differences between two interfering beams. The resolution of this system is limited only by the diffraction limit and aberration [15]. Optical interferometry has been used for measuring surface profiles, displacements, and optical distances with accuracy in the order of 1/100 of the wavelength of the light used [20]. A few develop method for static and surface characterization using interferometry techniques are discussed in the next chapter.

1.4 Interferometry Technique for Surface Profile and Static Behavior

Surface profiling is essential in fabrication of the microstructures for optimizing the process design. Static characterization of microstructures under static load is a requirement for fabricated microstructures before being used in working condition. The high-accuracy surface profile interferometry measurements include the heterodyne

interferometry method, the phase-shifting interferometry method, and sinusoidal phase modulating (SPM) interferometer [21]. Various microscopic interferometers have been developed for satisfying both requirements. Figure 1.4 shows a schematic layout of one of microscopic Mirau interferometer systems.

The principle in a Mirau interferometer is the same as in a Michelson interferometer. The difference between the two is in the physical location of the reference arm. The reference arm of a Mirau interferometer is located within the object arm and microscope objective assembly. The big advantage of this interferometer is that any vibration on the sample could be transferred equally to both paths. Hence, any mechanical movement of specimen due to vibration can not affect the result.

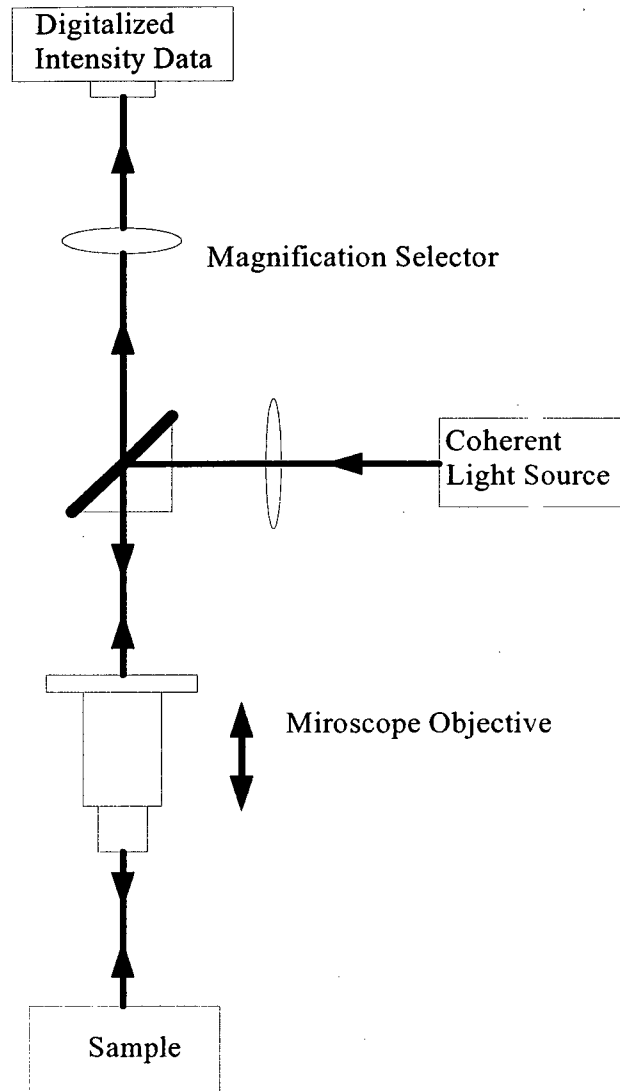


Figure 1.4 A schematic layout of Microscopic Mirau interferometer system.

1.4.1 Stroboscopic interferometer

Many MEMS and micro Opto-Electro-Mechanical Systems (MOEMS) devices are specifically designed as actuators, deflectors, motors or other moving systems. Hence dynamic and static behavior of these systems is of great interest. Although, vibratory motion of sample is detrimental to conventional interferometry, a stroboscopic source

illumination can capture repeated images of the sample at the same phase of oscillation so that the interference pattern would appear stable. Eguchi et al. and Nakano et al. adapted the stroboscopic technique to a phase-shifting interference microscope for measuring micro-mechanical systems in the early 1990's [22,23] and there are now a number of commercial instruments that offer this capability, including scanning white light interferometers.

The most recent work on stroboscopic interferometry was published by David A. Horsley from University of California. He collected dynamic and static measurements of surface profile of a bimorph deformable mirror (DM) used in adaptive optics system. Figure 1.5 shows a block-diagram of this phase-shifting interferometer. The instrument is a Twyman–Green interferometer in which a piezoelectric stage translates a reference mirror in order to introduce a controlled phase-shift between the light passing through the reference and measurement arms of the interferometer. Surface height variations in the DM create interference fringes when the reference and measurement beams are recombined, producing an interferogram that is captured and digitized using a CCD camera and a frame-grabber card. The surface profile of the DM is reconstructed using four interferograms collected at four distinct phase shifts (0 , $\pi/2$, π , $3\pi/2$) using Hariharan's algorithm [24].

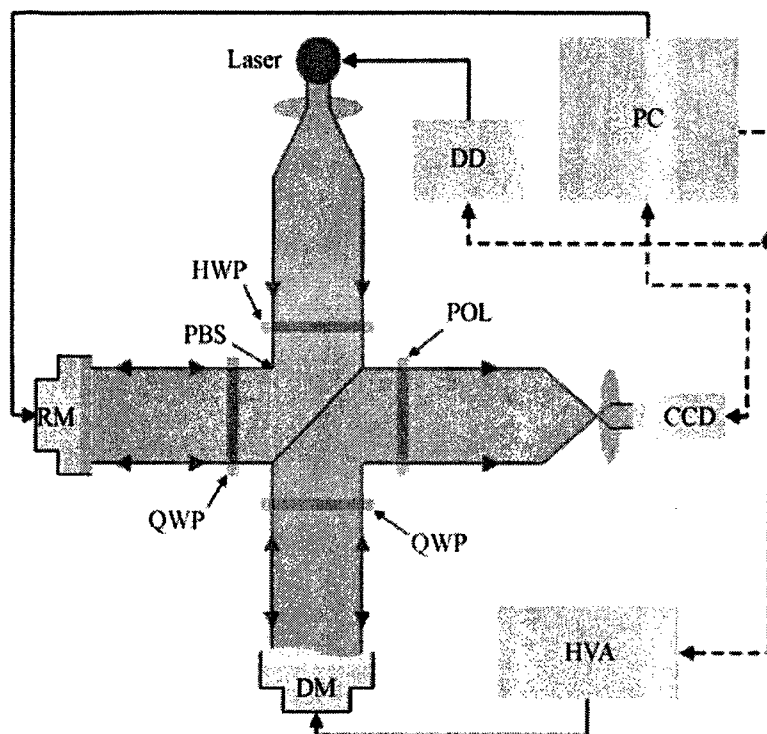


Figure 1.5. Stroboscopic interferometer block-diagram. RM: reference mirror, HWP: half-wave plate, QWP: quarter-wave plate, PBS: polarizing beam-splitter, POL: polarizer, DM: deformable mirror, HVA: high voltage amplifier, DD: digital delay [24].

The interferometer was outfitted with a pulsed diode laser to allow the DM surface profile to be measured in response to time-varying voltage inputs. Strobing the illumination source gates the image, allowing motion at frequencies much faster than the CCD frame rate (30 Hz) to be measured. The strobed illumination is synchronized to the high voltage line used to drive one of the actuators on the DM, and a programmable digital delay unit is used to control the time delay between the applied voltage and the optical pulse. Even though obtained result from this setup has high resolution, two issues should be discussed about this setup. First PZT is used on the reference mirror for

shifting the phase. PZT base phase shifters usually carry the mechanical error. In addition, non-linearity of PZT is the main source of error which is not ignorable in most cases [25, 26, 27, 28]. The second issue is that this set up is using LED as light source. Usually LEDs are not monochromatic and have restrictions in coherence length and frequency stability [19]. Using a He-Ne laser source and acousto-optic modulator (AOM) for pulsating the light would isolate the system from the error of LED and pulse generator.

1.4.2 Digital laser micro interferometer

A digital laser micro interferometer has a capability to measure both static and dynamic properties of MEMS and microstructures [29]. L.Yang et al [30] developed a universal digital laser micro-interferometer for measuring out-of-plane and in-plane displacements under either a static or a dynamic loading. Figure 1.6 illustrates the schematic layout of a digital laser micro-interferometer with a stroboscopic illumination. Developed system uses a long-distance microscope (LDM) incorporated with an out-of-plane or an in-plane digital speckle pattern interferometry (DSPI) and a stroboscopic illumination synchronized with vibration signal by a controller. The controller can generate both a continuous illumination (for static investigation or for vibration investigation by the time-average method) and a stroboscopic illumination (for dynamic measurement and analysis) without changing any optical arrangement in the setup. The disadvantage of this system is that the actuators use a synchronizing to vary the delay between two frequencies and they rely on commercial phase shifter for TPS. Developing a system which does not require any phase shifter can also avoid the error of phase shifter.

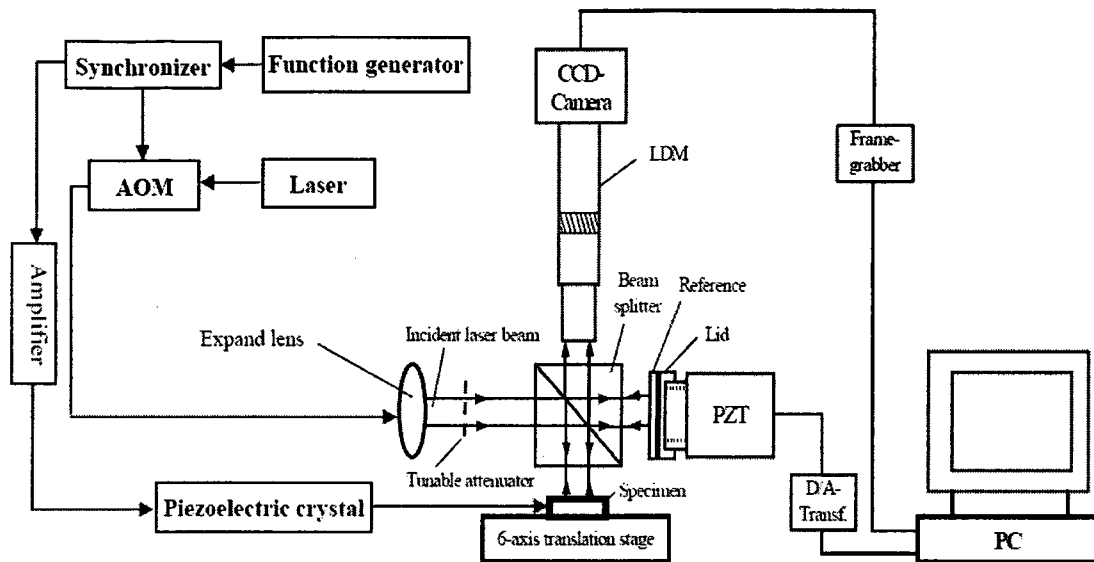


Figure 1.6 Schematic layout of a digital laser micro-interferometer with a stroboscopic illumination [30].

1.5 Processing of a Fringe Pattern

Fringe patterns (interferograms) produced by various types of optical techniques such as holographic interferometry, moiré interferometry, and fringe projection are used widely in the measurement of shapes, displacement and strain [31]. The measurement precision is influenced directly by processed fringe pattern [31]. The fringe patterns are usually analyzed automatically and the methods of processing fringe patterns are mainly classified as fringe tracking, and phase measurement methods.

1.5.1 Fringe tracking

Before the development of phase-measurement techniques, intensity-based techniques were the only image-processing tools available for the automatic analysis of

interferograms [32]. Fringe tracking involves a search for the locus of the fringe maxima (or minima) by examining the pixel values in all directions from the starting point (often determined manually) and moving the pixel locus in the direction along which the sum of the intensity is maximized (or minimized) or alternatively the gradient is a minimum. In this way only a limited set of the whole image array is examined [32].

Fringe tracking method currently is used, either manually or automatically, in applications where high precision is not needed and large fringe orders are involved in the analyses. This approach results in saving the cost of experimental design as a precision phase-shifting mechanism is not needed. Other advantage of this method is that only one image is required for the analysis leading to a saving of computation time [23, 33, 32]. Figure 1.7 illustrates the result of analyzing a holographic interferogram by automatic fringe analysis with a computer image processing system [32]

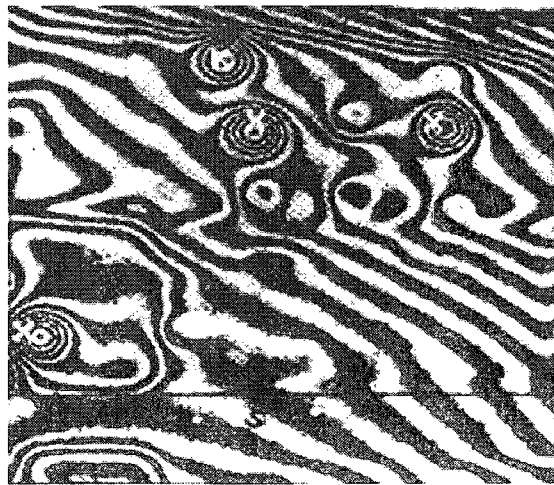


Figure 1.7 Result of analysing a holographic interferogram by automatic fringe analysis with a computer image processing system [32].

1.5.2 Fourier Transform method

Fourier transform methods (FTM) have been applied to various kinds of interferometric techniques such as holographic interferometry, shearography or Moire' interferometry [34]. The FTM usually involves introducing a known set of linear carrier fringes in order to modulate information fringes. This results in a simple fringe pattern with monotonically increasing or decreasing fringe order. If the spatial frequency content of amplitude variations of the information fringes is less than the spatial carrier frequency, the Fourier spectrum of the carrier modulated fringe pattern will exhibit three distinct peaks. The central peak represents the zero frequency component of the spectrum. One of the two outer peaks of the spectrum can be filtered from the rest, shifted to zero frequency and inverse transformed to yield a complex function for each pixel position of the digitized carrier-coded fringe pattern. Noise is removed by the proper selection of the filtering window in the spectrum domain. The phase of the original interferogram $\varphi(x, y)$ can be obtained by taking the arctangent of the ratio of the imaginary to the real parts of the complex function.

In Fourier transform method, better removal spatial noise improves the measurement accuracy. It is fast to perform and one interferogram is enough to analysis the fringe pattern. It has much better accuracy than fringe tracking method. How ever, it does not have the accuracy of the phase shifting method [32].

1.5.3 Phase shifting method

Earlier methods of extracting phase information and consequently, the connected parameters of interest, were very laborious and time-consuming and also suffered from the inherent inaccuracies of the procedures [19]. With the easy availability of computational and processing power and charge-coupled device array detectors, many automatic fringe evaluation procedures have been developed [15]. Table 1.2 provides information of different methods for phase evaluation and compare them with their performance.

Parameters	Fringe Tracking	Fourier Transform	Phase Shifting
Number of Interferograms	1	1	Minimum 3
Resolution	1 to $1/10 \lambda$	$1/10$ to $1/30 \lambda$	$1/10$ to $1/100 \lambda$
Inherent noise suppression	partially	No(yes)	Yes
Speed of evaluation	Low	Low	High
Experimental effort	Low	Moderate	High
Sensitivity to external influence	Low	Low	Moderate
Cost	Low	Moderate	High

Table 1.2 Comparison of different fringe analyzing method [35].

As seen in Table 1.2, the phase shifting method, because of its higher resolution and higher speed, can be considered promising of the phase evaluation method. Next chapter provides the detail information of the phase shifting method for characterizing.

1.6 Objective and Scope of the Thesis

The primary objective of this research work is to develop a new method of Temporal Phase Shifting (TPS) using the principle of stroboscopy for characterizing microstructures.

The scope of the work includes

- Developing Acousto-Optic Modulated Stroboscopic Interferometry (AOMSI) for performing new method of TPS without requiring any phase shifter.
- Design of simple MEMS microstructures to implement the developed method of TPS.
- Implementing the presented method for Surface profiling and static characterization
- Developing a stitching method for characterizing large structures.
- Validation of the results acquired using the developed TPS method with the results from the commercial interferometry profiler.

Chapter 2

Study of Phase Shifting Interferometer

2.1 Introduction and Background

Phase distribution is encoded in intensity distribution as a result of interference which can be retrieved from the interference pattern [32,36]. Techniques for determining the phase can be split into two basic categories, electronic and analytic. For analytical techniques, intensity data are recorded while the phase is temporally modulated, and then used to compute the relative intensity measurements. Electronic techniques are also known as heterodyne interferometry[37] is used extensively in distance measuring interferometers where the phase at a single point with a fast update is required. The analytic methods can be subdivided into two techniques, one that integrates the intensity while the phase is increased linearly, and a second where the phase is altered in steps between intensity measurements. The first method is referred to as integrating bucket phase-shifting, while the second is termed phase-stepping.

Phase-measurement technique has been applied to holographic and Moire' interferometers in the late 1970s and early 1980s [38] for the measurement of wave front in interferometers. Since then, various phase measurement methods have been developed. Phase-measuring interferometer technique is divided into two main categories taking the phase data sequentially (temporal phase shifting), and simultaneously (spatial phase shifting).

Currently the phase-shift method is the most popular in the field of the optical precision measurement. The limitations of this technique are due to phase-shift errors and the need for at least three interferograms for analysis. In applications involving high fringe

densities a good degree of accuracy can be obtained without using the phase-shift method [31, 33].

2.2 Available Methods for Shifting the Phase

2.2.1 Introduction

In order to measure accurately the wavefronts in broadband light, a phase shifting interferometer must be capable of obtaining zero path difference to give reasonably high-contrast fringes [40-41]. If two beams have a common source, phase shifting would happen because of the optical path differences. The value of phase can be calculated using Equation (2.1).

$$\Delta p = \frac{\lambda}{2\pi} \Delta\varphi \quad (2.1)$$

where $\Delta\varphi$ is the phase differences between two waves, Δp is the optical path difference

between them, and λ is the wavelength of the light source.

2.2.2 Linear reference surface displacement

In most phase-shifting interferometers phase shift is achieved by linear displacement of the reference surface using PZT actuators [26,42, 43]. Figure 2.1 shows the schematic of this technique.

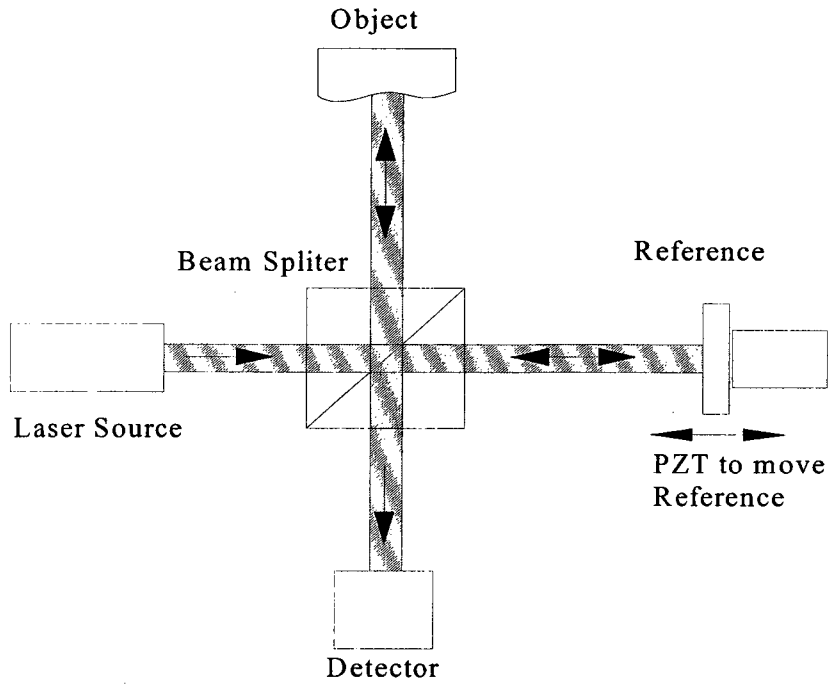


Figure 2.1 Phase shifting by linear displacement of the reference surface using piezoelectric.

Pierre Boher[44] developed a phase shifting interferometer for the characterization of nano devices using white light for illumination of the object. Both object and reference mirrors were excited sinusoidal using PZT. Figure 2.2 shows the schematic of the setup used for this purpose.

Phases are produced in real time at a rate of several Hertz and the system was not sensitive to the vibration. The above setup was used to estimate the profile of metallic electrodes on glass substrates [44].

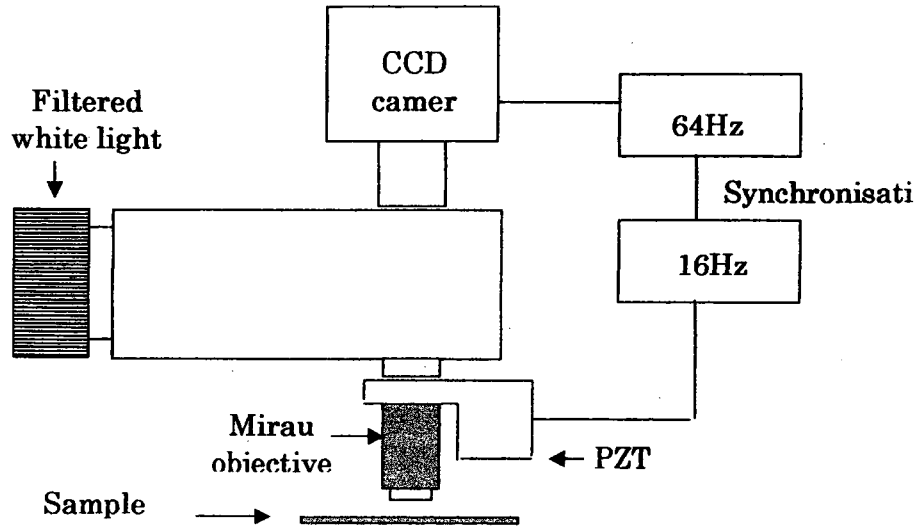


Figure 2.2 A schematic of a setup for phase shifting [44].

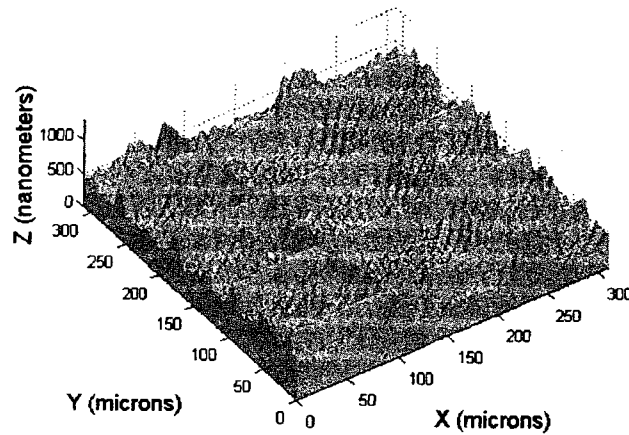


Figure 2.3 The profile of metallic electrodes on a glass substrate extracted by phase shifting method [44].

Although using PZT for moving the reference mirror for achieving phase shifting is relatively easy, it suffers from errors such as non-linearity, accuracy, and system vibration [45-47] and these errors are discussed in section 2.5 .

2.2.3 Using a glass plate

Creating phase shift between two beams by using a parallel glass plate in optical path of reference or object beam is also applied for phase shifting. Using this method can avoid the errors due to non-linearity of PZT, but vibration induced movement would still exist. Figure 2.4, shows the methodology of the phase shift produced by rotating a glass plate. This methodology is on the basis of increasing the path length of the reference beam by a fraction of wave length with respect to the object beam.

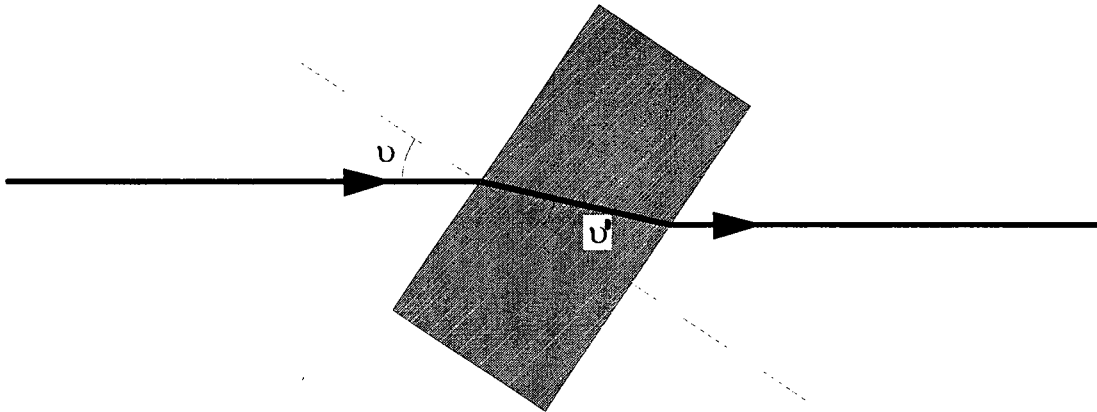


Figure 2.4 Phase shifting with rotating a glass plate.

The amount of shift achieved by rotating a glass plate can be calculated using Equation (2.2) [32].

$$\alpha = \frac{t}{k} \left\{ 1 - \frac{\cos(\alpha)}{n \cdot \cos(\alpha')} \right\} \sin(\nu) \Delta \nu \quad (2.2)$$

Where α is the amount of shift, t is the glass plate thickness, n is its refractive index, and $K = 2\pi / \lambda$. The angle ν and ν' are the angles between the normal to the glass plate and the light rays outside and inside of the plate, respectively.

2.2.4 Using a grating plate

Moving a grating plate perpendicular to the direction of the light was used by Suzuki et. for phase shifting[32]. As it is shown in Figure 2.5, the reflected beam could have a shift in the phase. Acousto-optic modulator (AOM) is considered as an alternative method for this purpose. It uses acousto-optic effect to diffract and shift the frequency of the light using sound wave and the phase of the diffracted beam will be shifted by the phase of the sound wave. This method is considered as better method as it provides better efficiency than moving grating plate, however it changes the direction of the light [15].

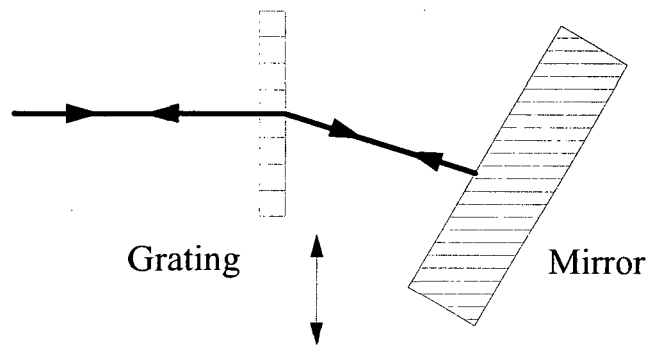


Figure 2.5 Phase shifting by moving grating and Bragg cell.

2.2.5 Polarization based phase shifting

In polarization based phase shifting usually a wave plate is used for polarizing the light. A wave plate is a simple birefringent crystal with a suitable orientation and thickness that shifts the phase between two perpendicular polarization components of light wave. In a polarization based phase shifting interferometer, the object and the reference beams are orthogonally polarized hence rotating a quarter wave plate in a particular angle is required. Phase shifts achieved by this method can be calculated by Equation (2.3).

$$\varphi = 2\Delta\theta$$

(2.3)

Where φ is the phase shift and $\Delta\theta$ is the small rotation of the wave plate.

The main source of error in this method is the inaccuracy of rotation of the wave plate[15], as this rotation is usually achieved by using mechanical instruments.

2.3 Phase Shifting Algorithms

Phase Sampling or phase shifting is on the basis of reconstruction of the phase $\delta(x,y)$ and it can be achieved by sampling a number of interferograms differing from each other by several of discrete phase $\delta(\varphi)$. If the plane is shifted, for instance temporally in n steps of φ , then n intensity values $I_n(x,y)$ are measured for each point in the fringe pattern. A general expression for an interferogram is written as

$$I_n(x,y) = a(x,y) + b(x,y) \cos[\delta(x,y) + \varphi_n] \quad (2.4)$$

With $\varphi_n = (n-1)\varphi_0$ $n=1 \dots m$, $m \geq 3$, and $\varphi_0 = \frac{2\pi}{m}$

Here $a(x,y)$ is the mean intensity and $\frac{a(x,y)}{b(x,y)}$ represents the visibility for each interferograms. Furthermore $\delta(x,y)$ is the phase of each pixel which should be calculated.

In Equation (2.4) there are three unknowns components a , b and δ . Hence only three intensity measurements are necessary for calculating the value of phase. However, with

more than three a better accuracy can be ensured using a least squares fitting technique. If the reference phase values φ_n are equally distributed over one or a number of periods, the orthogonal relations of the trigonometric functions provide simplified solution. Equation (2.4) can be rewritten in the form

$$I_n(x, y) = K(x, y) + L(x, y)\cos \varphi_n + M(x, y)\sin \varphi_n \quad (2.5)$$

where

$$\begin{cases} k(x, y) = a(x, y) \\ L(x, y) = -b(x, y)\cos\delta \\ M(x, y) = -b(x, y)\sin\delta \end{cases} \quad (2.6)$$

By making N phase steps ($i = 1, 2, \dots, N$), Equation (2.5) can be written in matrix form as

$$\begin{pmatrix} I_1 \\ I_2 \\ \vdots \\ I_N \end{pmatrix} = \begin{pmatrix} 1 & \cos\varphi_1 & \sin\varphi_1 \\ 1 & \cos\varphi_2 & \sin\varphi_2 \\ \vdots & \vdots & \vdots \\ 1 & \cos\varphi_N & \sin\varphi_N \end{pmatrix} \begin{pmatrix} K \\ L \\ M \end{pmatrix} \quad (2.7)$$

The values for K, L, and M can be calculated using the least squares solution to Equation (2.7).

$$\begin{pmatrix} K \\ L \\ M \end{pmatrix} = A^{-1}B \quad (2.8)$$

Where

$$A = \begin{pmatrix} N & \sum \cos\alpha_i & \sum \sin\alpha_i \\ \sum \cos\alpha_i & \sum \cos^2\alpha_i & \sum \cos\alpha_i \sin\alpha_i \\ \sum \sin\alpha_i & \sum \cos\alpha_i \sin\alpha_i & \sum \sin^2\alpha_i \end{pmatrix} \quad (2.9)$$

and

$$B = \begin{pmatrix} \sum I_i \\ \sum I_i \cos \alpha_i \\ \sum I_i \sin \alpha_i \end{pmatrix} \quad (2.10)$$

By applying the least square application, L and M can be calculated using Equations (2.11) and (2.12) [39]:

$$L(x, y) = \frac{2}{m} \sum_{n=1}^m I_n(x, y) \cdot \cos \varphi_n \quad (2.11)$$

$$M(x, y) = \frac{2}{m} \sum_{n=1}^m I_n(x, y) \cdot \sin \varphi_n \quad (2.12)$$

A combination of these equations delivers the basic equation for the phase shifting method where the minus sign is ignored because of the ambiguity of the sign in interferometry:

$$\delta(x, y) = \text{Arctan} \frac{M}{L} \quad (2.14)$$

Although obtained value using Equation (2.14) has modulus of π , with considering the sign of the numerator and denominator, the mod 2π wrapped phase distribution $\delta(x, y)$ can be measured. The unwrapping or demodulation of this wrapped signal delivers the continuous phase field as

$$\delta'(x, y) = \delta(x, y) + 2\pi N \quad (2.15)$$

where N is the integer fringe number.

2.4 Phase Shifting Methods

2.4.1 Three step method

Among the various phase-shifting algorithms available, the three-step algorithm requires a minimum number of frames and is the simplest to use [48]. The following equations describe the intensity values of the three measured fringe patterns:

$$I_1(x, y) = a(x, y) + b(x, y) \cdot \cos[\delta(x, y) - \beta] \quad (2.16)$$

$$I_2(x, y) = a(x, y) + b(x, y) \cdot \cos[\delta(x, y)] \quad (2.17)$$

$$I_3(x, y) = a(x, y) + b(x, y) \cdot \cos[\delta(x, y) + \beta] \quad (2.18)$$

Where $a(x, y)$ is the average intensity, $b(x, y)$ is the intensity modulation, $\delta(x, y)$ is the

phase, and β is the phase step size.

Even though β can be any value, the two commonly used ones are $\beta=\pi/2$ and $\beta=2\pi/3$ and

the formula for calculating the value of phase for those two particular shift is given by Equation (2.19) and (2.20) respectively.

$$\delta(x, y) = \tan^{-1} \frac{I_2 - I_1}{I_3 - I_1} \quad \text{for } \beta = \frac{\pi}{2} \quad (2.19)$$

$$\delta(x, y) = \tan^{-1} \frac{\sqrt{3}(I_2 - I_3)}{2I_2 - I_1 - I_3} \quad \text{for } \beta = \frac{2\pi}{3} \quad (2.20)$$

In this method the amount of phase shift should be known and three equal shifts should be achieved among three steps using any of the method mentioned in section 2.2, hence it is very sensitive to system error.

2.4.2 Four step method

This is also called the conventional 4-frame algorithm. In this method, it is required to shift the phase of either reference beam or object beam by $0, \pi/2, \pi, 3\pi/2$ and four phase

shifted images are acquired. Thus the intensity equations may be written as

$$I_1(x, y) = a(x, y) + b(x, y) \cdot \cos[\delta(x, y)] \quad (2.21)$$

$$I_2(x, y) = a(x, y) + b(x, y) \cdot \cos\left[\delta(x, y) + \frac{\pi}{2}\right] \quad (2.22)$$

$$I_3(x, y) = a(x, y) + b(x, y) \cdot \cos[\delta(x, y) + \pi] \quad (2.23)$$

$$I_4(x, y) = a(x, y) + b(x, y) \cdot \cos\left[\delta(x, y) + \frac{3\pi}{2}\right] \quad (2.24)$$

From these equations, the phase of the object can be calculated as

$$\delta(x, y) = \tan^{-1} \frac{I_4 - I_2}{I_1 - I_3} \quad (2.25)$$

Even though this algorithm is commonly used in phase shifting interferograms, it is not self-calibrating. So it is important that the phase shift should exactly be $\frac{\pi}{2}$ in order to achieve accurate results [15].

2.4.3 Carré method

The Carré algorithm is the one which is almost insensitive to linear error of phase shifter[49]. In this method four equal but unknown phase shift is needed. This algorithm is described by these intensity equations.

$$I_1(x, y) = a(x, y) + b(x, y) \cdot \cos[\delta(x, y)] \quad (2.26)$$

$$I_2(x, y) = a(x, y) + b(x, y) \cdot \cos[\delta(x, y) + \alpha] \quad (2.27)$$

$$I_3(x, y) = a(x, y) + b(x, y) \cdot \cos[\delta(x, y) + 2\alpha] \quad (2.28)$$

$$I_4(x, y) = a(x, y) + b(x, y) \cdot \cos[\delta(x, y) + 3\alpha] \quad (2.29)$$

From these equations, the phase of the object can be calculated as

$$\delta(x, y) = \tan^{-1} \sqrt{\frac{(3I_2 - 3I_3 - I_1 + I_4)(I_1 + I_2 - I_3 - I_4)}{(I_1 - I_2 - I_3 + I_4)^2}} \quad (2.30)$$

When light intensity change are purely sinusoidal, phase error of the Carré algorithm becomes zero [49].

2.4.4 The five step method

In this method, like Carré method there is no requirement for having a known shift. However the shift should be equal. The advantage of this method to Carré algorithm is that if the value of shift phase is large the five step method would give better accuracy [15]. The intensity equation in this method may be written as

$$I_1(x, y) = a(x, y) + b(x, y) \cdot \cos[\delta(x, y) - 2\alpha] \quad (2.31)$$

$$I_2(x, y) = a(x, y) + b(x, y) \cdot \cos[\delta(x, y) - \alpha] \quad (2.32)$$

$$I_3(x, y) = a(x, y) + b(x, y) \cdot \cos[\delta(x, y)] \quad (2.33)$$

$$I_4(x, y) = a(x, y) + b(x, y) \cdot \cos[\delta(x, y) + \alpha] \quad (2.34)$$

$$I_5(x, y) = a(x, y) + b(x, y) \cdot \cos[\delta(x, y) + 2\alpha] \quad (2.35)$$

From these equations, the phase of the object can be calculated as

$$\delta(x, y) = \tan^{-1} \left\{ 2 \sin \alpha \frac{I_2 - I_4}{2I_3 - (I_1 + I_5)} \right\} \quad (2.36)$$

In this method the phase shift of 90° would give the least error [15] and the value of phase can be calculated using the Equation (2.37).

$$\delta(x, y) = \tan^{-1}(-1) (2(I_2 - I_4)) / (2I_3 - I_5 - I_1)$$

2.5 Error in Phase Shifting Method

Though phase shifting is considered as one of the most accurate techniques, many research works have been done to study on minimizing the errors and achieving higher accuracy. As a result of these efforts, it was estimated that any steady phase-shift error has a spatial frequency twice that of fringe frequency [32,50]. Mudassar[51] obtained a maximum image intensity when fringe frequency was twice that of the cutoff frequency of the imager.

Different error sources have been presented for phase shifting method, but the main factors that influence the measurement accuracy of this method are vibration, air turbulence, phase-shifter errors, non-linearities of the detector, and quantization of the detector signal. The details of these error sources will be discussed in this context.

2.5.1 Vibration and air turbulence

The largest limitation of phase-shifting interferometry is its sensitivity to the environment, both vibration and air turbulence. Magee and Welsh in 1994 [32] announced that vibration and air turbulence are the most common source of temporal phase shifting. Hence for accurate results a proper isolation system is required [32]. While in simultaneous phase shifting interferometry and spatial carrier interferometry by using single-shot interferometric technique, the effects of vibration have been reduced. In temporal phase shifting using of a highly isolated table is considered as the easiest way for reducing vibration effects. Averaging the result is also considered as a useful method to reduce the effects of vibration and air turbulence.

2.5.2 Phase-shifter errors

PZT actuators are commonly used as a phase shifter in phase shifting interferometry [45,46,47]. Usually they are attached to the reference mirror and using advanced computer controlled devices, shift in the phase of reference beam is achieved. All PZT based phase shifters carry linear and non-linear phase errors. The linear error of the phase shifter is because of miscalibration of the phase shifter. Hence careful calibration of the phase shifter can eliminate this error or make it negligible. The important issue about non-linear errors of the phase shifters is that they are not easy to be detected or removed [15]. Dependency of non-linear or quadratic error to linear or miscalibration error of phase shifter varies among different algorithms. The three-frame algorithm, however, can cause large phase errors because of detector non-linearities, five-frame algorithm is the least sensitive to miscalibration [32]. Dependency of non-linear to linear phase error among some common phase shifting algorithms has been illustrated in Figure 2.6. As it

shown in this figure, Carré algorithm has excellent resistance to the non-linear phase error.

In the thesis work phase shifting is employed by AOMSI as there is no need to move the reference mirror for achieving phase shift. This would minimize linear or non-linear error of the phase shifter.

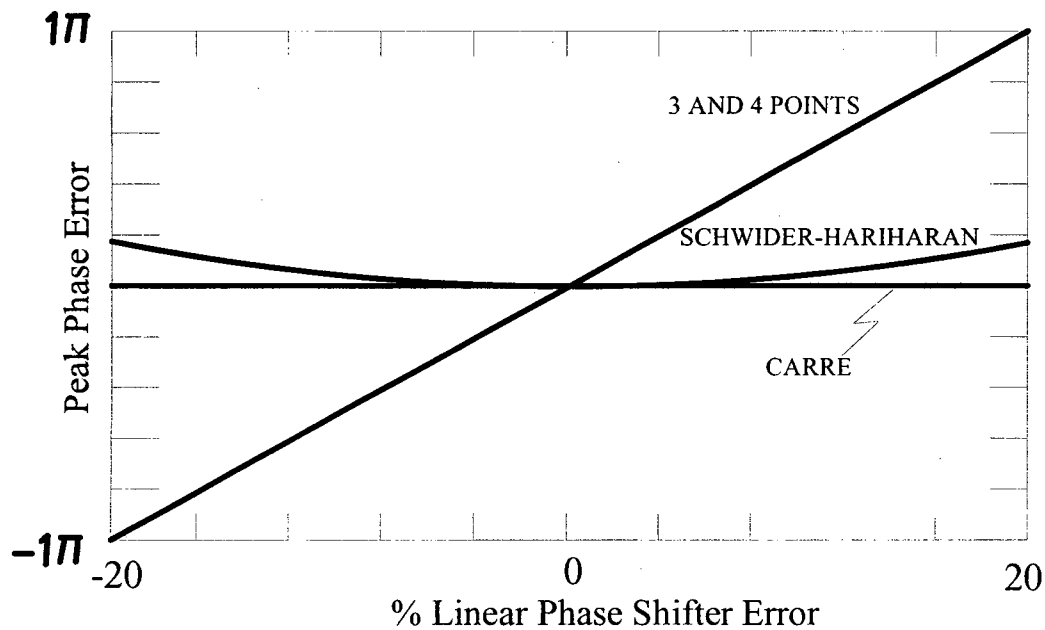


Figure 2.6 Dependency of non-linear phase error to linear error in different algorithms [52].

2.5.3 Non-linearity due to the detector

Even the phase error associated with the recording plane of interferometry is negligible, the amplitude error may still occur in phase-shifting interferometry (PSI) and it will affect both the amplitude and phase distributions of the reconstructed wave-front in original object plane when inverse Fresnel diffraction is involved [53]. Q. Liu[13]

proposed a method for correcting the wave front reconstruction errors caused by the nonlinearity of a detector by a special digital data processing algorithm. This algorithm was able to eliminate amplitude error the recording plane, and reduce both amplitude and phase errors significantly.

2.5.4 Quantization of the detector

Other factor that influences measurement accuracy is the quantization of detector signal. It is due to digitalization of the images, photon noise error and power fluctuation in laser in case tunable laser diode is used for phase shifting. For an intensity signal digitized to eight bits or more, the quantization error has an insignificant influence on the phase error and it is usually negligible when compared with other source of errors mentioned earlier [15,32].

2.6 Conclusion

The principle of phase shifting and various methods used to achieve the phase shift were discussed in detail. Different available methods for phase shifting and calculation of the phase were introduced. The advantages and disadvantages of each method were presented. In addition the errors associated with phase shifting method were discussed.

Chapter 3

New Temporal Phase-Shifting Technique for Static

Characterization of Microstructures

3.1 Introduction

Mechanical characterization of MEMS materials is increasingly important in view of improving reliability and assessing the life time of new devices. Various types of characterization would be required based on the application of the specimen. These methods include, surface profiling, static and dynamic characterization, tensile, torsion and fatigue testing of specially designed microstructures, particle characterization, performance characterization, etc. There are difficulties that exist in manufacturing and handling of small structures and determination of geometrical dimensions.

Unavoidability of residual stress in the fabrication of microstructures is another challenge for the designers. Layers in the surface micromachining, created by deposition or growth, usually are formed at higher temperatures which are very different from operating temperature of the microstructures. This is the main reason of existing residual stress in microstructures fabricated using surface micromachining method. Also the various thermal expansion coefficients on the device are the other reasons for residual stress. In most cases, the deformation of microstructure due to residual stress is undesirable yet unavoidable [63, 85]. Residual stress collapses the equilibrium configuration of the microstructure and shifts its resonant frequencies. Exploring the curvature of the deflection can uniquely determine structural residual stress [64]. Also the curvature can be used for calculating the Young's modulus of the device [65]. In this chapter, a simple phase shifting method is proposed for extracting the curvature of MEMS device formed due to existing residual stress.

The basic principle of various techniques and methods in the optical metrology, such as holographic, speckle, Michelson and Moiré interferometry is creating fringe patterns on the object. Fringe tracking, Fourier transform and phase shifting methods are three popular methods in optical characterization which were created on the fundamental of fringe pattern measurement techniques. Existence of inherent problems in the first two mentioned methods, has made researchers to consider phase shifting. Resolution and accuracy are lacking in fringe tracking method, because of the loss of directional information in the fringe formation process. In Fourier transform method, transformed intensity distribution to frequency distribution, requires individually adapted filters in the spatial domain [66].

Phase shifting interferometry is considered as a conventional method for characterization of a variety of physical parameters ranging from the surface properties to the displacement of solid objects [67]. Spatial and temporal phase shifting are two different techniques of phase shifting methods. In the first method, phase shifting is achieved by adding a substantial tilt to the wavefront but in the second method it is achievable by shifting the fringes through known phase increments such as by moving a mirror, tilting a glass plate, moving a grating or using a polarization based phase shifters [66]. Phase shifters which are located in either reference or object beam, create phase shifting between the object and reference beams. Although recent advances in computing and electronic circuit capability have made possible implementation of instant phase measurement system [68], it is difficult to obtain spatially uniform phase steps over a large aperture [69]. This is the reason that the non-linearity of phase-shifter in various

combination of electrical and mechanical loads is the subject of many research works [69, 70].

Though stroboscopic interferometry has been used for dynamic characterization of microstructures [42,71,72, 73] all the work done so far use either commercial phase shifter for temporal phase shifting method or use Fourier transform method for fringe analysis. In this work, the methodology of the new phase shifting technique is presented. This method utilizes the advantage of stroboscopic interferometry without requiring any phase-shifter.

The proposed simple technique, because of employing accurate phase-shifting methodology and avoiding non-linearity of phase-shift is expecting to provide accurate results. It does not require any additional software or equipment which makes the proposed method more practical for designers.

3.2 Stroboscopic Interferometry

Stroboscopic interferometry utilizes the advantage of principle of stroboscopy for creating frozen images from vibrating objects and analyzing the device behaviour from the acquired interferograms. In this interferometry, the object is vibrating at a particular frequency, and laser which is used for illumination of the object is pulsating at a frequency close to vibrating frequency of the device. Advanced capability of CCD cameras made them more capable for capturing images from the vibrating device in stroboscopic interferometry. Existing information on the captured interferograms are related to the frequencies of pulsating laser, driving frequencies of the device and their

frequency differences. Figure 3.1, shows the driving signal of the object and pulsating signal of the coherent laser in which there is a small difference between those two waves. It is obvious that $t_{\text{pulse}} = t_{\text{device}}$ results in frozen image.

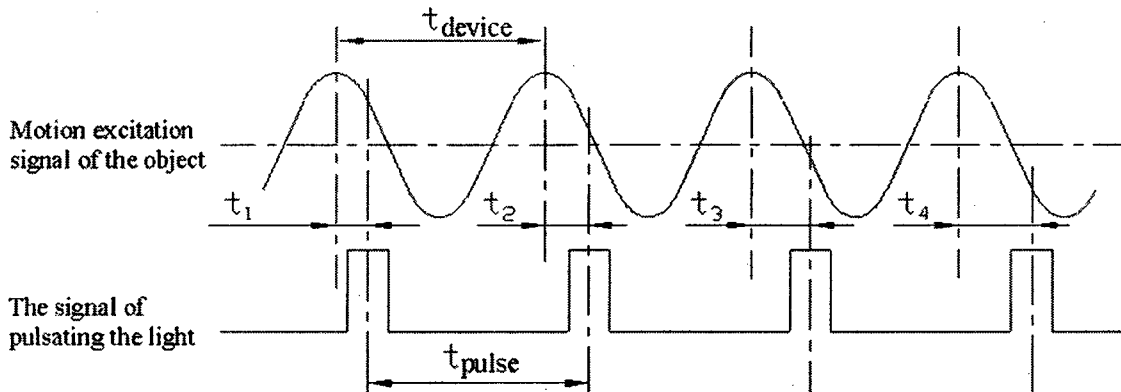


Figure 3.1 The phase motion because of existing small differences between two frequencies [14].

Stroboscopic interferometry requires a suitable instrument for pulsating the coherent laser [73]. A beam generated by a laser diode source, has a short coherence-length [74] and it is not monochromatic. Moreover it becomes unstable at higher pulsating frequencies [75]. Electronic shutters usually operate in the low frequency range [76] and can not be used in a stroboscopic interferometry that requires wide frequency range depending on the microstructures. MEMS devices usually operate at high resonance frequencies [25] and for characterization of these devices, a measurement system with higher frequency imaging system is required [26]. Acousto-optic modulator (AOM) has a variety of applications because of its capability to have a wide range of frequency. It is used in telecommunication for signal modulation and in spectroscopy for frequency control. Also

it can be used for controlling the power, frequency or spatial direction of a laser beam with an electrical drive signal.

Three main parts in an AOM are coupled to each other (see Figure 3.2). The key element is an acoustic optic transparent crystal (or piece of glass) through which the light propagates. A piezoelectric transducer attached to the crystal launches sound wave with a frequency of the order of 100 MHz through the crystal.

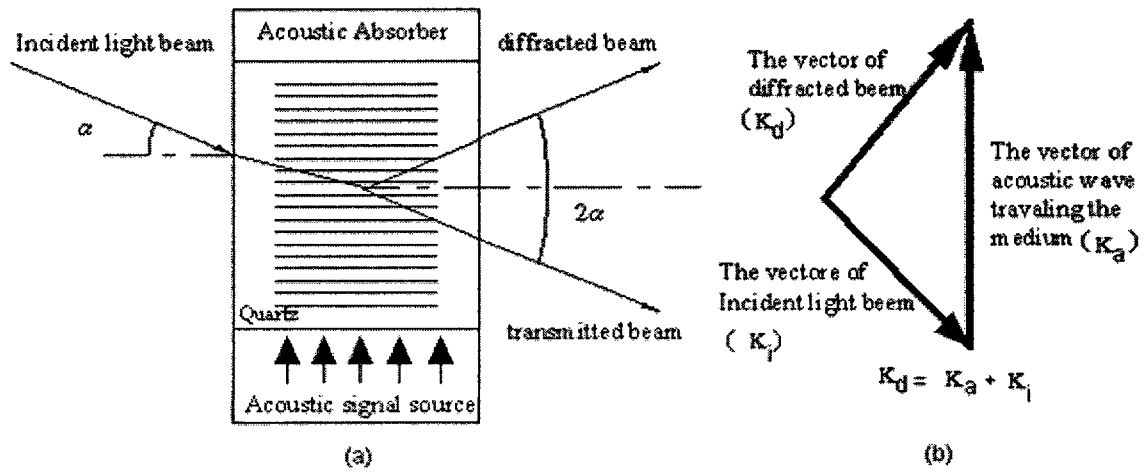


Figure 3.2 (a) Bragg angle and (b) Vector of diffracted beam in AOM.

Compressions and rarefactions of the traveling acoustic wave in AOM can be considered like spatially periodic density variations in the glass which modifies the index of refraction for propagation of the light in each point of the medium. For an acoustic wave with wave vector K_a , propagating in a material with the suitable acoustical and optical properties, the change in the index of refraction $\Delta n(r, t)$ is given by $\Delta n(r, t) \approx \Delta n$

$e^{i(k_a r - \omega_a t)}$, where $v_a = \frac{\omega_a}{k_a}$ is the speed of sound in the material (see Figure 3.2b).

The amplitude of the acoustic wave determines Δn and therefore controls the refraction of the electromagnetic radiation. A Raman-Nath parameter Q bigger than unity identifies incident of light in Bragg regime. It is defined by $Q = \frac{4\hat{w}}{\lambda_a^2} \lambda_i$, where λ_a is the wavelength of acoustic wave, \hat{w} is the width of AOM and λ_i is the wavelength of incident light [27]. Also the value of Bragg angle for an incident light can be calculated using $\sin \alpha = \hat{n} \frac{\lambda_i}{\lambda_a}$ [28] where λ_i and λ_a are the wavelengths of incident light and acoustic wave respectively, and \hat{n} is called diffraction order ($0, \pm 1, \pm 2, \dots$). In this work AOM was positioned in a calculated Bragg angle to the incident light which could transmit optimized diffraction angle with maximum intensity. Using TTL signal, the frequency of the strobing beam was controlled.

3.3 Experimental Methodology

The consequence of applying sinusoidal voltage on a piezoelectric (PZT) material would be compression and rarefaction of PZT because of rapidly changing polarity. This behavior of PZT makes it possible to vibrate the device mounted. The connection between applied sinusoidal voltage to a PZT and the location and stroke of the mounted device are shown in Figure 3.3 . Each point of sinusoidal applied voltage corresponds to particular location of the device along its stroke. In case of ignoring the backlash of PZT, points 'a' and 'f' in the sinusoidal wave represent the lowest (point 1) and highest (point 6) positions of the device respectively. Equal displacement of device on PZT would happen if the selected points on the sine wave have equal projected distances on vertical axis (see Figure 3.3).

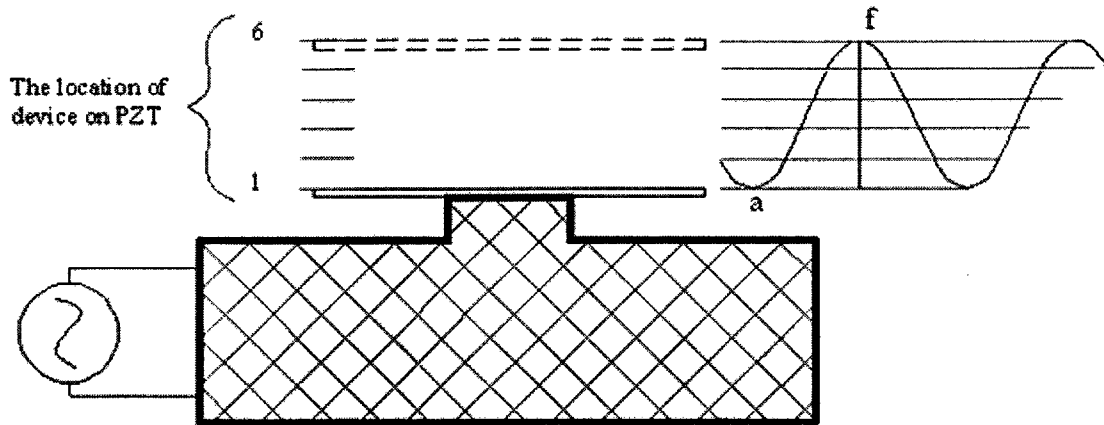


Figure 3.3 The vibration of mounted cantilever on PZT.

Acquiring phase-shifted images from this device is the objective in temporal phase-shifting. This would help creating phase differences between the laser beams reflected from the reference mirror and the object. Presented method takes advantage of stroboscopy and does not require any phase-shifter. It considers a small difference between the frequencies of pulsating light and vibrating object. This functions like the common way of creating phase differences using commercial phase shifter. The advantage of this method is that that the frequency can be adjusted to any small difference enabling phase shifted images within the linear phase of the PZT.

The device was vibrated in sinusoidal function using PZT at the natural frequency of the whole chip which was 2KHz. Strobe light was created using square function in AOM at the same frequency of vibration of device. A small difference, 0.01 Hz, in frequency of strobing could be applied. This would result in 100 seconds to pass one complete cycle of phase differences between them.

As shown in Figure 3.4, points 2, 3, 4, and 5 on the sinusoidal wave of vibrating object, present the time at which the images were captured. These points are the projection of points 2', 3', 4' and 5' on the vertical motion. As the distances between these four points are the same, those points present equal phase differences. Since nonlinearity and backlash of the piezostack between points 1 to 2 and 5 to 6 were affecting the value of phase differences between two waves, points 1 and 6 were not used for capturing images and just points 2,3,4 and 5 were used. This results in four unknown but equally phase shifted images.

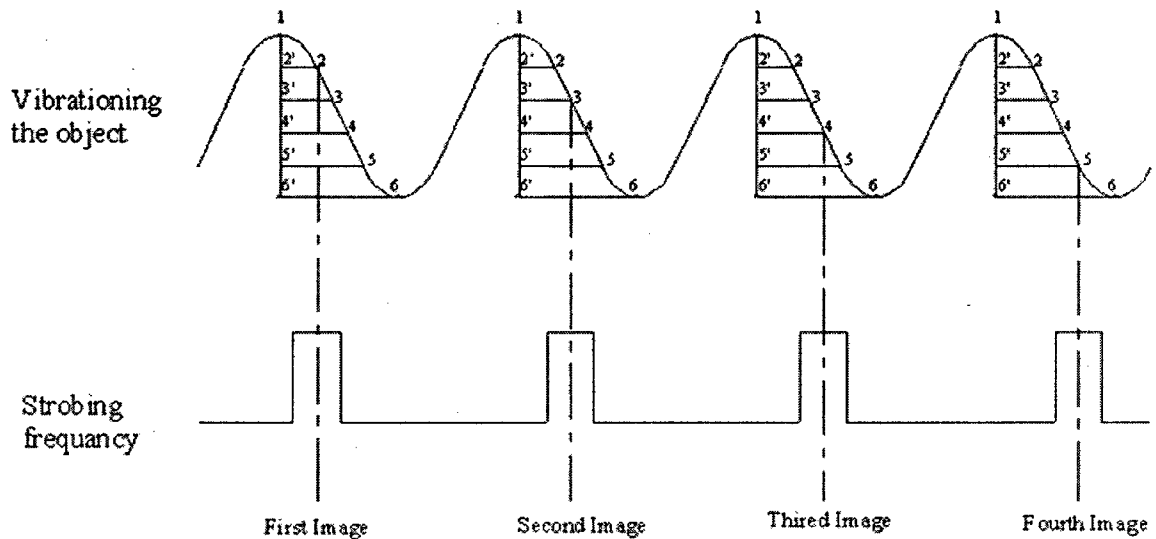


Figure 3.4 Capturing situations of four equal phase-shifted images.

3.4 Experimental setup

The same AOMSI Acoustic-Optic Modulated Stroboscopic Interferometer which was described earlier [84] is used in this experiment (see Figure 3.5). This setup was made on Twyman-Green interferometry. A real-time vision system was used by employing a CCD camera with 648 x 492 pixels which captured 30 images per second and transferred the data to a computer. In this experiment, a HeNe laser with 632.8 nm wavelength and 5 milliwatt power was used for illumination of the device. Also an acoustic-optic modulator (AOM-80) was used for laser pulsing. Bragg angle was calculated for used laser and AOM, and it was 0.7 mrad for the first order. The laser was adjusted to incident the AOM in Bragg angle to have maximum intensity. Two $\lambda/10$ mirrors were used to reflect zero and first order beams. The first order was used for the illumination of the device and the zeroth order was blocked (see Figure3.5).

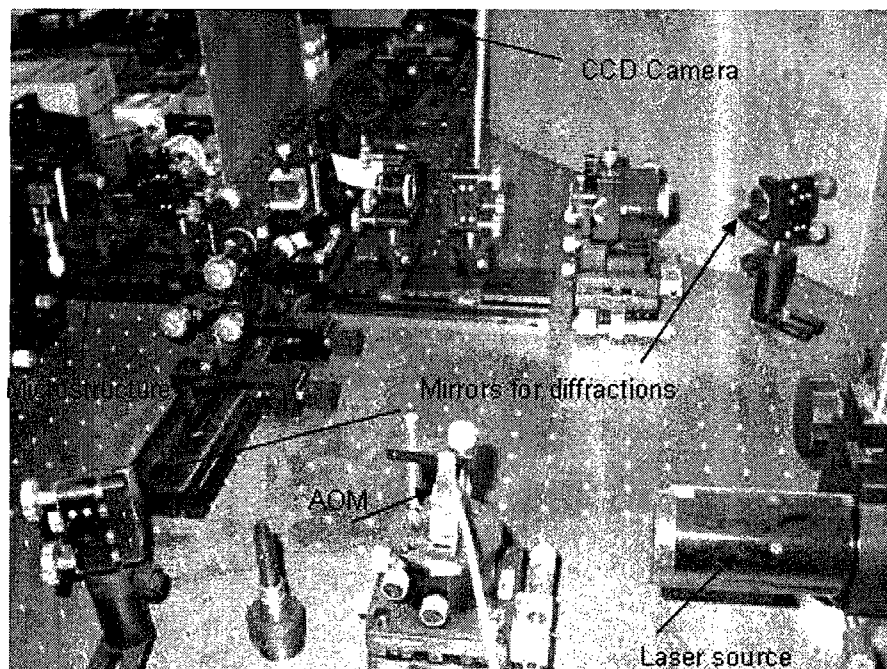


Figure 3.5 A digital image of used stroboscopic interferometer set up.

Using a function generator FG1, the micromirror mounted on the piezostack was excited by applying 10 volts at the frequency of 2 kHz and created phase shifting due to changing the path length of laser beam reflecting from the microstructure. Using another function generator, FG2 and using TTL signal and AOM, the first-order beam was strobed with the same frequency as that of excitation (see Figure 3.6). For strobing the laser, step function was used which could be adjusted for having suitable intensity on the images. For monitoring the motion of micro structure and frequency of strobing, both function generators were connected to an oscilloscope (see Figure 3.6).

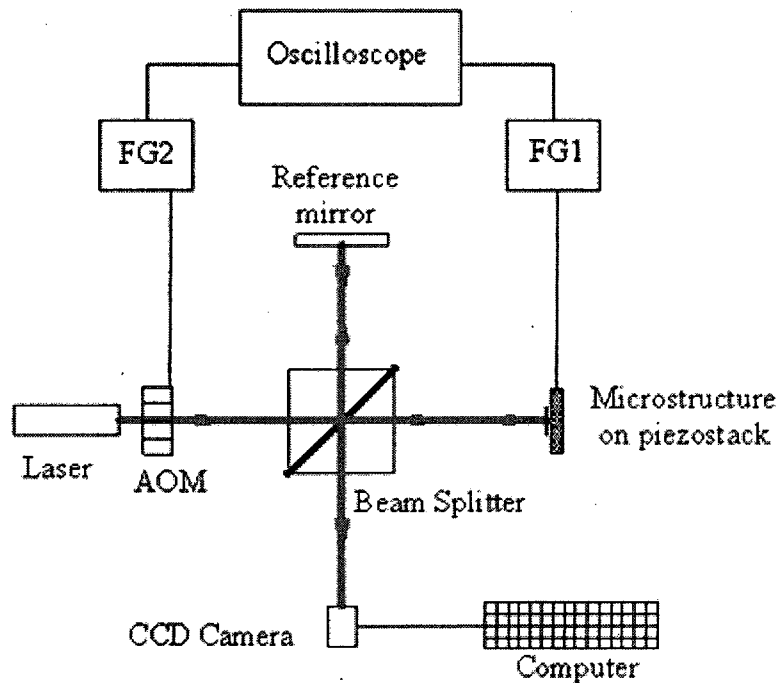


Figure 3.6 Schematic arrangement for the Acoustic-Optic Modulated Stroboscopic Interferometer for performing temporal phase shifting (AOM: Acoustic-Optic Modulator; FG: function generator).

3.5 Design of Microstructures

For testing the applicability of presented temporal phase-shifting stroboscopic interferometry method, two microstructures were designed. Both one dimensional and two dimensional structures were fabricated. The dimensions of the structures are given in Table 3.1, while Figure 3.7 and 3.8 show the SEM images of the structures. Micromirror is square shaped and torsionally hinged at both ends. The one dimensional structure is a cantilever as shown in Figure 3.8.

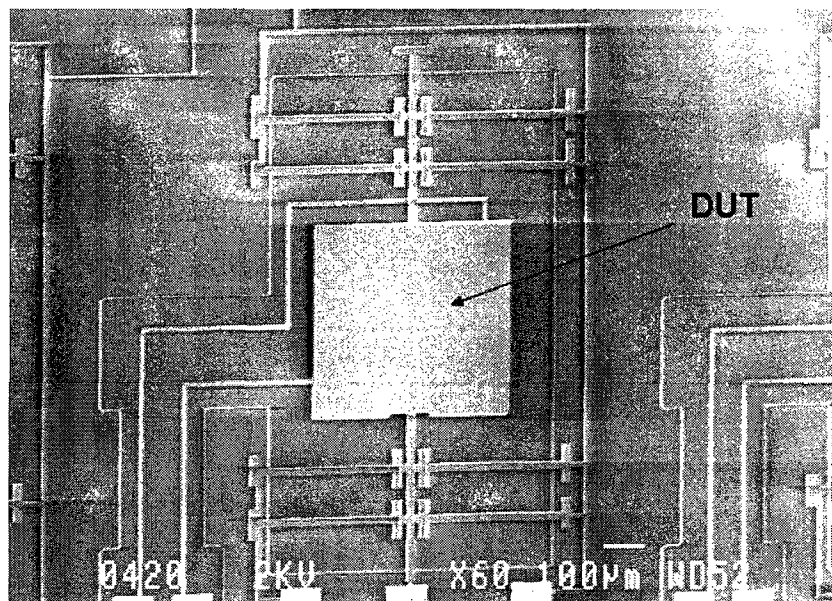


Figure 3.7 SEM image of designed micromirror for the test.

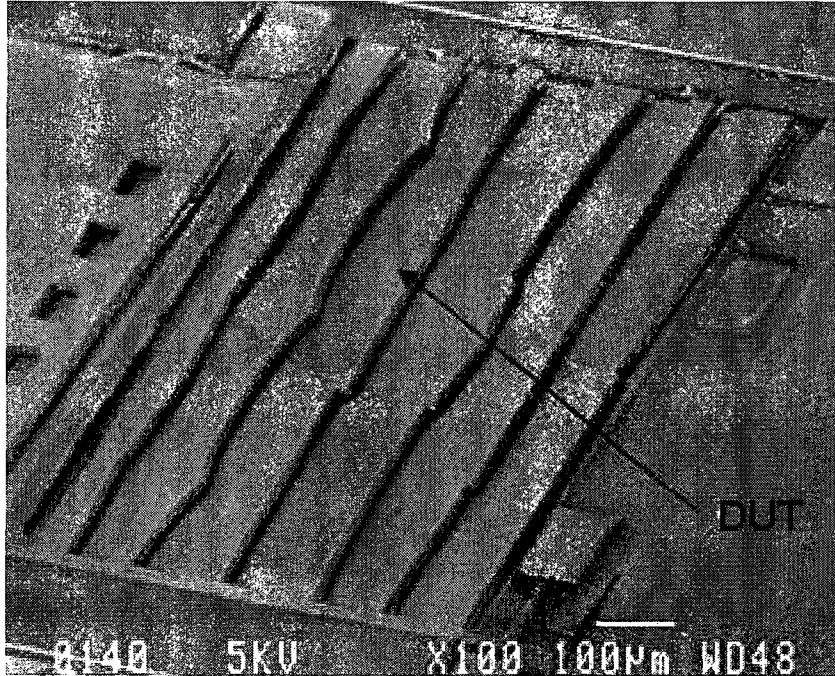


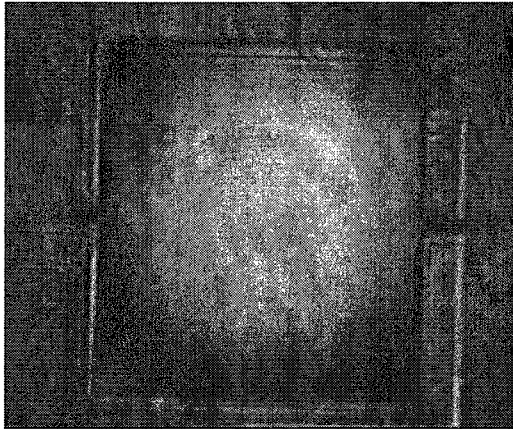
Figure 3.8 SEM image of an SOI MicraGem technology cantilever array (DUT shows the selected cantilever under test).

3.6 Results and Discussion

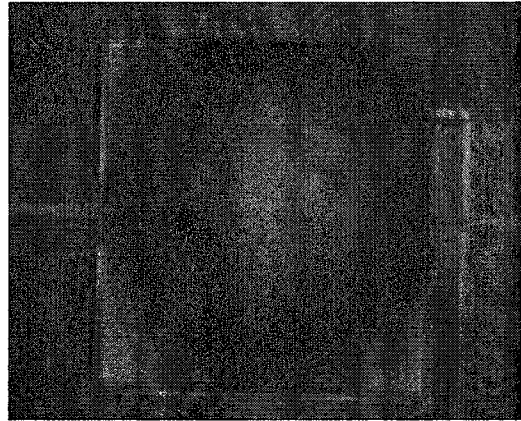
As discussed earlier, four unknown but equal phase shifted images were captured from a micromirror as shown in Figure 3.9. For this purpose, the device was placed in the test arm of the interferometry and aligned using a two-axis tilt stage to have the same axis for the reflected beam from object and reference beam, and it was focused to bring clear image of micromirror to the CCD camera. Since four unknown but equally phase shifted images were acquired, Carré algorithm was used for fringe processing. In Carré method a general expression for the recorded intensity in an interferogram is given by

$$I_n(x, y) = a + b \cos[\varphi(x, y) + n\alpha] \quad (3.1)$$

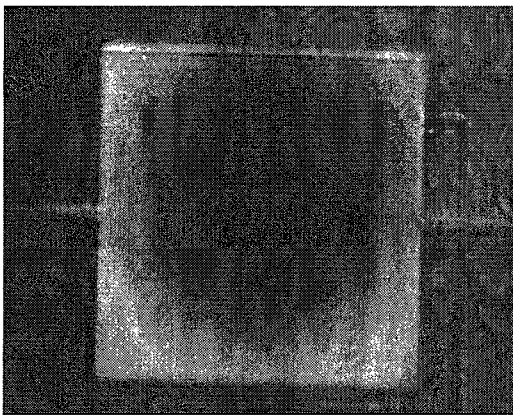
where n is a number showing the sequence of the images varying from 0 to 3, a and b are related to spatial variation in amplitude of the beams returned from the two interferometry arms, and $\varphi(x, y)$ is the phase distribution that encodes the surface-height variations over the object, which needs to be calculated [42].



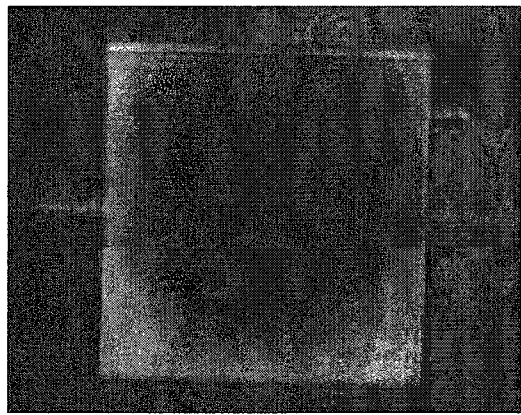
a) The first taken image from Micro mirror.



b) The second image after applying phase shift of φ .



c) The third image after applying phase shift of 2φ .



d) The fourth image after applying phase shift of 3φ .

Figure 3.9 Four interferograms which are taken in stroboscopic interferometry from micromirror, a is the first, b, c and d are the second, third, and fourth taken image respectively

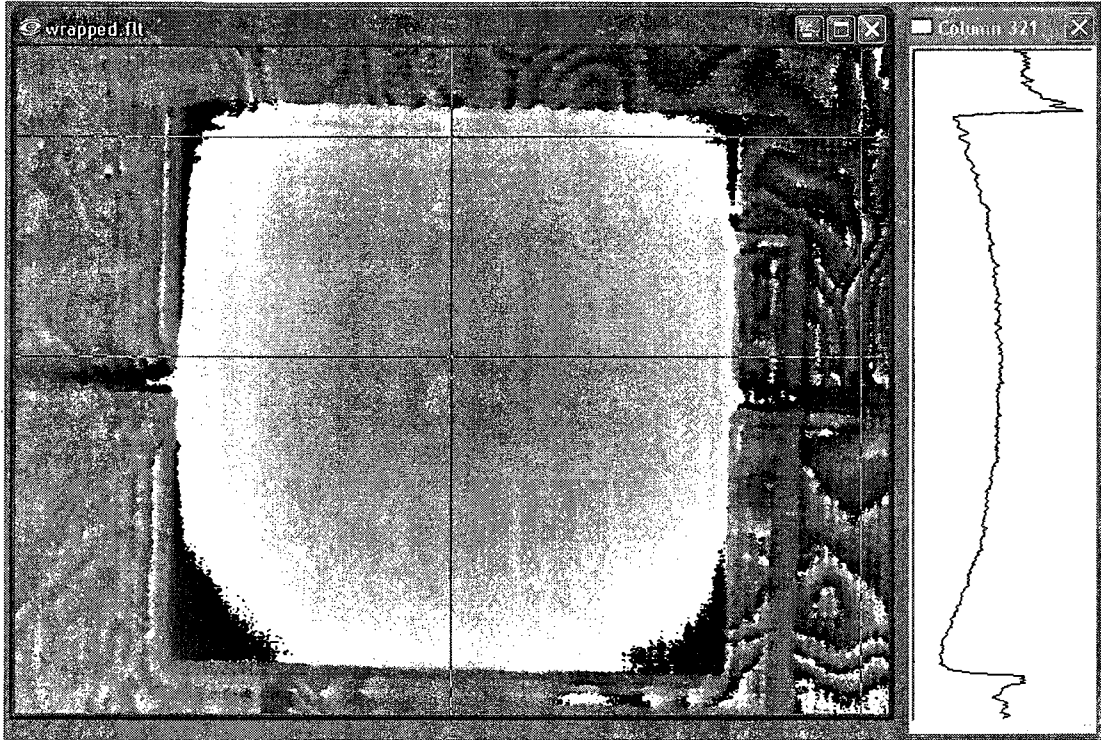


Figure 3.10 Wrapped image obtained from Micromirror.

This equation has four unknown parameters requiring four intensity measurements. Having a sequence of measurements of I for four captured images in each pixel, using Fringe Processor TM, The Wrapped image from the DUT were extracted as is shown in Figure3.10.

The values of the phase also can be calculated using following equation.

$$\varphi(x, y) = \tan^{-1} \sqrt{\frac{(3I_2 - 3I_3 - I_1 + I_4)(I_1 + I_2 - I_3 - I_4)}{(I_1 - I_2 - I_3 + I_4)^2}} \quad (3.2)$$

This value represents wrapped phase value of the image, but it is a multivalued arctan function and the solution for φ will be a sawtooth function. It will have discontinuities every time φ is changing by 2π [32]. Hence ‘phase unwrapping’ is required to unwrap or

integrate the phase along a line (or path) counting the 2π discontinuities. It is needed to add 2π each time the phase angle jumps from 2π to zero and to subtract 2π if the change is from zero to 2π [32].

The absolute value of phase in each pixel after the unwrapping process was converted to the surface-height information of the microstructure using

$$h(x, y) = \varphi(x, y) * \frac{\lambda}{4\pi} \quad (3.3)$$

where $\varphi(x,y)$ and λ are the values of phase in each pixels and the wavelength of used laser, respectively. Also the pixel number was converted to the length of the micromirrors considering the magnification factor of the setup. Figure 3.11 shows the results of this conversion and the shape of microstructure because of its residual stress.

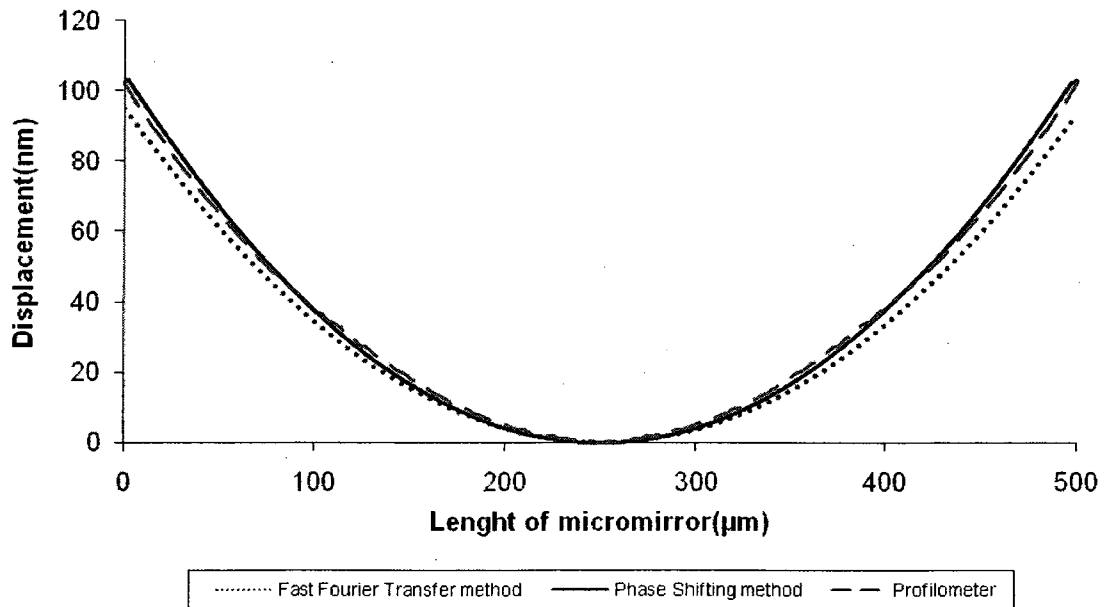


Figure 3.11 Extracted out of plane variation of micromirrors using new method of temporal phase shifting method

For verifying the result achieved using the presented method of temporal phase shifting, the device was tested in a commercial optical profiler (Wyko NT1100). Optical profiler employs coherence scanning interferometry (or white-light interferometry) and uses vertical scanning interferometry to produce high quality two and three-dimensional surface maps of the object under test. This system delivers rapid and non-contact measurements from a few nanometers up to a few millimeters of the object, with sub-nanometer resolution. The outcome results for the shape of micromirrors using profiler was in good agreement with the result using present method (maximum variation was about %1). Also the results were compared with the published [84] result of same device using Fast Fourier Transform FFT method. The Fourier Transform is a mathematical procedure that transfers a function from time domain to the frequency domain. FFT is an efficient algorithm, to compute the discrete Fourier transform (DFT) and frequently used in optical field. Intensity distribution and its evaluation by Hamming window, creating the modulus of its Fourier transform, wrapping the phase function and reconstructing phase function after the unwrapping procedure are the sequence of stages in FFT method. Figure 3.11, shows the results from the developed method having reasonable agreement with the results from commercial profiler.

Further work was done on a cantilever and the same method was used to acquire four phase-shifted images from a MicraGeM technology cantilever array. Figure 3.8 shows SEM images of this MicraGeM cantilever array and the selected cantilever for the analysis.

To identify the curvature of the cantilever, the cantilever was adjusted to have no fringes on the base (see Figure 3.12a) making the base of microstructure as the reference of the measurement. Figure 3.12 shows four unknown but equal phase shifted taken images from the cantilever. Because the field of view of AOMSI employed in this work was limited to around 510 μm , it would not cover all the length of cantilever which is 810 μm in length.

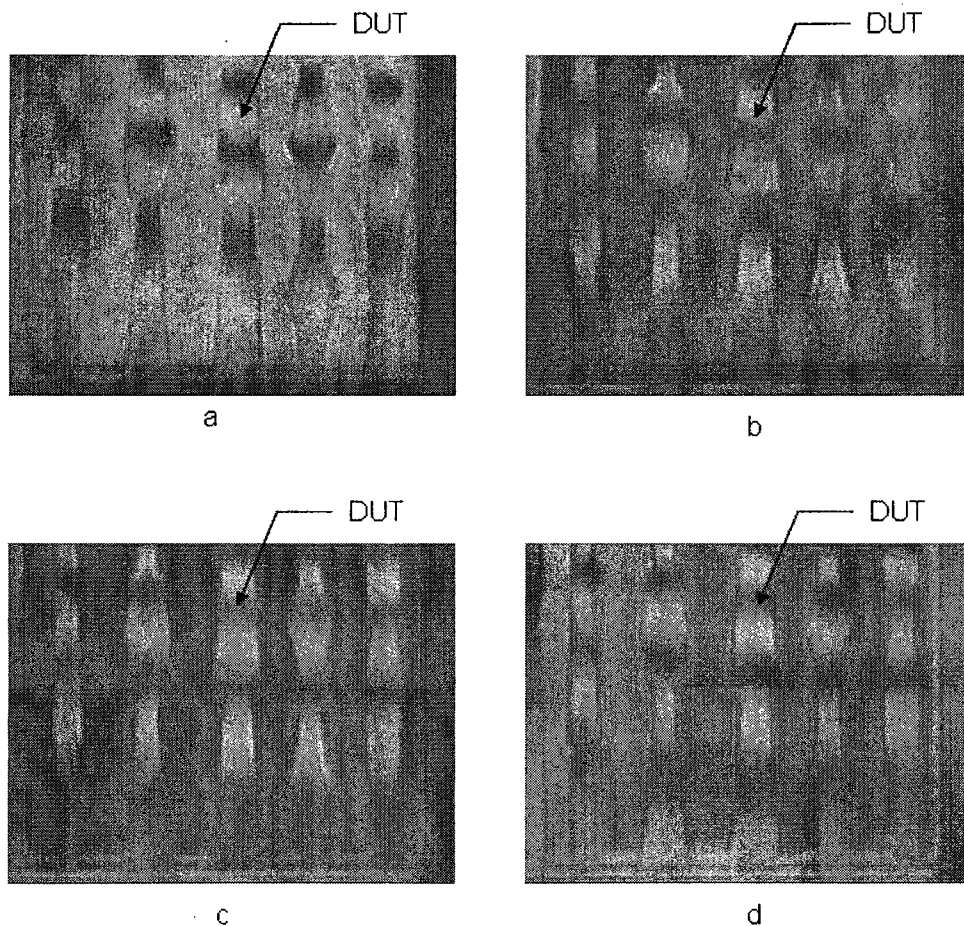


Figure 3.12 Captured interferograms from MicraGem technology cantilever array(a is the first, b, c and d are the second, third and fourth respectively taken image.

Obtained fringe pattern for the cantilever, shown in Figure 3.12, was analyzed and the phase value of each pixel was extracted. Figure 3.13 shows the wrapped phase value of pixels along the cantilever. The absolute value of phase for each pixel in unwrapping process was calculated and it was converted to surface-height information of cantilever. Figure 3.14 shows the shape of microstructure due to its residual stress after subsequent low pass filter on the unwrapped image.

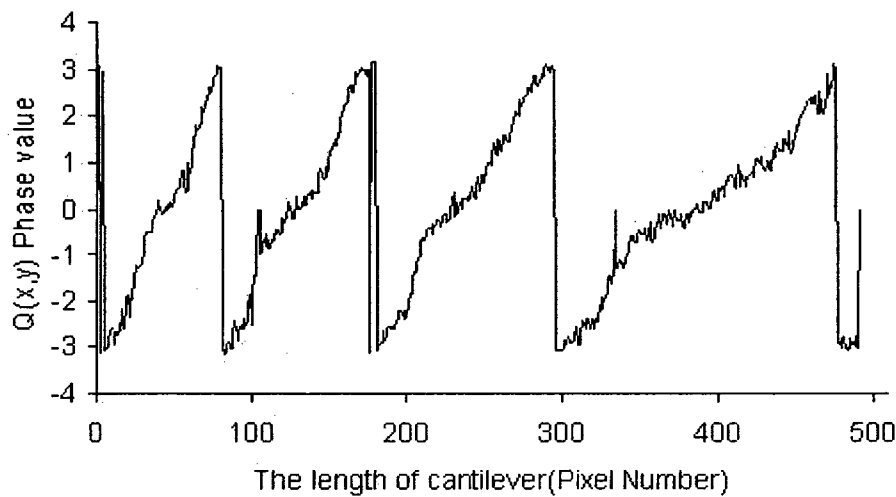


Figure 3.13 The wrapped phase value of pixels along of selected cantilever.

One of the most advantages of using this method of phase shifting is that the number of fringes is not restricted, in analysis of the fringes, unlike Fourier Transform Method. This graph shows the value of surface-height information of the cantilever due to residual stress where x-axis gives is along the length of cantilever which is 539 μm and y-axis shows the out of plane distribution which is 112 nm on the tip.

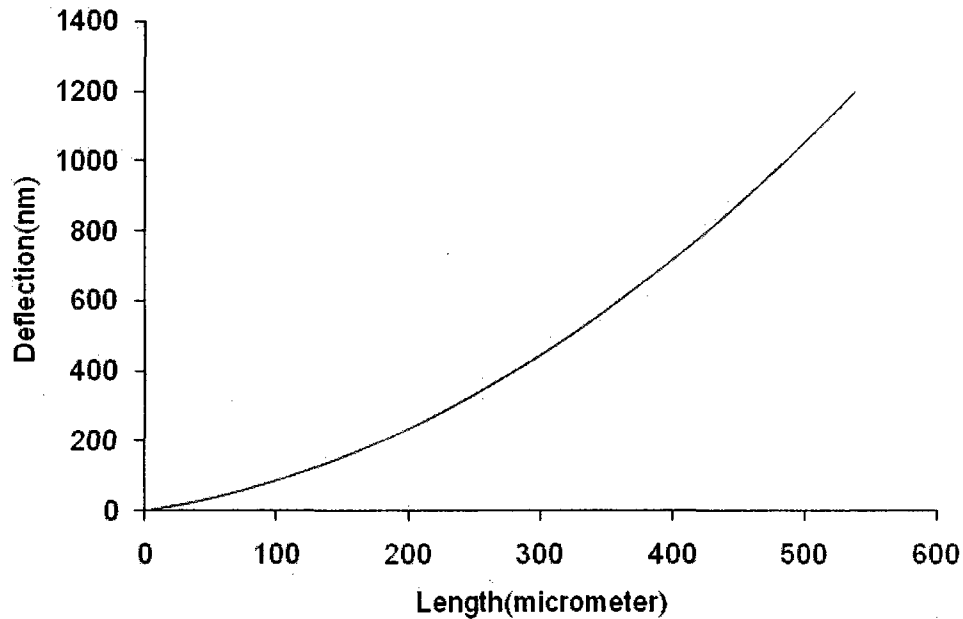


Figure 3.14 Surface-height information of the selected cantilever.

Name of designed microstructure	The method of manufacturing	Dimensions(μm)		
		Length	Wide	Thickness
Micromirrors	MicraGem	500	500	10.5
Microcantilever	MicraGem	810	~ 30	10.5

Table 3.1 Designed microstructures for the test.

3.7 Conclusion

A new method of temporal phase shifting using Acoustic-Optic Modulated Stroboscopic Interferometry was presented. This method, unlike common temporal phase shifting methods does not require any phase-shifter which has the error of phase-shifter nonlinearity. As an illustration of accuracy of the presented method, the experiments were done on a MicraGem technology torsional micromirror and the results were in

excellent agreement with the result of the same device under a commercial white light profiler (Wyko NT1100). Also the obtained results were in good agreement with the previous published results on the same micro device using Fourier Transform method.

Further work was done on a MicraGem cantilever to explore the curvature of the cantilever because of residual stress.

Chapter 4

Static Characterization of Microstructures Using Developed AOMSI and Temporal Phase-Shifting

4.1 Introduction

Electrostatic MEMS is a rapidly maturing field that has found verity of applications in automotive and industrial sectors. It includes switches, micro-mirrors, micro resonators and sensors [76-77]. All of them employ a diaphragm or cantilevered structure as part of a variable capacitance sensor geometry. As an example, Figure 5.1 shows an array of three MEMS RF switches.

Electro static actuators are used in harsh environment and their behavior under different mechanical loads is the subject of many research works [77-78]. A Failure in MEMS device may happen due to high stresses, striction and electric short circuits. Further more, these devices may face shock loads and unexpected electrostatic force [79]. Hence characterization of these devices is highly required for optimizing their design and its commercialization. Characterization will help to identify the region of stable operation and the situation of instabilities. Figure 5.2 shows the schematic of a capacitor-type Fixed-Free cantilever beam and its deflection after applying electrostatic load.

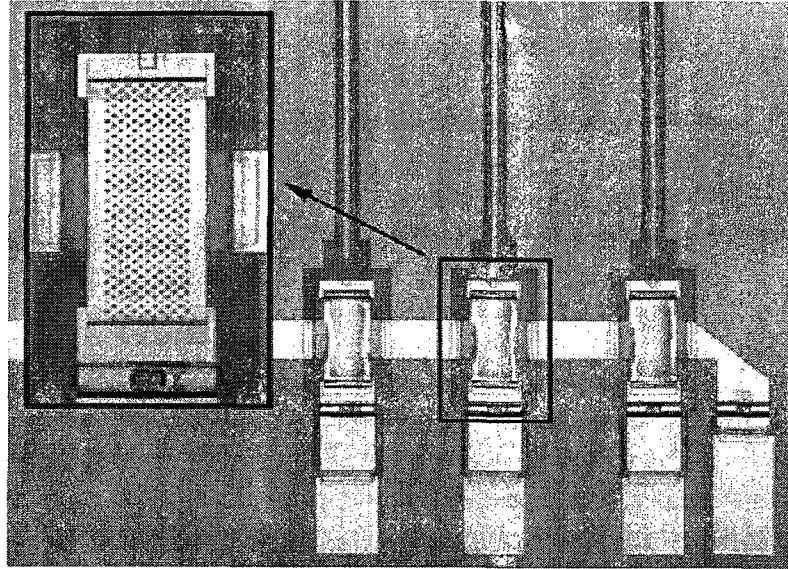


Figure 4.1 An array of three MEMS RF switches [3].

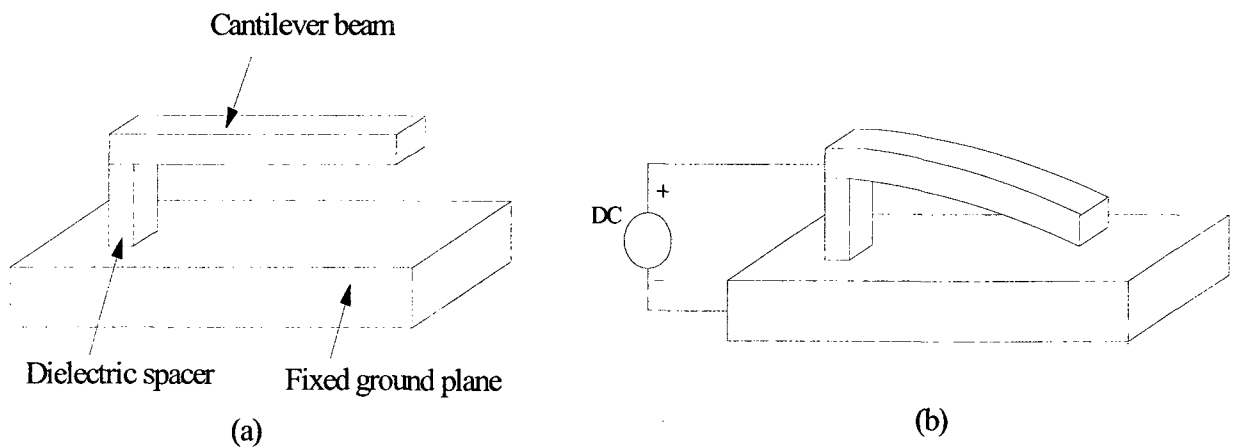


Figure 4.2 (a) A capacitor-based fixed-free cantilever beam, (b) Deformed beam under electrostatic force.

Well-known phenomenon of ‘pull-in’ voltage is considered the most important issue for characterization of capacitive-type sensors and actuators [80-81]. These sensing

structures operate in the constant voltage drive mode and collapses on the backplane if the bias voltage exceeds certain limit. In other word, collapse happens when electro static pressure in the device exceed the elastic restoring pressure. Identifying this limit is critical for capacitive-type sensors and actuators; hence theoretical model of these devices is necessary before performing any tests on these devices.

4.2 Theoretical analysis

In this section, the fixed-free capacitor based cantilever shown in Figure 4.3 is analyzed with the help of a developed theoretical [19]. Initially the formulation of developed theoretical model will be studied briefly and later the response of device under various applied electro static load will be discussed. Figure 4.3 shows the schematic of the selected device for theoretical modeling of the DUT.

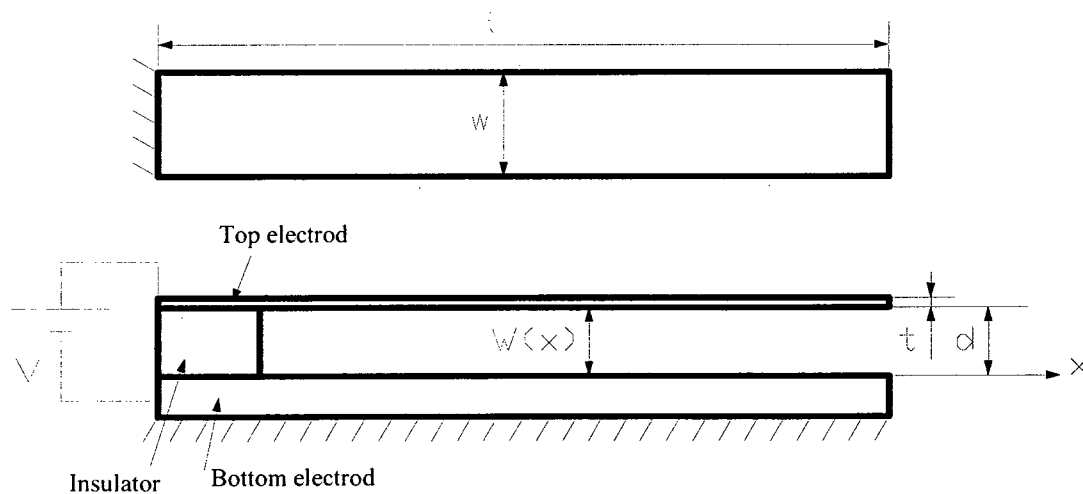


Figure 4.3 Schematic of assumed capacitor-base cantilever for the experiment.

Using energy approach, the transverse deflection of a beam is approximated as

$$W(x) = \sum_{n=1}^N c_n \phi_n(x) \quad (4.1)$$

where c_n are the deflection coefficients of the cantilever and ϕ_n are the orthogonal polynomials. Using energy method for solving the Equation (4.2), requires the strain energy and the electrostatic potential energy. The equations for these energies can be written as in Equations (4.2) & (4.3).

$$U_b = \frac{Et^3w}{24L^3} \int_0^1 (W''(x))^2 dx \quad \text{strain energy} \quad (4.2)$$

$$U_p = \frac{\epsilon_0 \epsilon_r LV^2w}{2d} \int_0^1 \left[1 + \frac{W(x)}{d} + \frac{W(x)^2}{d^2} \right] dx \quad \text{electrostatic potential energy} \quad (4.3)$$

where E is the young modulus, t is the thickness, w is the width, L is the length, ϵ_0 is the permittivity of the free space, ϵ_r is the relative permittivity of the dielectric medium, d is the gap between cantilever and base, and V is the applied voltage.

Using energy method after minimizing potential energy, the elastic shape of the cantilever can be obtained using Equation (4.5)

$$\frac{\partial}{\partial c_j} [U_b + U_p] = 0 \quad (4.4)$$

For $j = 1, \dots, N$

$$\sum_{j=1}^N [E_{ij}^{22} - S_1 E_{ij}^{00}] c_j = S_2 \int_0^1 g(x) \phi_i(x) dx \quad (4.5)$$

For $i = 1, \dots, N$

in which

$$E_{ij}^{22} = \int_0^1 \phi_i'(x) \phi_j'(x) dx \quad (4.6)$$

$$E_{ij}^{00} = \int_0^1 \phi_i(x) \phi_j(x) dx \quad (4.7)$$

And the constant value of S_1 and S_2 can be calculated using Equation in (5.7)

$$S_1 = \frac{12\varepsilon_0\varepsilon_r L^4 V^2}{Et^3 d^3}, S_2 = \frac{6\varepsilon_0\varepsilon_r L^4 V^2}{Et^3 d^2} \quad (4.8)$$

Using this model, the deflection of the cantilever beam under electrostatic load was extracted. Table 4.1 shows the parameters considered for the calculation and Figure 4.4 illustrates the cantilever response for 10V, 20V, 30V, and 40V of applied electrostatic loads.

Parameters	Value
Length (L)	1200(μm)
Thickness (t)	10.5(μm)
Gap (d)	11(μm)
Widths (w)	63(μm)
Young's Module (E)	129(GPa)
Density(ρ)	2320($[\text{kgm}]^{-3}$)
Considered shape	Rectangle

Table 4.1 Used parameters for the calculation.

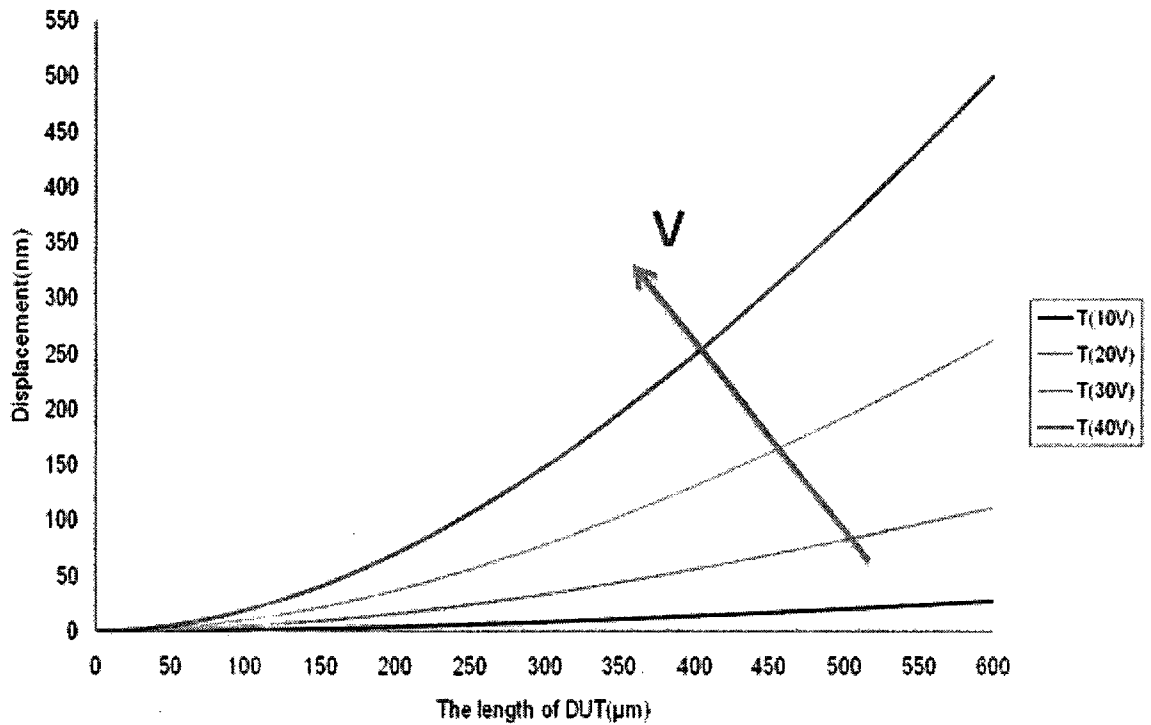


Figure 4.4 Predicted displacement of the cantilever under different applied voltages.

As it is shown in Figure 5.4, the deflection of the cantilever is increased with raising the applied electro static loads. The increasing deflection is non linear due to reducing the gap 'd' with increasing the applied voltage.

4.3 Experimental Methodology

A capacitor-base MicraGem[19] cantilever with properties shown in Table 5.1 was considered for the experiment. Developed AOMSI explained in chapter 4.2 was used for the experiment. the DUT chip was mounted in the test arm of the AOMSI (explained in 3.2) and it was adjusted to obtain clear images from the cantilever. As the FOV of the system was limited to ~610 μm, the root portion of the device was focused in the setup.

One of the requirements of the developed new method is to vibrate the DUT at the natural frequency of the structure. A vibration frequency of 2354 Hz was obtained as the natural frequency of vibrating cantilever by sweeping the input excitation frequency of sinusoidal voltage applied on PZT. The natural frequency can be tracked with a big movement of fringes in the image. Then the laser in AOMSI is strobed at this frequency to obtain frozen images of the fringes on the cantilever. A D.C power supply system for applying electrostatic load and an A.C power supply for exciting piezoelectric actuator were used in the experiment as shown in Figure 4.5.

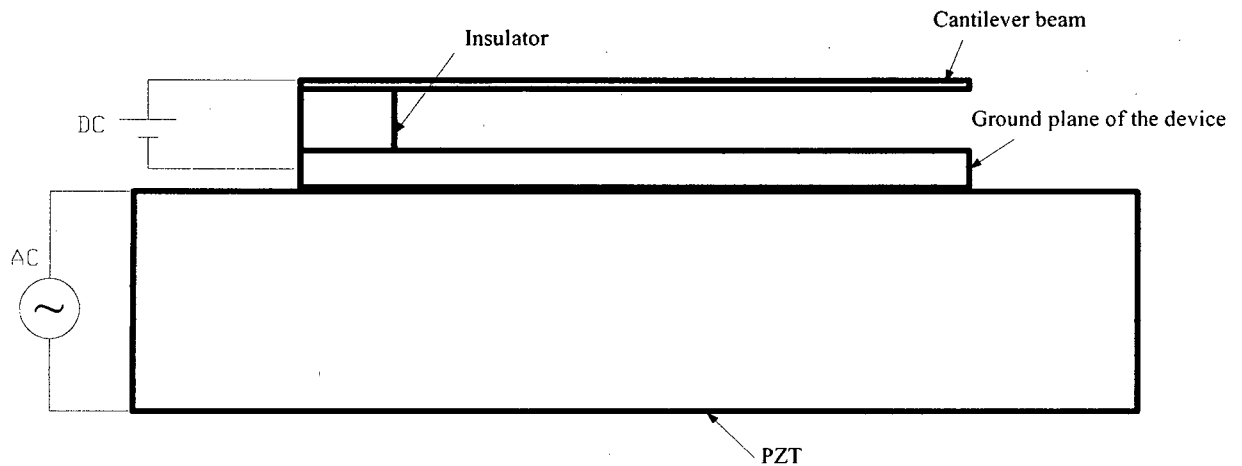


Figure 4.5 Electrostatic excitation of microcantilever.

In order to identify the range of applied loads for static characterization of the device, the behavior of the DUT was studied using theoretical model. The tip deflection of DUT was extracted by applying wide range of voltages between 5V&85V with an interval of 5V. Figure 5.6 illustrates the result of tip deflection for applied electro static loads. As it shown in this figure, the expected pull in voltage for the DUT is around 85 Volts.

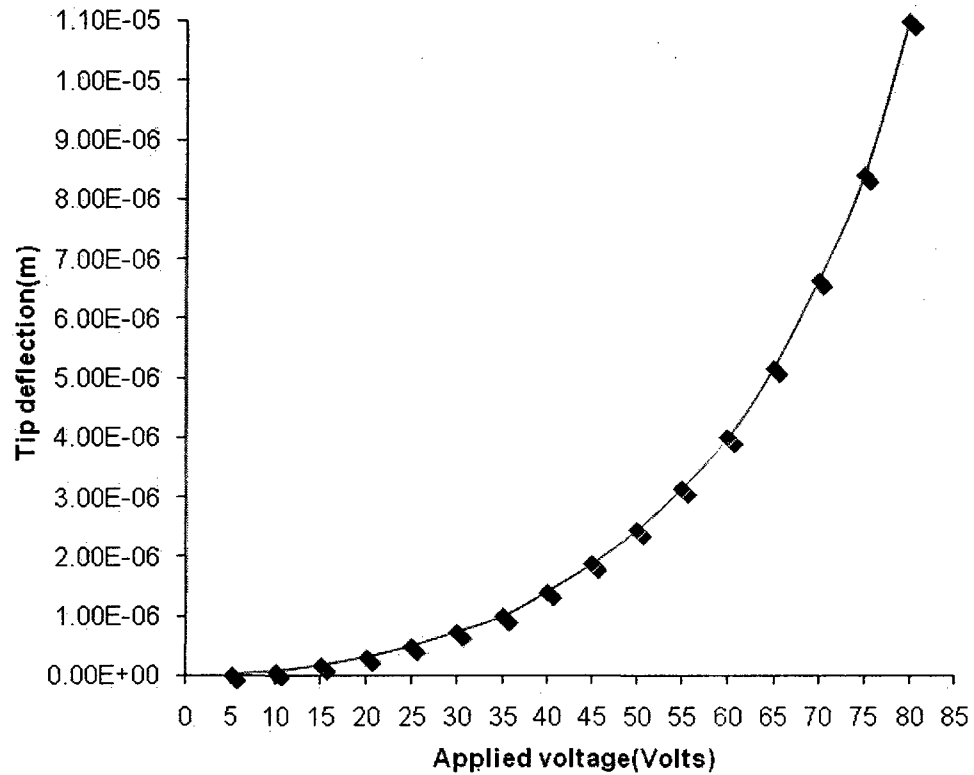


Figure 4.6 Tip deflection of the beam because of the electrostatic loads.

Hence the voltage range has to be carefully chosen, so that the cantilevers will not pull in during experiment. Also in the developed method of TPS, the object is vibrated externally using a PZT actuator to achieve phase shift. Considering these the maximum voltage for performing static characterization using AOMSI was kept at 40V.

4.4 Results and discussion

Using the developed TPS method, four unknown but equally phase shifted images of the DUT were acquired as shown in Figure 5.7.

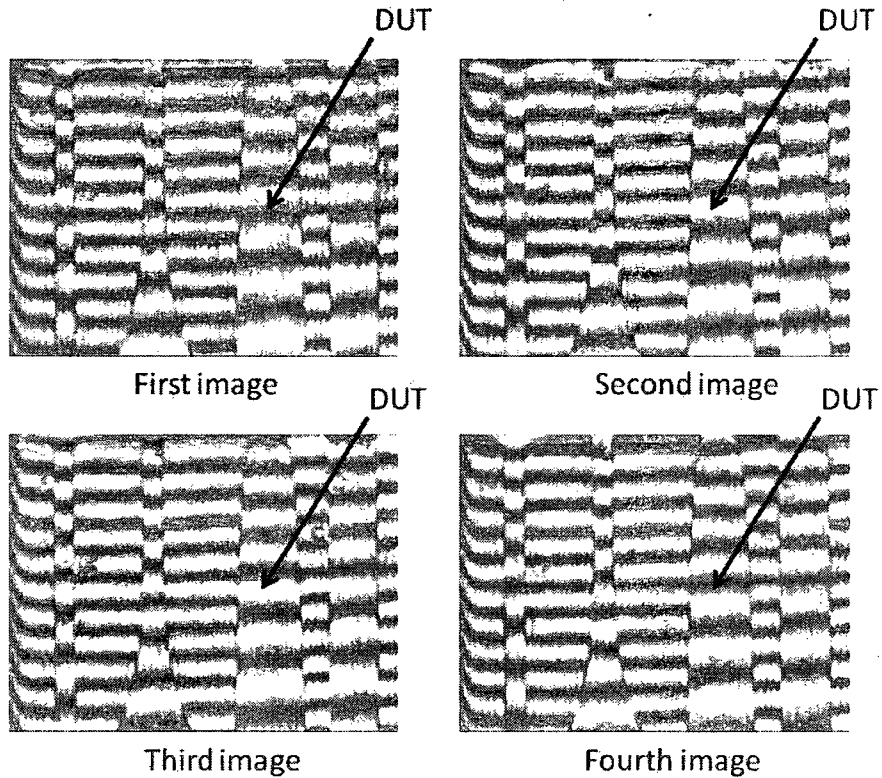


Figure 4.7 Four equally phase-shifted images from DUT when no voltage was applied.

In the first step, there was not any voltage applied to the cantilever. The purpose was acquiring initially shape of the cantilever. Hence, after acquiring four phase-shifted images the value of phase for each pixel on the cantilever was calculated and it was converted to the surface-height information of the cantilever as explained in section 3.3.

In the next step, electrostatic load was applied on the cantilever by applying 10V on the cantilever. This would make the free beam to bend towards the fixed ground plane. The technique used in the first step was repeated in order to explore the shape of the structure under a electrostatic load. For obtaining the deflection of the structure under particular electrostatic load, the original shape of the cantilever at '0V' was subtracted. The same

process was performed with applying 20V, 30V, and 40V to the structure. Figure 4.8 illustrates the deflection of the cantilever as a result of electrostatic load on the cantilever.

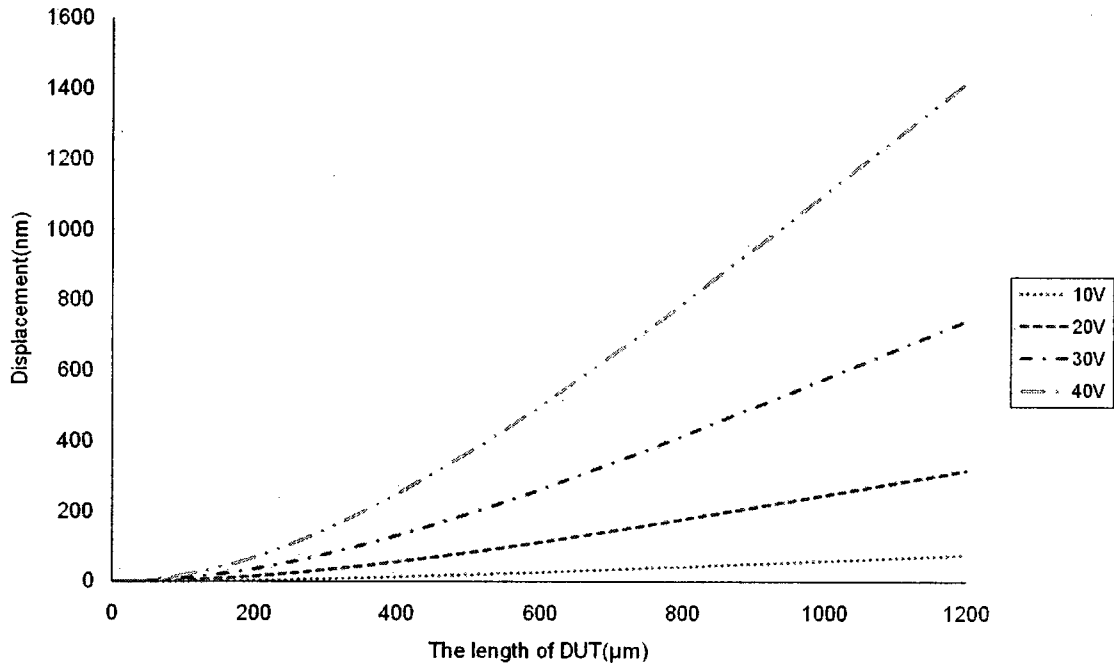


Figure 4.8 Displacement of the cantilever because of applied voltage in AOMSI.

In order to compare the results between theoretical model and the results from AOMSI, deflections of DUT was predicted at bias voltage of 10V, 20V, 30V, and 40V. Figure 5.9 illustrates the comparison of the results between the experimental and theoretical results.

As shown in Figure 5.9 there are two distinct variations. One in the magnitude of the deflection and the other is the overall shape of deflection. The magnitude of the tip deflection measured experimentally in about 7 to 8% lower than the theoretical prediction. The reason for this is due to the residual stress. The cantilever has an upward bend even without applying any electrostatic loads (Figure 3.14 for one designed MicroGem cantilever). This residual stress have not considered for the theoretical modeling, where the gap between the cantilever and the base is considered as 11μm. In

reality since the cantilevers bend upwards due the gap increases thereby reducing the electrostatic forces. This reduces the amount of deflection measured.

Since the gap increases non-linearly along the length of the cantilever, this also affects the profile of the cantilever. Moreover the variations in the profile are attributed in part to spherical aberration in the setup also.

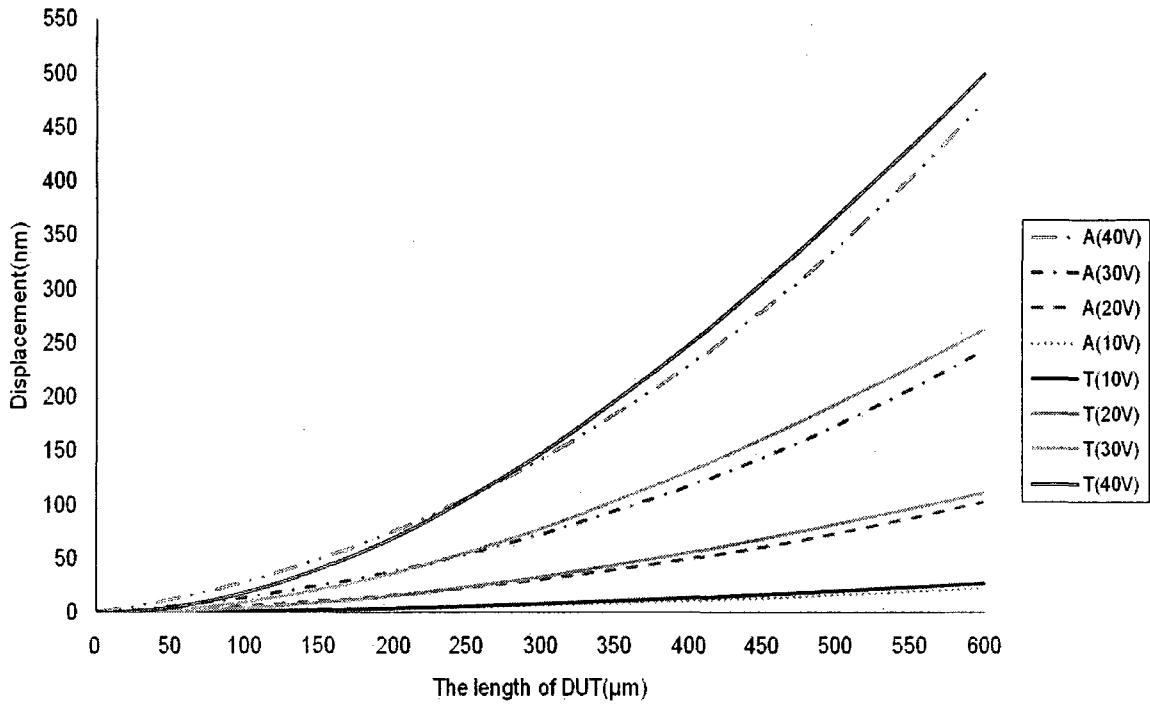


Figure 4.9 Comparison of the results in developed AOMSI and theoretical model.

As it shown in Figure 5.8 there is a good agreement between the results and variation of less than 8% was acquired. Two reasons are primary for the variations. Firstly the initial existing tilt on the cantilever due to residual stress was not considered in the theoretical modeling of the cantilever. And it was considered to be flat. Secondly existing of the abbreviation error in the set up makes the result of experiment in AOMSI to be varied form the theoretical model.

4.5 Conclusion

A brief explanation about the importance of static characterization for micro structures was explained. A brief theoretical model for a fixed-free capacitor-base cantilever was also presented. Using the developed method of temporal phase shifting the shape of the cantilever under electrostatic load was extracted. There was a good agreement between the results of AOMSI and theoretical model.

Chapter 5

Stitched Acousto-Optic Modulator Stroboscopic

Interferometry for Characterizing Large Structures

5.1 Introduction

Acquiring a large field of view (FOV) along with high resolution is one of the main requirements of present imaging interferometric technologies. As an example, large field of view is essential in order to study the anatomy of the organism with 3D high-resolution image [87]. The most advanced technology which is used for imaging with high spatial resolution is suffering from the limitation of FOV, while those imaging system with large FOV has the problem of spatial resolution. Hence, a system that can provide images with high resolution with large field of view would be useful. Sub-aperture stitching method is considered as a practical method which can overcome both FOV and resolution limitation [87].

The sub-aperture stitching method involves obtaining a series of sub-aperture maps from entire specimen and combining them to get a full field map of the object [88]. Sub-aperture maps can individually have enough accuracy and combining the maps would enable a full aperture map of the specimen with required resolution. Usually there is a trade off between field of view and resolution [89] as it is difficult to obtain both in the same time and usually an optimization procedure is employed in order to obtain a

reasonable objective. A stitching method suggests 20 % overlap between subsequent images as an optimized tradeoff between FOV and resolution [90].

Although the present of sub-aperture stitching technology aims to minimize the errors of stitching, they are not sufficient to provide the precision some applications [90]. As an example, those measurement systems which are using microscopic stage for tilting the specimens are not able to provide enough accuracy because the physical coordinates provided by the microscope stage are not precise enough to allow reconstruction ("Stitching") of the whole image from individual image stacks[87]. While scanning either the wave front or the sample with respect to the other increases the FOV without affecting the spatial resolution, they are not able to provide real time measurements.

Various stitching methods with different ways of describing the overlap area have been used for stitching long specimens. Although having an overlapping area is common in all stitching methods, its length can be a significant and effective parameter for stitching process [90]. It is known that having long overlapping region can make the result more accurate when there is no constraint on the number of images. But, in contrary, more maps would result in more errors due to the variation in imaging conditions. As result, an optimized overlapping length should be considered in stitching methods.

Furthermore, consideration of data in overlapping region is another significant issue in stitching process. In some areas, where the displacement is high and not accurate require only averaging of the data sets of overlapping portion. While in the case of requirement for higher accuracy the data in the overlapping portion should be analyzed using different

mathematical functions. Hence, different coarse and fine strategies have been developed for the overlap area in order to obtain higher accuracy in stitching process [87].

For any measurement system including stitching, obtaining a suitable mapping system with higher resolution is essential. Interferometry technique which is usually used for the test of microstructures carries higher resolution [91]. Hence many accurate profilers have been made on the basis of interferometric system. In this work three simple stitching methods employing an Acousto-Optic Modulator Stroboscopic Interferometer (AOMSI) without requiring any calibrated high precision stages are proposed. This interferometer system using Temporal Phase-shifting (TPS) method is able to extract surface information of the microstructure with a few nanometer resolutions. The applicability of these methods for micro devices is discussed and the results of different stitching approaches are presented in comparison with the whole field results obtained using a commercial white light profilometer.

5.2 Stitching Methods

Stitching is required when the FOV of measurement system is smaller than the size of the specimen. Stitching procedure requires having a common area in two adjacent images to merge the data from two images onto one image. In this thesis three different stitching methods based on geometric, size and combination of geometry and size as a reference are presented for stitching large specimens.

5.2.1 Size reference method

In size reference method, a known size of the specimen is considered as a reference. This allows identifying overlapping areas in two sequential images (shown in Figure 5.1) and enables stitching. There is no constraint for the shape of specimen in this method except that entire specimen must be covered in two adjacent acquired images. The specimens that are equal or larger than two FOVs can not be characterized using size reference methodology. For the case of stitching with size reference, two methodologies based on edge or overlap area is introduced in this section and the results of experiment for both approaches are also presented.

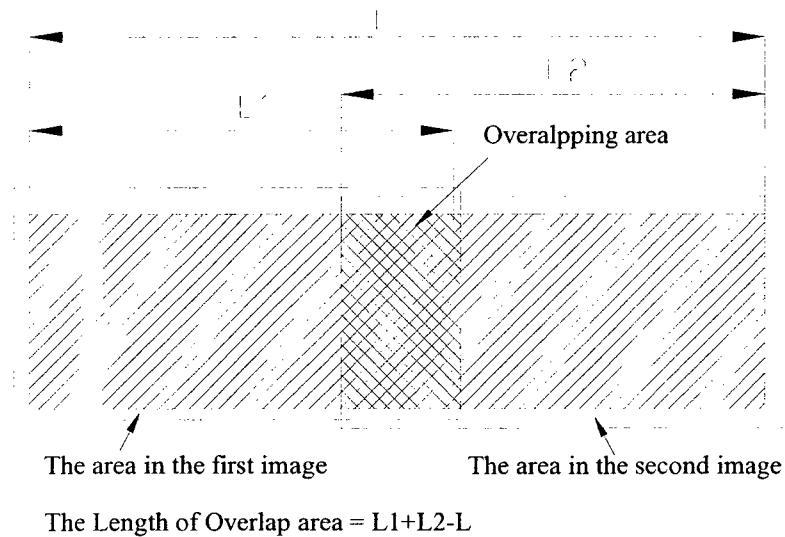


Figure 5.1 Scheme for the dimension of a specimen for stitching using size reference method.

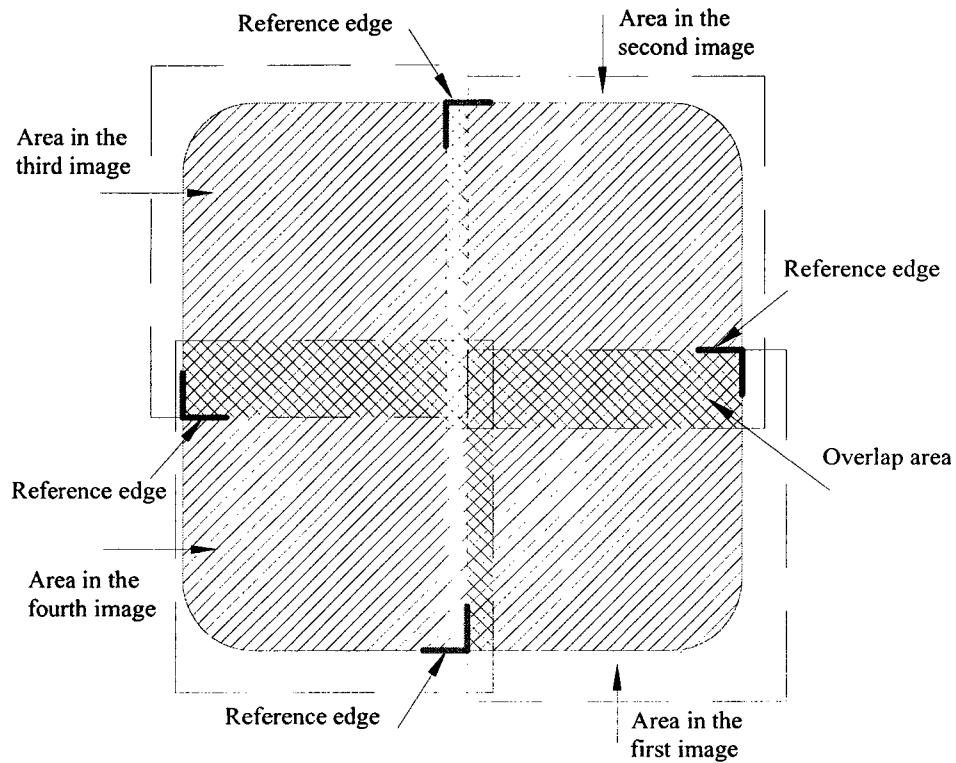


Figure 5.2 A 2-D specimen in which the FOV of taken adjunct images and the reference edges for stitching using size reference has been illustrated.

In “edge consideration” approaches one of the top or bottom edges of the specimen in the FOV is considered as reference for stitching and the result from whole of the image is used and remaining portion of the specimen from other image is added to it. Stitching using size reference can be applied to 2-D and 1-D specimens, while in 1-D specimens just having a reference line will be enough for the stitching. Figure 5.2 shows a 2-D specimen in which the FOV of adjacent images and references for the stitching using size references are shown.

In the second methodology of using size reference “overlap area consideration” approach, unlike previous method the data from overlap area in two adjacent images are functioned and used in the stitching process. The way of functioning the data sets in overlap area can be different depends on the circumstance of the measurement system, specimen and required accuracy [88] while a simple function would be averaging the data in overlap area. The overlap area consideration approach provides a better accuracy than edge approach, as it uses both the data in overlap area for stitching.

5.2.2 Geometric reference

Various components such as micromirrors arrays and cantilevers require a high accuracy characterization, but limitation in the FOV of measurement systems makes this difficult. For devices with at least one structural discontinuity, geometric reference can be used where these points are considered as reference during stitching of the images. This method is not applicable for specimens which do not carry any geometrical change in the structure or having them while the distance between them is larger than the FOV of the acquired image. In this method, extracted information from all images is added to each other with equalizing the data in reference points. Figure 5.3 and Figure 5.4 show schematic of 2-D and 1-D specimens respectively which have at least one structural discontinuity in each FOV and stitching method with geometric reference can be used for extracting surface information of the whole specimen. The FOV of the adjunct images, the reference points and overlap areas also has been shown on these figures.

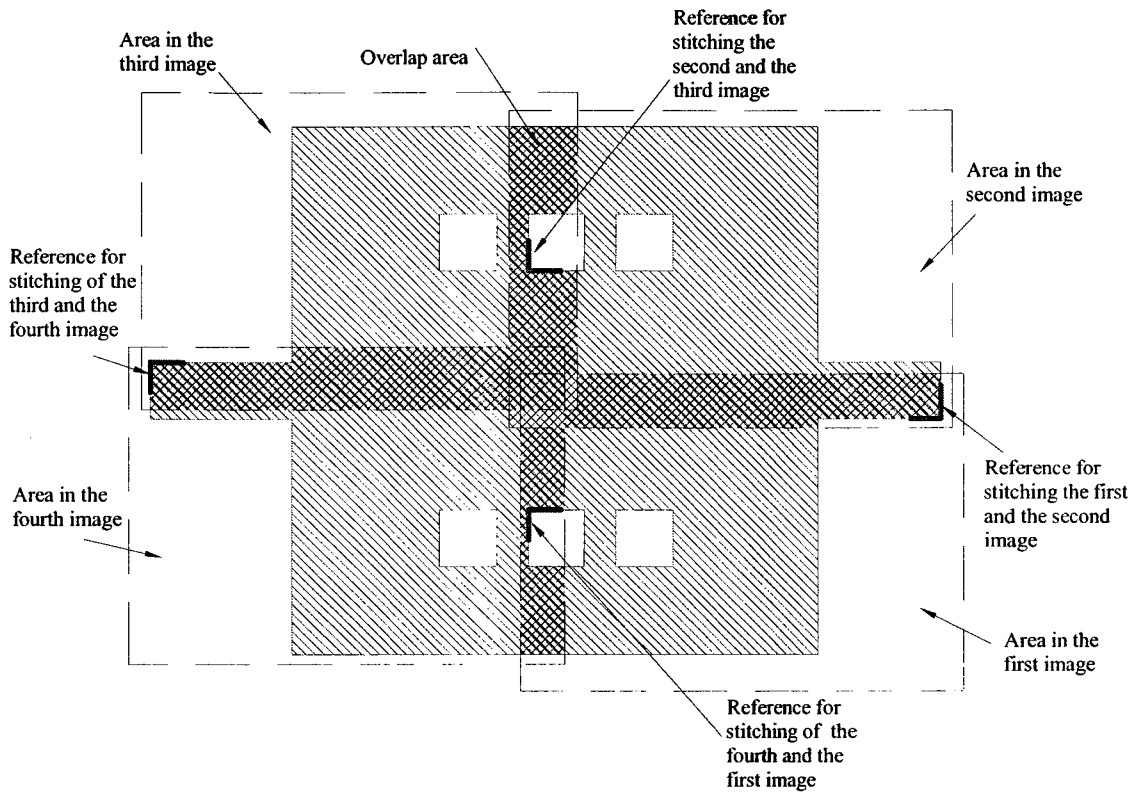


Figure 5.3 The area of the adjunct images and references for stitching them on the basis of geometric reference.

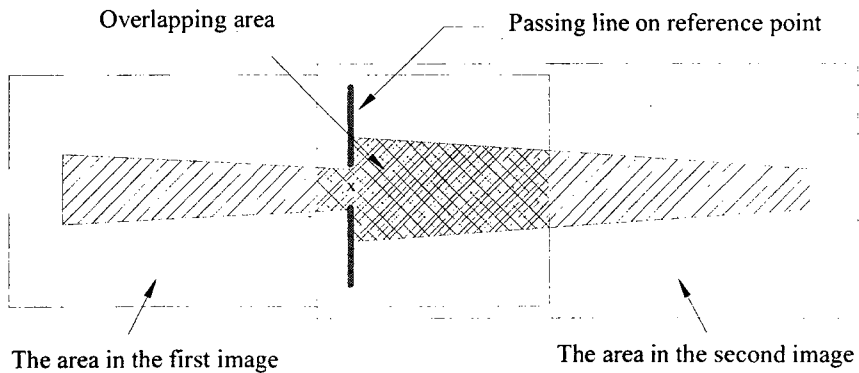


Figure 5.4 The area of two images and references for stitching them on the base of geometric reference.

5.2.3 Combination of size and geometrical reference

Combination of geometric reference and size reference is considered more practical method for larger specimens. This method gives possibility of characterizing many big specimens which were not possible using any explained stitching methods. Figure 5.5 shows a rectangular specimen which has a few cut outs in the central area. This specimen because of having larger area than the FOV of testing system it is not possible to be tested without using any stitching method. Further more as the distance between the cut outs and the edge of the specimen (L_1 or L_4) is larger than the FOV and there is not any structural discontinuity in this area, hence using any of the previous stitching methods is impractical. A combination of size and geometrical reference method can be used for stitching the images of this specimen as it shown in Figure 5.4. Initially I_{11} , I_{12} , I_{13} , and I_{14} are stitched to I_{21} , I_{22} , I_{23} , and I_{24} respectively, using size reference method. The same way I_{51} , I_{52} , I_{53} , and I_{54} can be stitched to I_{61} , I_{62} , I_{63} , and I_{64} respectively. Also the adjacent images in the central area of the specimen because of having one cut out in common area of them can be stitched using geometrical reference.

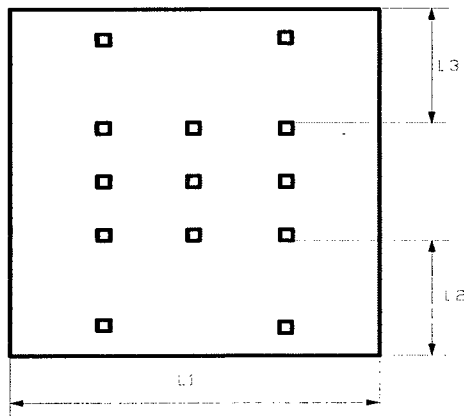


Figure 5.5 Scheme of a 2-D specimen and its dimension for stitching using combination of size and reference method.

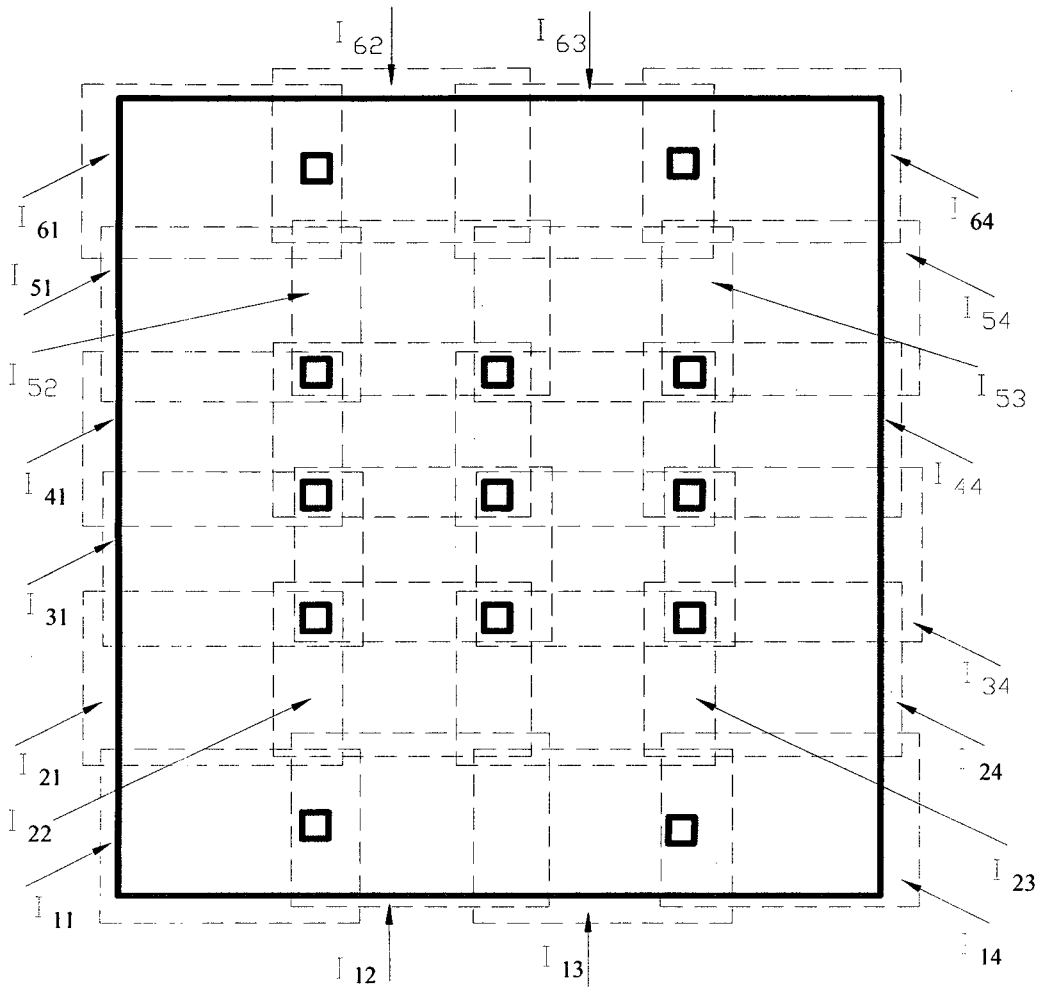


Figure 5.6 A sample 2-D specimen in which the FOV of the images with overlap areas is shown, can be analyzed using combination of size and geometric references.

5.3 Results and Discussions

For studying practically presented stitching methods, the experiments were done on a MicroGem cantilever which is $810\mu\text{m}$ length, $35\mu\text{m}$ minimum width and $10.5\mu\text{m}$ thick. Figure 5.7 shows the image of used cantilever array in which the selected cantilever for the test has been identified.

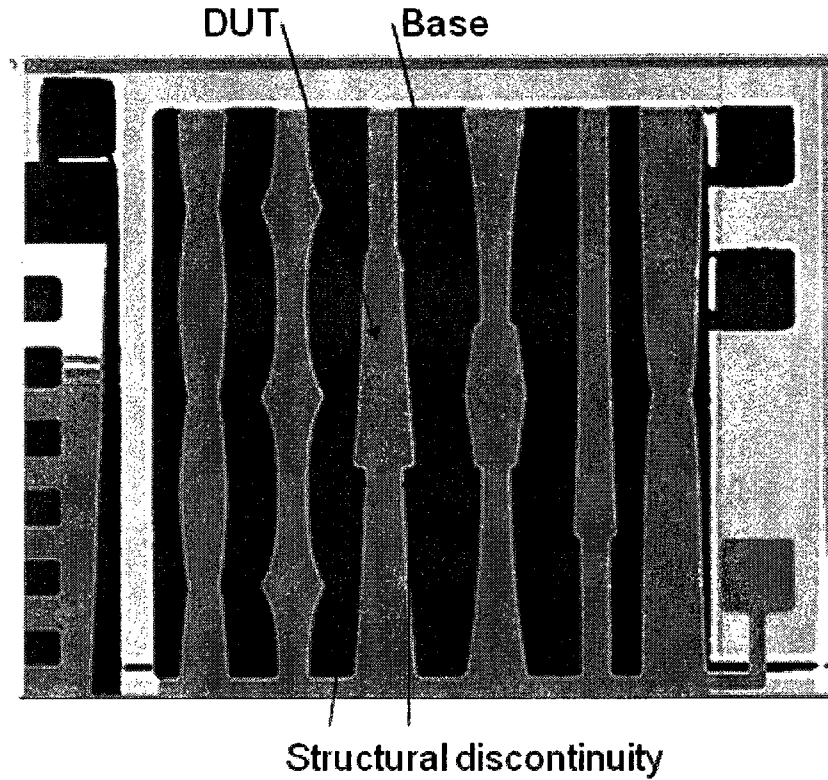


Figure 5.7 MicroGem made cantilever array and selected cantilever for the test.

The device was mounted on a two-axis stage of the interferometer and it was focused to bring clear image of the microcantilever to CCD camera. In the first step of the experiment four unknown but equal phase shifted images from the root of the device were taken as shown in Figure 5.8. As the field of view (FOV) of the optical equipment used in the experimental set up was limited to around $610\mu\text{m}$, a portion of the microcantilever from the root has been placed in the FOV.

Four captured images were studied using Carré algorithm and the value of phase for each pixel over the selected cantilever was calculated. Expression

$$I_n(x, y) = a + b \cos[\varphi(x, y) + n\alpha] \quad (5.1)$$

in which $\varphi(x, y)$ is the phase distribution that encodes the surface information over the object, n is a number showing the sequence of the images varying from 0 to 3 and letters a and b are constant value related to spatial variation in amplitude of the beams returned from the two interferometry arms is used for this calculation.

Extracted phase value for the pixels is a saw function and has discontinuities of 2π . For this reason the extracted data was conducted to obtain the absolute value for the phase.

In optical methodology obtaining the surface information from phase value requires a transformation which is related to the methodology and used experiment. Equation (2) in which $\varphi(x,y)$ and λ are the values of phase in each pixels and the wavelength of used laser respectively, is used expression for transferring the phase value to surface information in this work.

$$h(x, y) = [(\varphi(x, y) * (\lambda / 4\pi)] \quad (5.2)$$

Extracted data presenting the surface information of the root of test cantilever is shown in Figure 5.9.

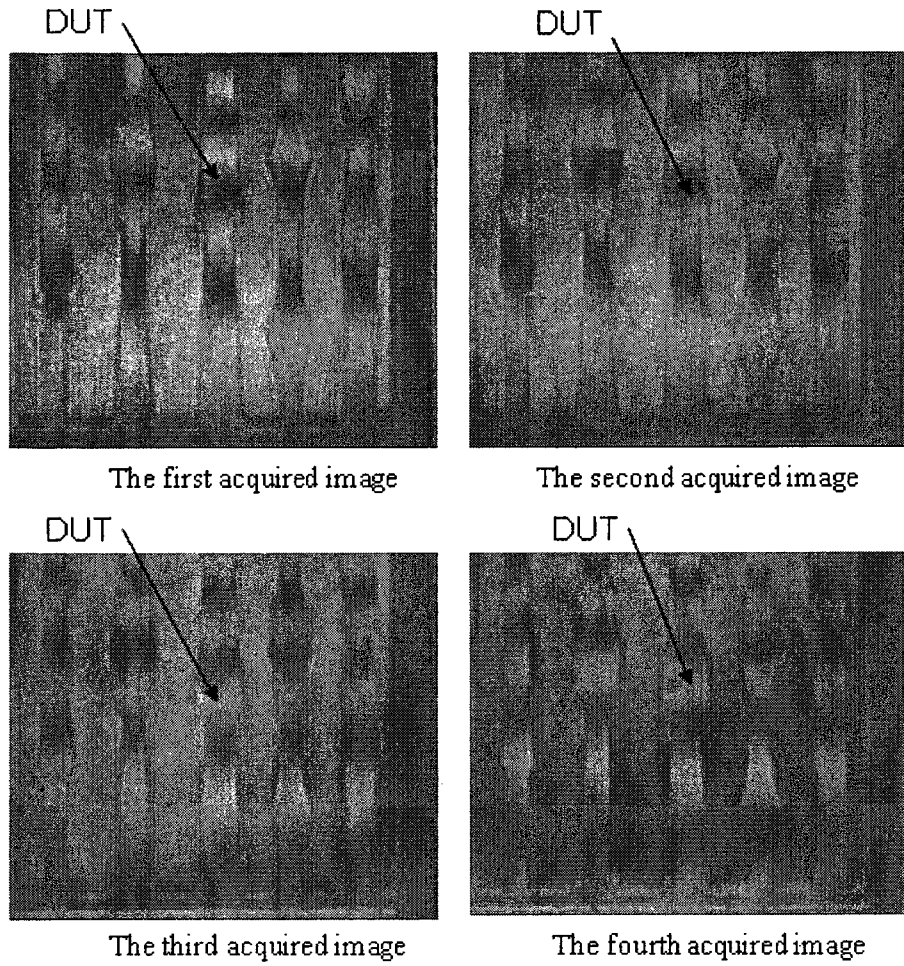


Figure 5.8 Four unknown but equally phase-shifted captured images from used microcantilever for the test in the sequence of acquiring in the first step.

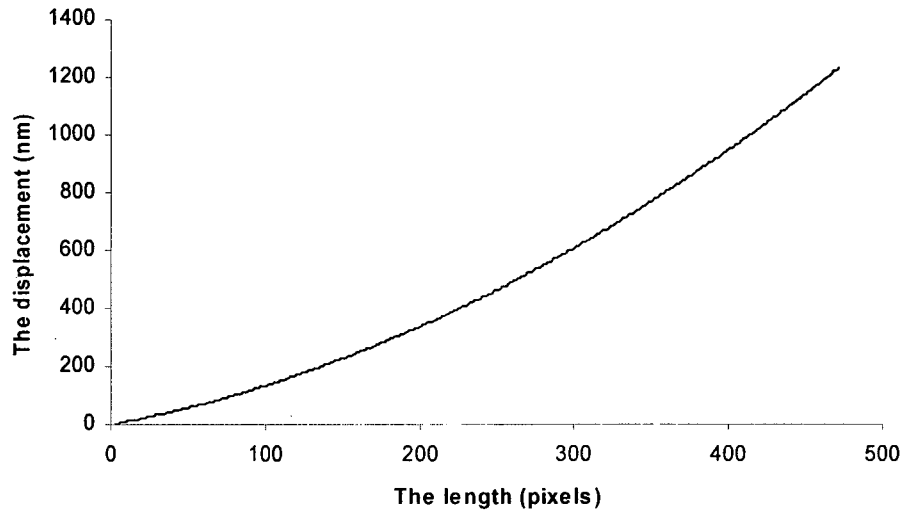


Figure 5.9 Extracted deflection information for the root portion of the DUT.

As the FOV of the measurement system was shorter than the size of the DUT, another set of images were required, from the tip portion of the device, to stitch the information in two sets and extract surface information for whole the DUT. In the second step of the experiment, mounted DUT on the stage was moved to have the image of tip portion of the cantilever in CCD camera without making any tilt in the device. Figure 5.7, Shows captured four unknown but equally phase-shifted images from the device in this step. The same process was performed in the second step to obtain the phase value and surface information for the tip portion of the cantilever. Figure 5.11 shows this value for 442 pixels of the can

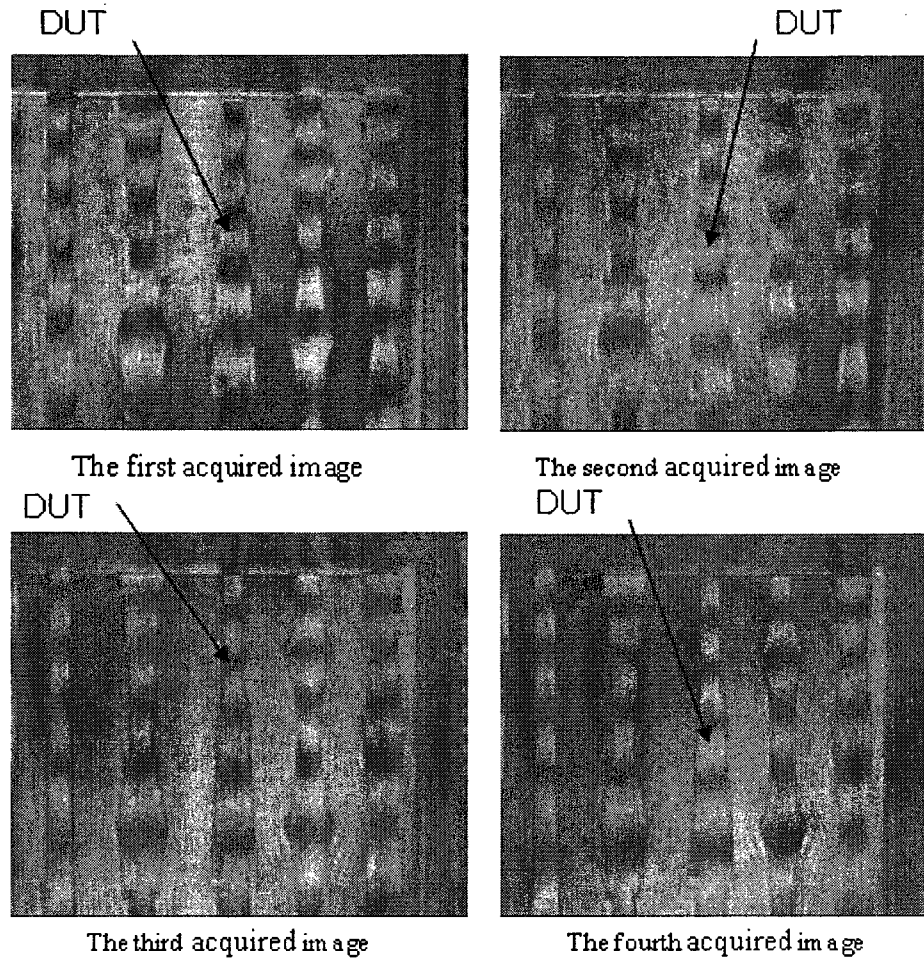


Figure 5.10 Four unknown but equally phase-shifted captured images from used microcantilever for the test in the sequence of acquiring in the second step.

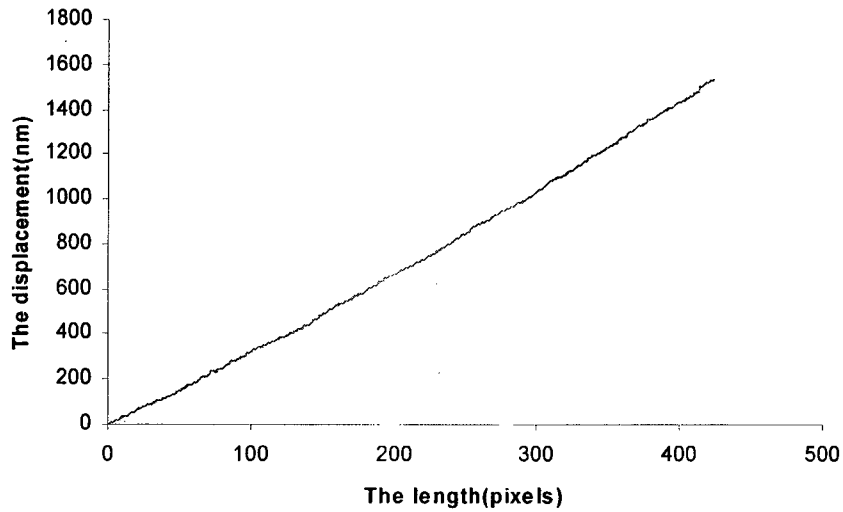


Figure 5.11 Extracted surface information for the tip portion of the DUT.

Existing structural discontinuity in the DUT, as shown in Figure 5.7, and also having the size of DUT known made possible to stitch acquired two set of images using size and geometrical references. Figure 5.12-5.15 illustrate the result of stitching in different approaches and the inserts in the figures show the reference consideration and methodology of stitching. Comparison of the results of four different approaches shows that the maximum variation between them is less than 0.75% which is well within the acceptable range.

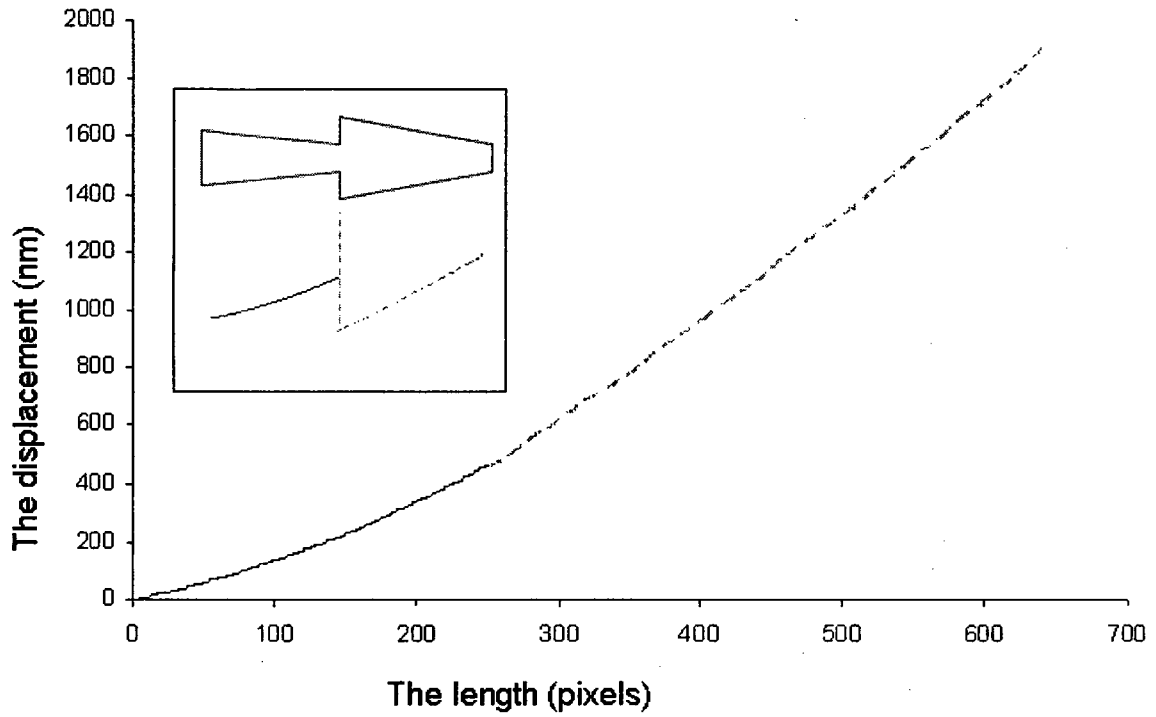


Figure 5.12. Extracted surface information for DUT after stitching using geometric reference.

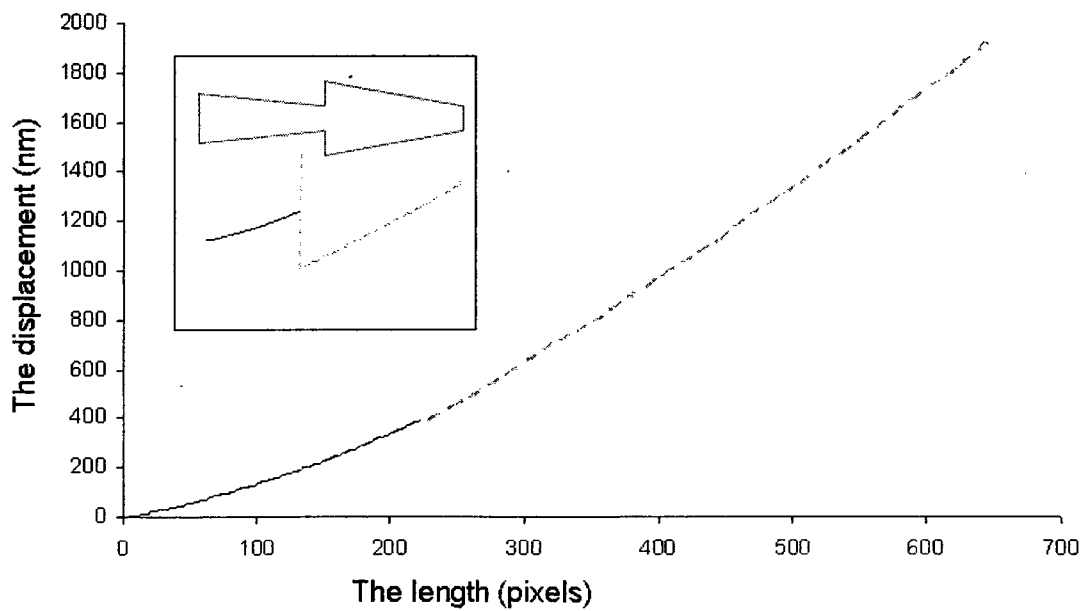


Figure 5.13. Extracted surface information for DUT after stitching with size reference and considering whole tip configuration.

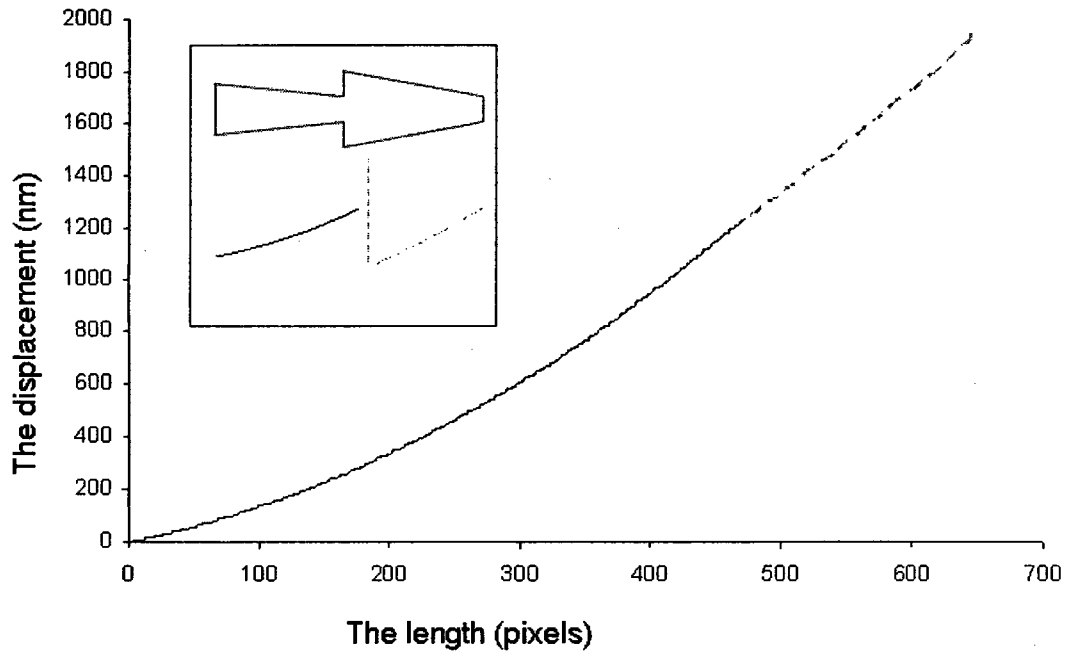


Figure 5.14. Extracted surface information for the DUT after stitching with size reference and considering whole root configuration.

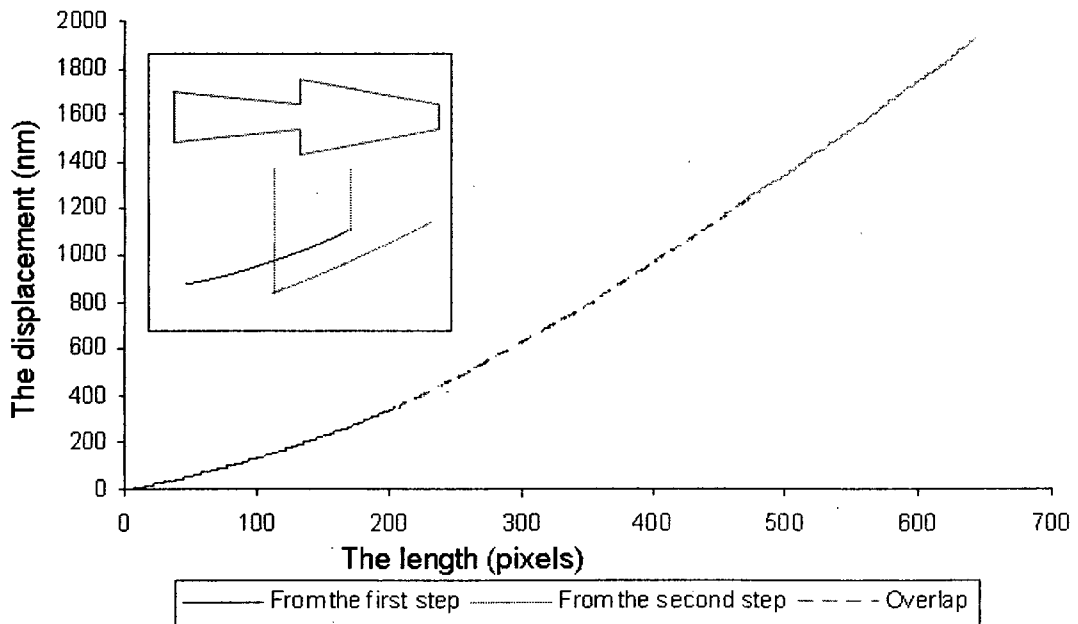


Figure 5.15. Extracted surface information for the DUT after stitching with averaging overlapping areas.

Even though, starting of the experiment the device was adjusted to have a parallel base with reference mirror, appearing fringes in the base (as can be seen in acquired images in Figures 5.8 and 5.10) proves having a small tilt on the device. For compensating this tilt on the extracted surface information for the cantilever the value of tilt of device was calculated using the same process on the base as explained for the cantilever. Figure 5.16 shows the extracted result for the tilt, the surface information for the DUT after stitching with averaging overlapping area and surface of the DUT after compensating the tilt.

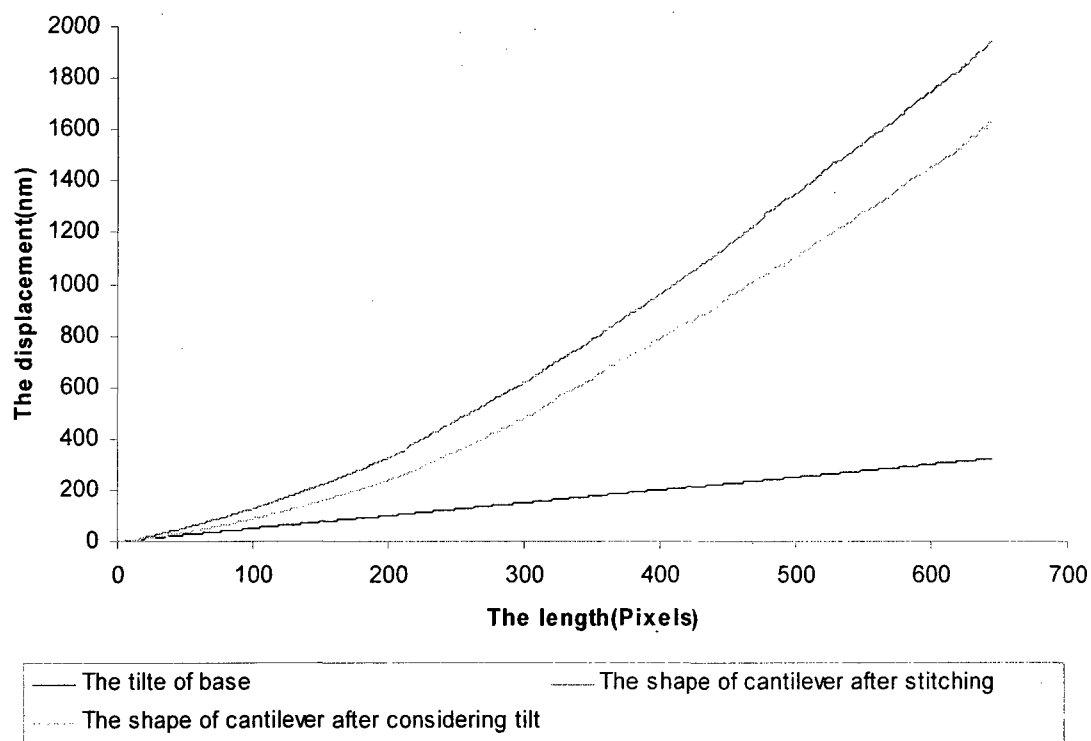


Figure 5.16 Extracted information for DUT after compensating the tilt.

Though the results from various stitching approaches mentioned in this work are repeatable with an error of less than 1%, it does not show the accuracy of the stitching process yet. In order to verify the outcome of the accuracy of presented method of stitching, the device was tested in a commercial optical profiler (Wyko NT1100) with a FOV larger than the DUT. Figure 5.17 illustrates both the results from profiler and stitching, while table 1 compares the result from profiler with different proposed stitching approaches. Even though the Figure 5.17 shows good agreement between the result from profiler and stitching, the variation between them is remarkable.

The First reason for this variation is that the tilt in the profiler is autocorrected, while in proposed stitching method the tilt and the profiler of the DUT was calculated separately. Moreover the cantilever which carries huge amount of residual stress has two shapes; the first image closer to the root is curved, while the second image is almost linear. This is another reason, and the third reason is the small spherical aberration in the developed interferometer [75].

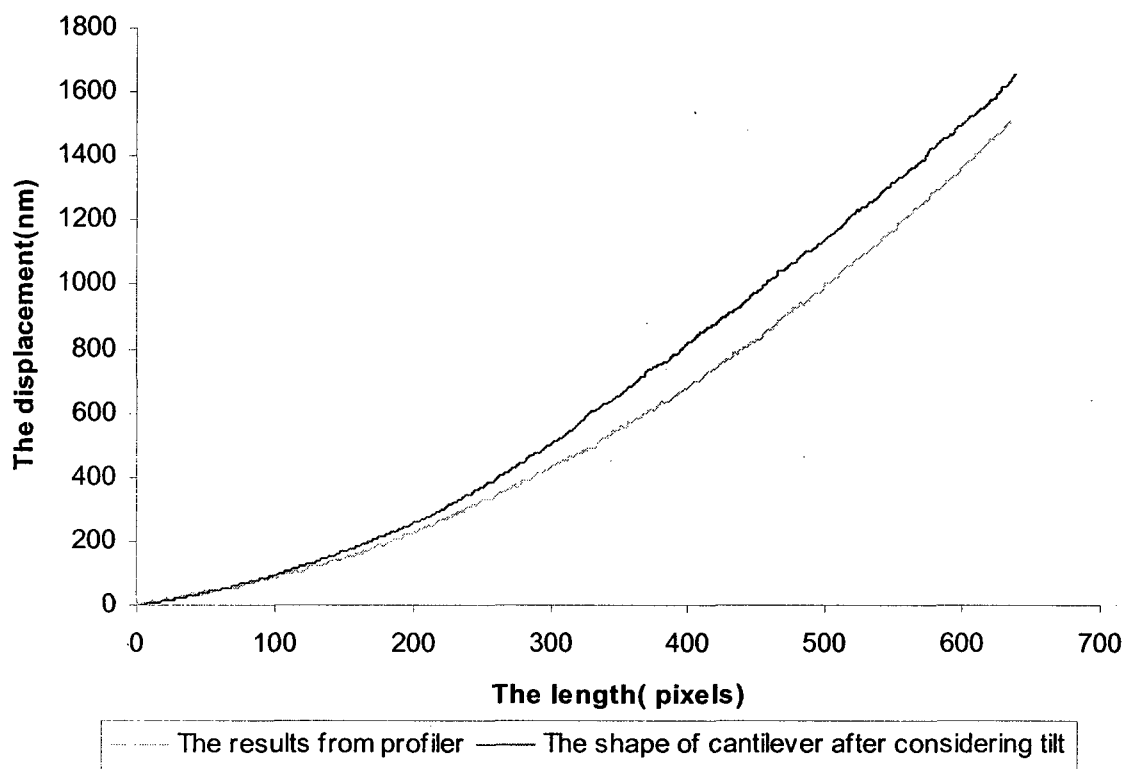


Figure 5.17 Extracted information for the test cantilever after considering the tilt using AOMSI and profilometer.

	Stitching with geometric reference	Stitching with size reference considering whole the first image configuration	Stitching with size reference considering whole the second image configuration	Stitching with size reference averaging the data in overlap areas
Extracted profile of the cantilever (nm)	16103	1612.5	1623	1607
Variation from profilometer(1505nm)	6.99%	7.14%	7.84%	6.77%

Table 5.1 Comparing the result of four used stitching methods and profilometer

5.4 Conclusion

Three simple techniques for stitching of long specimens were presented. These techniques taking advantage of structural discontinuity or known length of the structures as reference and do not require any computer control stage. As the field of view of the used experiment set up was larger than the length of cantilever, experiments were done in two steps. In the first step the root portion of cantilever were tested and in the second step the tip portion. Surface information for the root and tip portion of the cantilever individually extracted and in four different methods the images were stitched to have the whole view of the microstructure. For confirmation of the result the device was tested in full field of view with commercial profilometer. Obtained result was in good agreement with the result of stitching.

Chapter 6

Conclusions and Future Work

6.1 Conclusions

Phase shifting interferometry is considered as a conventional and reliable method for surface, static and dynamic characterization of microstructures. A simple yet viable Acoustic-Optic Modulated Stroboscopic Interferometer (AOMSI) was developed for implementing a new method of temporal phase shifting for surface profiling and static characterization of microstructures. The developed AOMSI uses a continuous wave laser which is pulsed with an Acousto Optic Modulator (AOM). This developed setup has ability for characterizing a variety of microstructures using the presented temporal phase shifting method. The proposed method unlike other temporal phase shifting methods, utilizes the principle of stroboscopy for phase shifting and does not require any phase-shifter that has the inherent error due to nonlinearity.

As an illustration of accuracy of the presented method, experiments were done on a MicraGem technology torsional micromirror and the results were in excellent agreement with the result of the same device under a commercial white light profiler (Wyko NT1100). Also the obtained results were in good agreement with the previous published results on the same micro device using Fourier Transform method.

The importance of static characterization for micro structures was presented. An energy based theoretical model was discussed. For predicting the static behavior of

microstructures using the developed theoretical model, the deflected shape of cantilever was predicted under 10V, 20V, 30V, and 40V and they were compared with experimental results using developed AOMSI. There was a good agreement between the experimental and theoretical results. The variation was noticed on the order of about 7 to 8% in the tip deflection. This could be due to the presence of residual stress on the cantilever which was not considered in the theoretical prediction. Other possible reason for variation could be spherical aberration in the setup. The non uniform gap due to the presence of residual stress could also influence the validation.

Further work was done for characterizing structures which are larger than the FOV of the developed interferometer using temporal phase shifting method. Three simple techniques for stitching the large specimens were presented. These techniques do not require any computer control stage as they use structural discontinuity or physical sizes for reference. The experiments were done on MicraGem cantilevers. As the FOV of the experimental set up was smaller than the length of cantilever, experiments were done in two steps. In the first step the root portion of cantilever was tested while in the second step, the tip portion was tested. Obtained information from the root and tip were stitched using three proposed methodologies. The results of stitching were compared with the full-field view measurements carried out using a commercial profilometer. The results were found to be in good agreement.

6.2 Future Work

For obtaining a high precision metrology and extending the application of developed AOMSI, temporal phase shifting following future work is suggested.

To improve the resolution of the developed AOMSI using this new method of temporal phase shifting two important error sources should be considered. Since the set up is developed in an open area with a laser source, reflection of the light from other equipments was affecting the results. Implementation of fiber-optic system can reduce this noise. Moreover, during all the experiments done towards this thesis, images were acquired manually, as explained in Section 3.3. This not only reduce the repeatability which capturing the four phase shifted images, but also increases the time required for capture. Electronic system for automating the acquiring of images would be highly recommended for future work, as this will ensure repeatability and reduce operating time.

The most important improvement of this work would be the dynamic characterization using temporal phase shifting. Implementation of dynamic characterization using the developed method of temporal phase shifting would make the presented method more whole some, and would make it attractive for comprehensive characterization of microstructure.

References:

- [1] Mohamed Gad-el-Hak, (2006), "The MEMS Handbook: MEMS Introduction and Fundamentals" CRC Press, 1(2), pp.1-5.
- [2] <http://www.mems-issys.com/technology.shtml>, (2008), "Technology: Introduction to MEMS"(chk: February 2009).
- [3] Rebello, K., (2004), "Applications of MEMS in Surgery" Proc IEEE, 92(1), pp.43-55.
- [4] Oliver, W., and Pharr, G., (1992), "An Improved Technique for Determining Hardness and Elastic Modulus Using Load and Displacement Sensing Indentation Experiments" Materials Research, 7(6), pp.1564-1583.
- [5] French, P. and Evans, A., (1985), "Polycrystalline Silicon Strain Sensors" Report University of Southampton.
- [6] Wen H., (2007), "Trends and frontiers of MEMS", Sensors and actuators, 136(1), pp.62-67.
- [7] Ivan, O., (1999), "Comparison of optical and non-optical methods for measuring surface roughness" The International Society for Optical Engineering, 3(1), pp. 456-467.
- [8] http://www.inems.com/MEMS_course_AREA/01_introduction/MEMS_History.htm, (2006), "History of MEMS Technology"(chk: February 2009).
- [9]<http://mmc.la.coocan.jp/info/magazine/46e/06-micro-english.pdf>, (2004), "(chk: November 2008).
- [10] Kovacs, G.T.A., Maluf, N.I. and Petersen, K.E., (1998), "Bulk micromaching of silicon" Proc IEEE, 86(8), pp.1536–1551.
- [11] Pribo M., (2009), " Status of the MEMS industry", Report Yole Development.

- [12] Espinosa, H., Prorok, B. and Fischer, M., (2003), "A methodology for determining mechanical properties of freestanding thin films and MEMS materials" *Mech. Phys. Solids*, 51(1), pp.47-67.
- [13] Chang, H., Chen, J., Fu X., Hu, X., (2004), "Micro-Motion analyzer used for dynamic MEMS characterization", *Optics and Lasers in Engineering*, 47(3), pp512-517.
- [14] Mohammadalizadeh, D., Manohar, M. , Sivakumar, N., Packirisamy, M., " Novel temporal phase-shifting stroboscopic Interferometer for surface characterization of microstructures", *Measurement* (submitted November 2008).
- [15] Sivakumar N., (2002), "Non-Mechanical and Instantaneous Phase Shifting technique for surface profiling, PhD Thesis Nanyang Technological University, pp.3-40
- [16] Danilatos, G., (1988), "Foundations of environmental scanning electron microscopy" *Advances in electronics and electron physics*, 71(3), pp.109-250.
- [17] http://en.wikipedia.org/wiki/Atomic_force_microscope, Atomic force microscope (chk: March 2008)
- [18] http://www.azom.com/Details.asp?ArticleID=3281#_Environmental_Controls, Scanning Probe Microscopy and Atomic Force Microscopy, Recent Updates and an Overview of The Technology - Supplier Data By Veeco" (chk: April 2008).
- [19] Manohar Pai, M., (2008), "Acousto Optic Modulated Stroboscopic interferometer for characterizing of microstructures", MAs Thesis, Concordia University, pp2-13.
- [20] Onodera, R., Wakaumi, H., Ishii, Y., (2005), "Measurement technique for surface profiling in low-coherence interferometry", *Optics Communications*, 254 (1), pp. 52–57.

- [21] Guotian, H., Changrong, L., Helun, J., Lu, Y., Shanglian, H., (2007), "Real-time surface profile measurement using a feedback type of sinusoidal phase modulating interferometer", *Applied Optics*, 32(9), pp.5624-5630.
- [22] Grigg, D., Felkel, E., Roth, J., Colonna de Lega, X., Deck L., (2004), "Static and dynamic characterization of MEMS and MOEMS devices using optical interference microscopy", *SPIE Photonic Europe*, 5455(55), pp.532-538.
- [23] Groot, P., (2006), "Stroboscopic white-light interference microscopy", *Applied Optics*, 45(23), 5840-5844.
- [24] Horsley, A., Park, H., Laut, S., Werner, J., (2006) "Characterization of a bimorph deformable mirror using stroboscopic phase-shifting interferometry", *Sensors and Actuators*, 134(1), pp.221–230.
- [25] Spengen W., Puers R., Mertens R., Wolf I., (2004), "Characterization and failure analysis of MEMS: high resolution optical investigation of small out-of-plane movements and fast vibrations", *Microsystem Technologies*, 10(1), pp.89-96.
- [26] Rembe, C., Muller, R., Fellow, L., (2002), "Measurement System for Full Three-Dimensional Motion Characterization of MEMS", *Microelectromechanical System*, 11(5), pp. 479 – 488.
- [27] Neev, J., Kowalski, F., (1990), "Optical frequency scanning without deflection using an acoustooptic modulator", *Quantum Electronics*, 26(10), pp.1682-1685.
- [28] Spirou, G., Yavin, I., Weel, M., Mikaelian, T., (2003), "A High- Speed Modulated Retro-reflector for Lasers", *Canadian Journal of Physics*, 81(1), 625–638.
- [29] Yang L., (2003), "Digital laser microinterferometer and its applications", *Optical Engineering*, 42(5), pp.1417-1424.

- [30] Yang, L.X., Schuth M., Thomas D., Wang Y.H., Voelsing F., (2009), "Stroboscopic digital speckle pattern interferometry for vibration analysis of microsystem", *Optics and Laser in Engineering*, 47(1), pp.252-258.
- [31] Padilla, C.E. Karlov, V.I. Matson, L. Chun, H.M., (1998), "Advanced fringe tracking algorithms for low-light levelground-based stellar interferometry", *American Control Conference, Philadelphia, PA, USAIEEE*, Vol.(3), pp. 1585-1589.
- [32] Kjell, J., Gasvik, (2002), "Optical Metrology", John Wiley & Sons, Ltd., Third Edition, pp.269-295.
- [33] Frazin R.A., (1998), "Optical path stability and fringe tracking in optical stellar interferometry", *Optics Communications*, 153(4), pp.323-330.
- [34] Peleg K., (1998), "Fast Fourier Transform based calibration in remote sensing", *International Journal of Remote Sensing*, 19 (12), pp. 2301 – 2315.
- [35] Sirohi, R. S., Mahendra, P., (1991), "Optical components, system and measurement techniques", Marcel Decker, pp.235-249.
- [36] Sirohi, R. S., and Siong Chan, F., (1999), "Optical methods in metrology: Whole field techniques and its applications", Marcel Decker, pp. 173-299.
- [37] Ngoi, B.K.A., Venkatakrishnan, K. and Tan, B., (2000), "Laser scanning heterodyne-interferometer for micro-components", *Optics Communications*, 173(6), pp.291-301.
- [38] Takasaki H., (1970), "Moire topography", *Applied Optics*, 9(7), pp.1467–1472.
- [39] Osten, W., Elandalousii, F., and Stache, M., (2000), "Handbook of Fringe Evaluation", Bremer Institut für angewandte Strahtechnik, pp.25-34.

- [40] Yat Hei Lo., Somervell A.R.D., Barnes T.H., (2005), "Wavefront measurement with a phase-shifting lateral-shearing Sagnac interferometer operating in broadband light", *Optics and Lasers in Engineering*, 43(1), pp.33–41.
- [41] Nakadate, S., Saito, H. and Nakajima, T., (1986), "Vibration Measurement Using Phase-shifting Stroboscopic Holographic Interferometry" *Journal of Modern Optics*, 33(10), pp.1295-1309.
- [42] Hart, M., Conant, R., Lau, K. and Muller, R., (2000), "Stroboscopic interferometer system for dynamic MEMS characterization", *Microelectromechanical Systems*, 9(4), pp.409-418.
- [43] Sreenivasan, M., Sivakumar, N. and Packirisamy, M., (2006), "Theoretical modeling of acousto-optic modulated stroboscopic interferometer", *SPIE*, Vol.6343, pp.6343221-6343228.
- [44] Boher, P. , Philippe Piel J., Louis Stehel J., (2007), "Phase shifting interferometer for the characterization of nanodevices", 25(11), pp.5842-5848.
- [45] Hariharan, P., Oreb, B. and Eiju, T., (1987), "Digital phase-shifting interferometry: a simple error-compensating phase calculation algorithm" *Applied Optics*, 26(13), pp.2504-2506.
- [46] Brophy, C.P., (1990), "Effect of intensity error correlation on the computed phase of phase-shifting interferometry" *Journal of the Optical Society of America A: Optics and Image Science*, 7(4), pp.537-541.
- [47] Schmit, J. and Creath, K., (1995), "Extended averaging technique for derivation of error-compensating algorithms in phase-shifting interferometry" *Applied Optics*, 34(19), pp.3610-3619.

- [48] Peisen S. Huang and Song Zhang, (2006), "Fast three-step phase-shifting algorithm", *Applied Optics*, 45(21), pp.5091
- [49] Adachi M., (2008), "Phase-Shift Algorithm for White-Light Interferometry Insensitive to Linear Errors in Phase Shift", *Optical Review*, 15(3), pp.148–155.
- [50] YU Y., Wei C., Chen M., Guo H., (2000), "Effective error reduction method in phase-shifting interferometer", *Proceeding of SPIE*, 4101(1), pp. 283-290.
- [51] Mudassar A., Harvey A. R., Greenaway A. H., Jones J., (2005), "Band pass active aperture synthesis using spatial frequency heterodyning", *Journal of Physics*, 15(1), pp.290–295.
- [52] Malacra D., Manuel S., and Malacra Z., (1998), "Interferogram analysis for optical testing" *Marcel Dekker*, Vol. 6 , pp. 247-283.
- [53] Liu Q., Cai L.Z., He M.Z., (2004), "Digital correction of wave-front errors caused by detector nonlinearity of second order in phase-shifting interferometry", *Optics Communications*, 239 (1), pp. 223–228.
- [54] Rembe C., Hart M., (2000), "Stroboscopic Interferometer with Variable Magnification to Measure Dynamics in an Adaptive-Optics Micromirror", *Journal of Physics*, 6257(8), 72-73.
- [55] Packirasamy M., (2000), "Boundary conditioning concept applied to the synthesis of Microsystems using fuzzy logic approach", PhD Thesis, Concordia University, Montreal, pp.22-38.

- [56] Spacek M., Brown Keith B., Ma Y., Robinson Alexander M., Lawson Ron P.W., Allegretto W., (1999), "CMOS Cantilever Microstructures As Thin Film Deposition Monitors", Electrical and Computer Engineering, IEEE Canadian Conference on, Vol. 3, pp.1648-1651.
- [57] Bosseboeuf A., Petitgrand S., (2003), "Characterization of the static and dynamic behaviour of M(O)EMS by optical techniques", *Micromechanics and Microengineering*, 13(1), S23–S33.
- [58] Rinaldi G., Packirisamy M., Stiharu I., (2004), "An improved method for predicting microfabrication influence in atomic force microscopy performances", *International J. of Nanotechnology*, 1(3), pp.292-306.
- [59] Rembe C., Kant R., Muller R., (2001), "Optical Measurement Methods to Study Dynamic Behavior in MEMS", *Proceedings of SPIE*, Vol. 4400, pp.127-137.
- [60] Rinaldi G., Packirisamy M., Stiharu I., (2007), "Dynamic testing of micromechanical structures under thermo-electro-mechanical influences" *Measurement*, 40(6), pp.563-574.
- [61] Hu X., Hu C., (2007), "Measuring in-plane and out-f-plane coupled motions of microstructures by stroboscopic microscopic interferometry", *Optics & Laser Technology*, 39(6), pp.1176-1182.
- [62] Chiu Y., Wei C., Zhuang Z., Chiou J., (2006), "Integration of SO1 and SU-8 in a Surface-Micromachining-Like Process and Its Application in Micro-Optical Systems", Report National Chiao Tung University, Taiwan.
- [63] Stanbridge A., Martarelli M., Ewins D., (2004), "Measuring area vibration mode shapes with a continuous-scan LDV", *Measurement*, 35(2), pp.181-189.

- [64] Zhang Y., Zhao Y., (2006), "An effective method of determining the residual stress gradients in a micro-cantilever", *Microsystems Technologies*, 12(4), pp.357-364.
- [65] Roy S., Furukawa S., Mehregany M., (1996), "Determination of Young's modulus and residual stress of electroless nickel using test structures fabricated in a new surface micromachining process", *Microsystems Technologies*, 2(2), pp.92-96.
- [66] Osten W., (2006), "Optical Inspection of Microsystems", CRC Press, Third edition, pp.220-230.
- [67] Millered J., Brock N., Hayes J., Morris M., Novak M., Wyant J., (2007), "Pixelated phase- Mask Dynamic Interferometer", Report 4D Technology Corporation, Tucson, AZ 85706.
- [68] Novak M., Millered J., Brock N., Morris M., Hayes J., Wyant J., (2005), "Analysis of a micropolarizer array-based simultaneous phase-shifting interferometer" *Applied Optics*, 44(32), pp6861-6868.
- [69] Bitou Y., Inaba H., (2005), "Phase-shifting interferometry with equal phase steps by use of a frequency-tunable diode laser and a Fabry-Peort cavity", *Applied Optics*, 44(26), pp5403-5407.
- [70] Oded R., (2005), "Geometrically nonlinear behavior of piezoelectric laminated plates", *Smart Materials and Structures*, 14(4), pp785-798.
- [71] Liu S., Dan T., Praveen S., Lian Y., (2007), "Vibration measurement of MEMS by digital laser microinterferometer", Report Department of Mechanical Engineering, Oakland University, Rochester, MI 48309, USA.

- [72] Christian R., Pamela C., Richard W., Richard M., (2007), "Stroboscopic interferometry for characterization and improvement of flexural plate-wave transducers", Report Berkeley Sensor & Actuator Center, University of California, Berkeley, USA.
- [73] Marshall Space Flight Center, Alabama. (2005), "Stroboscopic Interferometer for Measuring Mirror Vibrations", Report NASA Tech Briefs.
- [74] Xu R., Liu H., Luan Z., Liu L., (2005), "A phase-shifting vectorial-shearing interferometer with wedge plate phase-shifter", *Journal of Optics*, 7(11), pp617-623.
- [75] Pai M., Rinaldi G., Packirisamy M., Sivakumar N., (2008), "Metrology, static and dynamic characterization of microstructures using acousto-optic-modulated-stroboscopic-interferometry", *Measurement*, 42(3), pp337-345.
- [76] Dakin J., (2006), "Handbook of optoelectronics", CRC Press, Second edition, pp 918-925.
- [77] Chowdhury S., Ahmadi M., Miller W. C., (2005), "Pull-In Voltage Calculations for MEMS Sensors with Cantilevered Beams", The 3rd International IEEE-NEWCAS Conference, Vol. 22, pp143-146.
- [78] http://www.ansys.com/industries/mems/images/app_rf_switch_pullin_array.jpg(chk: November 2008).
- [79] Pamidighantam S., Puers R., Baert K, and Tilmans H., (2002), "Pull-in voltage analysis of electrostatically actuated beam structures with fixed-fixed and fixed-free end conditions", *Micromechanics and Microengineering*, 1317(32), pp458-464.
- [80] Abdel-Rahman E., Younis M. and Nayfeh A., (2002), "Characterization of the mechanical behavior of an electrically actuated microbeam", *Micromechanics and Microengineering*, 1317(51), pp759-766.

- [81] Chowdhury, S., Ahmadi, M., Miller, W. C., (2005), "A Comparison of Pull-in Voltage Calculation Methods for MEMS-Based Electrostatic Actuator Design", 1st International Conference on Sensing Technology Palmerston North, New Zealand November 21-23, Vol.(11), pp1345-1353.
- [82] Mohammadalizadeh D., Narayanswamy S., Packirisamy M., (2008), "A new method of temporal phase shifting using Acoustic-Optic Modulated Stroboscopic Interferometer (AOMSI) for identifying the shape of microstructures due to residual stress", Canadian Institute for Photonic Innovations(PHOTONS), 6(2) , pp30-33.
- [83] Rinaldi G., Packirisamy M., Stiharu I., (2007), "Quantitive Boundary support characterization for cantilever MEMS", Sensors, 7(10), pp2062-2079.
- [84] Manohohar Pai M., Rinaldi G., Sivakumar N., Packirisamy M., (2008), "Low-frequency static characterization of microstructures using acousto-optic modulated stroboscopic interferometer", Optics and Lasers in Engineering, 17(2), pp230-236.
- [85] Huang S., Zhang X., (2007), "Gradient residual stress induced elastic deformation of multilayer MEMS structures", Sensors and Actuators. A, 134(1), 77-185.
- [86] Younis M., Miles R. and Jordy D., (2006), "Investigation of the response of microstructures under the combined effect of mechanical shock and electrostatic forces", Micromechanics and Microengineering, 16 (1), pp. 2463–2474.
- [87] Preibisch S., Saalfeld S., Tomancak P., (2007), "Fast Stitching of Large 3D Biological Datasets", Report Max Planck Institute of Molecular Cell Biology and Genetics, Dresden, Germany.
- [88] Donald G., (2004), "Method for self-calibrated sub-aperture stitching for surface figure measurement", United States Patent 6956657.

[89] Jansen1M., Schellekens1P. , Haitjema1H., (2006), ” Development of a double sided stitching interferometer for wafer characterization”, Report The Netherlands Annals of the CIRP Vol.55/1.

[90] Wyant J. C., Schmit J.,(2008), “Large Field of View, High Spatial Resolution, Surface Measurements”, Report University of Arizona, Tucson, Arizona 85721, USA.

[91] Bhushan B., Wyant J. C., Koliopoulos C., (1985), ” Measurement of surface topography of magnetic tapes by Mirau interferometry”, Applied Optics, 24(10), pp1489-1494.

Appendix

List of Publications

- I. Mohammadalizadeh D., Narayanswamy S., Packirisamy M., (2008), “A new method of temporal phase shifting using Acoustic-Optic Modulated Stroboscopic Interferometer (AOMSI) for identifying the shape of microstructures due to residual stress”, PHOTONS, 6(2) ,30-33.
- II. Mohammadalizadeh D., Packirisamy M., Narayanswamy S., (2009)” Temporal phase shifting method using acoustic-optic modulated stroboscopic interferometer (AOMSI) for characterization of microstructures”, SPIE Photonics North (SPIE proceeding in print).
- III. Mohammadalizadeh D., Manohar Pai M., Narayanswamy S., Packirisamy M., (2009), “Novel temporal phase-shifting stroboscopic Interferometer for surface characterization of microstructures”, Measurement (under review).
- IV. Mohammadalizadeh D., Packirisamy M., Narayanswamy S., (2009), ” Stitched Acousto-Optic Modulator Stroboscopic Interferometry for characterizing large structures “, Measurement (under review).